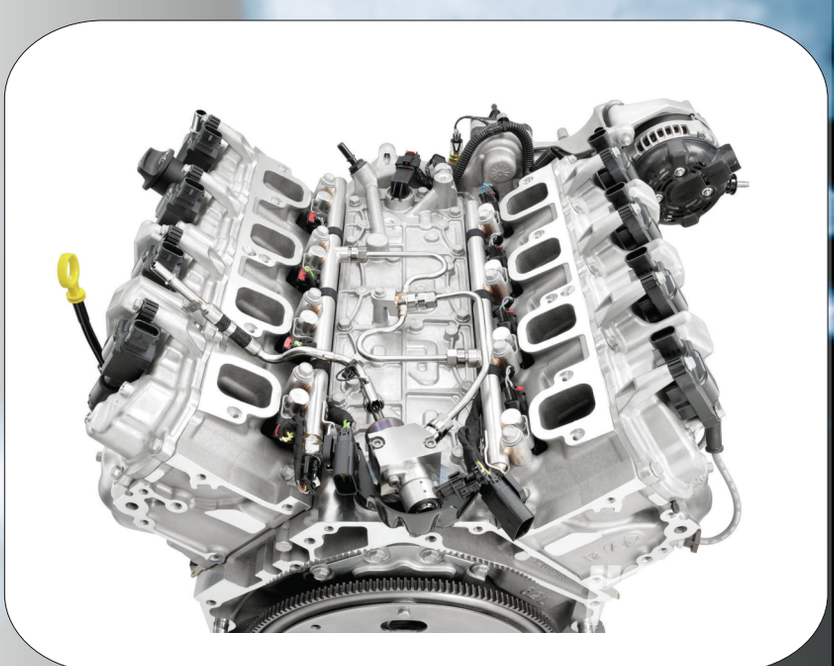
International virtual journal for science, technics and innovations for the industry

MTM

MACHINES TECHNOLOGIES MATERIALS

YEAR VIII Issue 12 / 2014 ISSN 1313-0226



Published by
Scientific technical
Union of Mechanical Engineering

MACHINES, TECHNOLOGIES, MATERIALS

INTERNATIONAL VIRTUAL JOURNAL

PUBLISHER

SCIENTIFIC TECHNICAL UNION OF MECHANICAL ENGINEERING

108, Rakovski Str., 1000 Sofia, Bulgaria
tel. (+359 2) 987 72 90,
tel./fax (+359 2) 986 22 40**,**
journal@mech-ing.com,
www.mech-ing.com/journal

ISSN 1313-0226
YEAR VIII ISSUE 12 / 2014

EDITORIAL BOARD

Editor-in-chief: Prof. Dr. Mitko Mihovski – Chairman of the Scientific Council of the STUnion of Mechanical Engineering

AKADEMIC CONCEPTIONAL BOARD
Acad. Vassil Sgurev
Acad Yachko Ivanov
Acad Vladimir Klyuev
Acad. Rivner Ganiev
Corr. mem. Georgi Mladenov
Corr. mem. Dimitar Buchkov
Corr. mem. Stefan Hristov
Corr. mem. Venelin Jivkov
Corr. mem. Anatoliy Kostin
Corr. mem. Edward Gorkunov

EDITORIAL COUNCIL
Prof. D.Sc. Georgi Popov
Prof. D.Sc. Alexander Skordev
Prof. D.Sc. Nikola Rashkov
Prof. D.Sc. Dimitar Stavrev
Prof. D.Sc. Hristo Shehtov
Prof. Dr. Todor Neshkov
Prof. Dr. Dimitar Damianov
Prof. Dr. Kiril Arnaudov
Prof. Dr. Snejana Grozdanova
Prof. Dr. Vassil Georgiev
Assoc. Prof. Lilo Kunchev

EDITORIAL BOARD – EXPERTS AND REVIEWERS

FROM BULGARIA
Prof. D.Sc. Nyagol Manolov
Prof. D.Sc. Vitan Galabov
Prof. D.Sc. Emil Momchilov
Prof. D.Sc. Emil Marinov
Prof. D.Sc. Dimitar Katzov
Prof. D.Sc. Stavri Stavrev
Prof. D.Sc. Georgi Raychevski
Prof. D.Sc. Ivan Yanchev
Prof. D.Sc. Marin Stoychev
Prof. D.Sc. Roman Zahariev
Prof. D.Sc. Vassil Mihnev
Prof. D.Sc. Valentin Abadjiev
Assoc. Prof. Dimitar Stanchev
Assoc. Prof. Milcho Angelov
Assoc. Prof. Mihail Mihovski
Assoc. Prof. Radi Radev
Assoc. Prof. Georgi Todorov
Assoc. Prof. Simeon Petkov
Assoc. Prof. Petar Dobrev
Assoc. Prof. Nikolay Piperov

FOREIGN MEMBERS
PD. D. PE Assoc. Prof D.Midaloponlas
Prof. Dr. Athanasios Mihaildis
Prof. Amos Notea
Prof. Dr. Eng. Airon Kubo
Prof. Dr. Eng Georg Dobre
Prof. Dr. Dimitrov Dimitar
Prof. Dr. Mohora Cristina
Prof. Dr. Popa Marcel
Prof. Dr. Sobczak Jerzy
Prof. Dr. Tamosiuniene Rima
Prof. Alexander Dimitrov
Prof. dr. Marian Tolnay
Prof. dr. Mikolas Hajduk

The current issue and the first issue of journal and the conditions for publication can be find on www.mech-ing.com/journal

CONTENTS

SURFACE MORPHOLOGY OF PURE TITANIUM AFTER ANODIZATION
Dikova Ts. 3

USER EVALUATIONS: APPLYING A COST-BENEFIT APPROACH TO HUMAN COMPUTER INTERACTIONS
Katz A. 8

PRODUCTION OF ALUMINA NANOPARTICLES (AL2O3) USING PULSED LASER ABLATION TECHNIQUE IN ETHANOL SOLUTION
Adel K. M. 12

COMPARISON BETWEEN PROJECT MANAGEMENT AND SOFTWARE PROJECT MANAGEMENT
Ivanova M. 16

THERMOMECHANICAL STRENGTHENING AND STABILITY OF AUSTENITIC Cr18Ni10N STEEL
Kaputkina L.M., A. G. Svyazhin, D.E. Kaputkin, I. V. Smarygina, V. E. Kindop 20

IN-SITU STRESS-STRAIN TESTING OF STEELS IN CO2-CONTAINING SALINE SOLUTIONS
Pfennig A., S. Trenner, M. Wolf, C.-P. Bork 23

ROBUST BI-CRITERIA APPROACH TO OPTIMIZE THE COMPOSITION AND PROPERTIES OF TITANIUM ALLOY
Tontchev N., Y. Kalev 26

ANALYSIS OF THE APPROACHES FOR IMPROVEMENT OF THE ENERGY EFFICIENCY OF ELECTRIC RESISTANCE FURNACES
Dimitrov B., O. Zhekov 31

CREATING AND RESEARCHING SUSTAINABLE DESIGN OF CORRUGATED CARDBOARD FURNITURE WITH ADVANCED TECHNOLOGICAL MEANS
Dovramadjiev T., P. Bratanov, K. Cankova, G. Jecheva 35

NUMERICAL SIMULATION AND EXPERIMENTAL INVESTIGATION OF EQUAL-CHANNEL ANGULAR PRESSING OF POROUS POWDER BILLETS
Ryabicheva L., D. Usatyuk, A. Dyadichev 37

PULSED DISCHARGE TECHNOLOGIES OF PROCESSING AND OBTAINMENT OF NEW MATERIALS (Review)
Sizonenko O., A. Vovchenko 41

THE ROLE OF SEVERE PLASTIC DEFORMATION IN THE FORMATION OF HIGH ELECTRICAL PROPERTIES OF ALUMINUM ALLOY
Raab G.I., E. I. Fakhretdinova 45

DISSIMILAR WELDING AUSTENITIC STAINLESS STEEL S316 WITH FERRITIC STRUCTURAL STEEL GRADE 300NZS
Cvetkovski S., D. Brkovski 48

COMBINED APPROACH FOR MODELING OF MANUFACTURING EXECUTION SYSTEMS
Antonova I. D. 52

SURFACE MORPHOLOGY OF PURE TITANIUM AFTER ANODIZATION

Assoc. Prof. Dr Dikova Ts.
Faculty of Dental Medicine, Medical University of Varna, Varna, Bulgaria

E-mail: tsanka_dikova@abv.bg

Abstract: *Present paper deals with the investigation of the surface morphology of pure titanium after anodization. Round samples of CP Ti were anodized at different voltages (16V, 20V, 25V, 30V and 40V) in an electrolyte containing 0.5 wt.% HF. The process duration varied from 30min to 7 hours. The samples' surface was observed and EDX analysis was made by SEM. Surface morphology of CP Ti after anodization is defined by the surface roughness before anodization, electrolyte type and process parameters – voltage and duration. It was established that the surface of pure titanium after 3h-7h anodization at all voltages characterizes with large number of craters increasing the surface micro-roughness. At short-term processes only pores with about 2μm diameter were observed. Depending on the regimes used different oxide nanostructures were observed. After short-term anodization in lower voltages the titanium surface was covered with nanodots, nanorods and nanoflakes. Increasing the voltage up to 25 V led to originating of nano-tubular structure in some areas and sponge-like nano-structure at 30 V and 40 V. Increasing the process duration caused increase of the proportion of nanotubes and sponge-like structure to that of nanorods.*

Keywords: PURE TITANIUM, ANODIZATION, SURFACE MORPHOLOGY, TITANIUM OXIDE NANOTUBES AND NANOSTRUCTURES

1. Introduction

An implant is an artificial structure whose purpose is to replace or stabilize damaged body functions and include many different types such as hip and knee joints, spinal implants, dental implants etc. [1]. The principal requirements of all medical implants are corrosion resistance, biocompatibility, bioadhesion, biofunctionality, processability and availability. The design of implants could be divided in four levels: macro-design, mini-design, micro-design and nano-design. The last two aspects refer to the surface roughness at micro-level and to the molecular organization of the implant surface at nano-level. From that point of view, the surface topography of the implant should consists of hierarchical structure, composed of micro- and nano-components, which mimic the structure of the natural bone [2,3].

Pure titanium is preferable material for production of implants because its mechanical properties and elastic modulus are close to that of the bone tissues. Its good corrosion resistance and biocompatibility depends upon the formation of a solid oxide layer. As the geometry, roughness and other surface characteristics importantly influence the surface–tissue interaction, the biocompatibility of the implant can be enhanced by surface modification. Transformation of the solid oxide layer into porous or tubular structure can give such a decision, because TiO_2 NanoTubes (NT) can mimic the dimensions of the components of natural bone.

The simplest, rapid and inexpensive method for preparation of strongly adherent layer of TiO_2 NT is anodization [4,5]. The nano-tubular structures are obtained during anodization in fluorine electrolyte solutions with applied voltage lower than the dielectric breakdown. In the most electrolytes containing fluorides, nanotubes can be grown with diameter of 40-150nm at anodic voltages in the range of 5-30V [3-5]. It was found that the diameters of the nanotubes were determined by applied voltage while the final length of the tubes was independent of the anodization time. The thickness of the formed tubular-structure oxide layer can be from a few hundred nanometers up to a few microns by controlling pH and electrolytes.

As the geometry and roughness of the surface strongly influences on the implant's biocompatibility, the aim of the present paper is to investigate the surface morphology of pure titanium after anodization in water solution of HF at different regimes.

2. Experimental methods

Round samples with dimensions 24mm x 3mm (diameter x thickness) were made of commercially pure (CP) Ti Grade-2 (99,5%). The samples' surface was grinded with sandpaper 300, 600 and 800. After grinding they were ultrasonically cleaned consecutively in acetone, ethanol and deionized water for 15 min in each media and dried with compressed air. On the next stage the samples were etched for 30 min in 0.5 wt.% HF acid, immediately rinsed with deionized water and dried. They were anodized at different voltages (16V, 20V, 25V, 30V and 40V) in an electrolyte containing 0.5 wt.% HF acid using a DC power supply with a graphite electrode as cathode. The process duration varied from 30min to 7 hours. Immediately after anodization the samples were rinsed several times with deionized water and dried with compressed air. The surface morphology was observed and EDX analysis was made on high resolution field emission scanning electron microscope FEI Quanta 400 ESEM FEG (ESEM2). The phase composition was investigated by XRD analyzer Rigaku D/Max in Cu Kα irradiation.

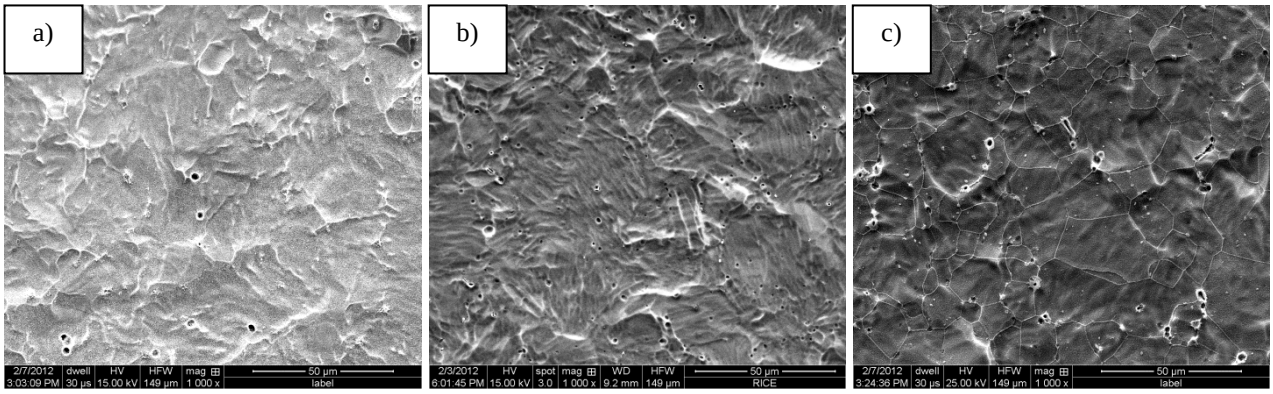


Fig. 1 *Surface morphology of pure Ti-Gr2, after 30 min anodization at different voltages: 20V - a); 30V - b); and 40V – c).*

3. *Results and analysis*

Results obtained

The surface of CP Ti after anodization characterizes with large number of craters increasing the surface micro-roughness. The first single pores with diameter of about 2μm are observed in 1h anodization even in lower voltages – 16 V. Their quantity slowly increases with increasing of the voltage up to 40 V (Fig. 1), while their sizes remain unchanged. The process duration influences stronger. With increase the time from 30 min up to 6h (Fig. 2) the number of pores and their diameter increase while their shape changes to crater-like. Fig. 2c-1 and Fig. 2d-1 show large number of well-shaped craters with different sizes on the sample's surface after 3h and 6h anodization. The new formed pores of about 2 μm can be seen both inside the craters with larger sizes and outside them. The craters' diameter after 1h anodization varies between 5-7 μm; it is up to15 μm after 3h and up to 25 μm after 6h processes.

The grain boundaries can be clearly seen on the samples surface after anodization in the all regimes, whether increasing the voltage (Fig. 3) or the process duration (Fig. 2d-2). White formations with irregular shape and dimensions of about 1-2 μm are observed on the joints of three grains and mainly along the grain boundaries (Fig. 3).

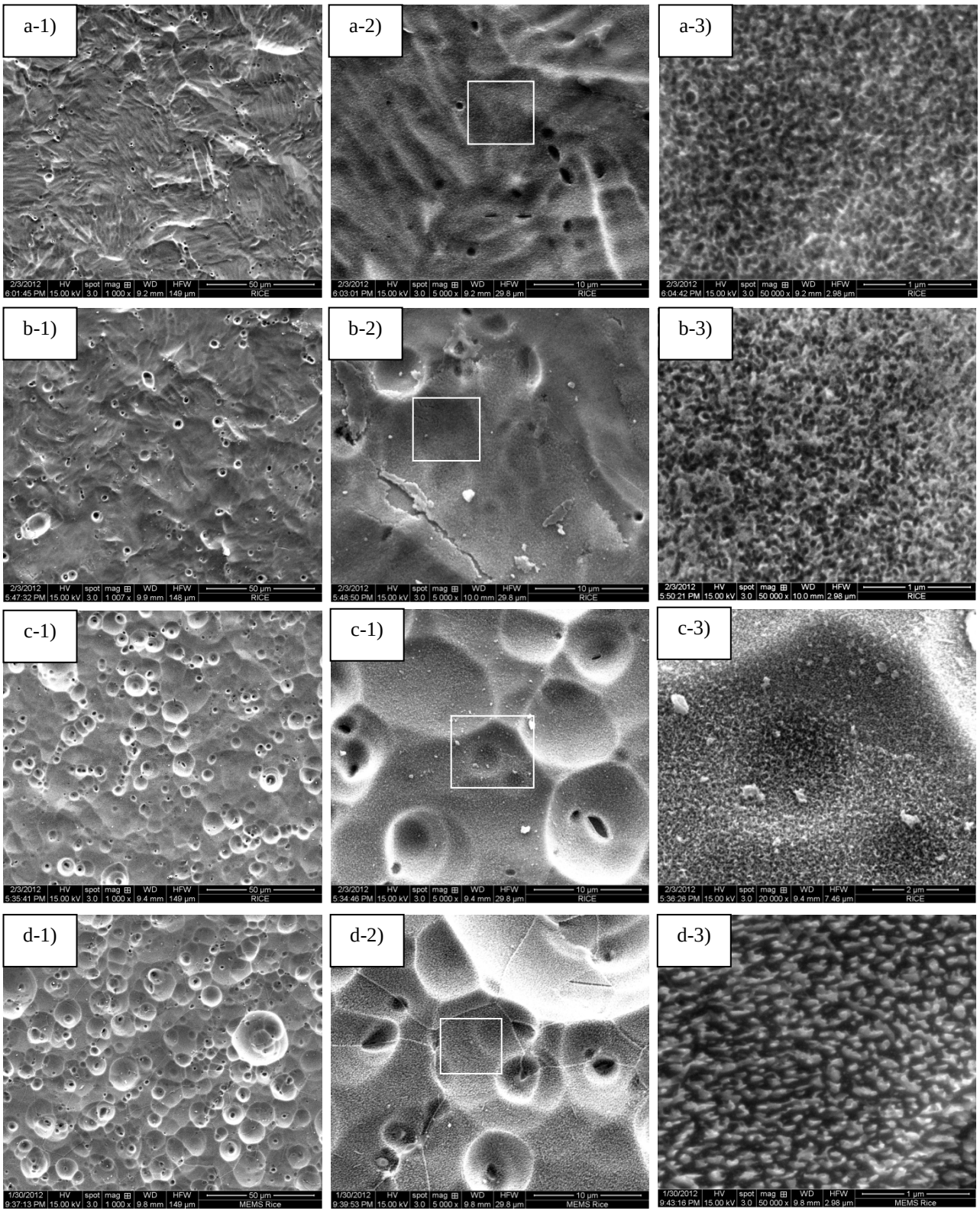


Fig. 2 *Surface morphology of pure Ti-Gr2, after anodization at 30V in different duration: 30min - a); 1h - b); 3h - c); and 6h - d).*

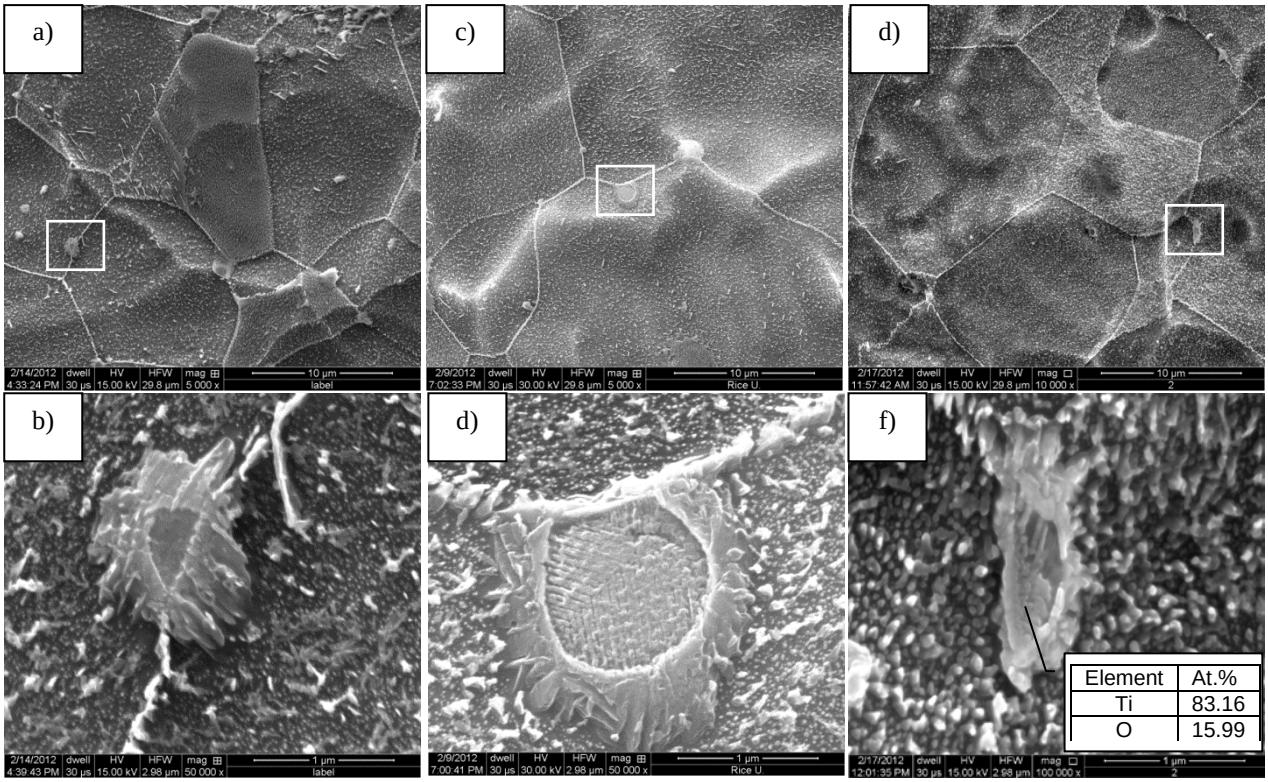


Fig. 3 *Surface morphology of pure Ti-Gr2, after 1h anodization at different voltages: 16V - a) and b); 20V - c) and d); and 25V – e) and f).*

They originate at the all anodization voltages after 1h and can be even seen after 6h process (Fig. 4). They are composed of titanium oxide (Fig. 3f and Fig. 4).

The surface morphology after short term (30 min) anodization in low voltages (20 V) is very similar to that of the etched sample (Fig. 5). Only oxide nanodots and the beginning of nanorods and nanoflakes formations can be seen. Increasing of voltage doesn't lead to significant changes. Only porous sponge-like nanostructure (Fig. 2a-3) originates in several spots on the surface after anodization at 30 V and 40 V, while the rest part is covered by nanorods. Increasing the process duration leads to formation of different type of titanium oxide nanostructures. After 1h anodization in lower voltages (16 V and 20 V) the samples surface is covered with nanodots, nanorods and nanoflakes (Fig.3a-d). The first nano-tubular structure originated in small spots scattered over the entire sample's surface after 1h anodization in 25V. The structure is rather sponge-like consisting of pores with irregular shape and sizes [6]. Well-shaped NTs with average internal diameter 82 nm could also be observed in some zones. The rest surface is covered with nanorods. The sample surface after 1h anodization in 30 V is covered with porous spong-like nanostructure (Fig.2a-3) and nanorods in ratio 30%/70%. Increasing of the process duration leads to increase the portion of nanotubes and sponge-like structure to that of nanorods and increasing the NTs diameter as well. After 6h anodization at 25 V the average NTs diameter is 109 nm and the NTs/nanorods ratio is 60-70%/40-30% (Fig. 4). While after 30 V process with the same duration the sponge-like/nanorods ratio is 60%/40% (Fig. 2d-2). EDX analysis on Fig. 4 shows that all types of nanostructures consist of titanium oxide with amorphous structure [6].

Discussion

Surface morphology of pure titanium after anodization is defined by the surface roughness before anodization, electrolyte type and process parameters – voltage and duration. During anodization field-enhanced oxidation and field-enhanced dissolution run simultaneously with the chemical dissolution of the titanium and titanium oxide in HF acid. But the field-enhanced processes run with different rate at the particular micro-regions because of the micro/nano-roughness of the surface, obtained after etching [6]. As a result the formation of thin oxide layer on the sample's surface is embarrassed and the first TiO_2 nanostructures originate in small spots. The fluorine electrolyte solutions determine the nano-porous or nano-tubular structure of the oxide layer during anodization which is obtained in voltages much lower than the dielectric breakdown – 93 V [5, 7, 8]. Our results show TiO_2 nano-tubular structure at 25 V and nano-porous sponge-like structure at higher voltages - 30 V and 40 V. The formation of nano-porous sponge-like structure at higher voltages is probably due to the intensive release of oxygen on the anode (1) which occurs during anodization in water solutions [7] and may cause inhomogeneity of the ordered structure.

$$H_2O \rightarrow O_2 + 4H^+ + 4e^- \quad (1)$$

The titanium oxide is a dielectric and has higher resistivity than the electrolyte and the metallic substrate. Therefore the applied voltage will mainly drop over the oxide film on the anode. High O_2 at the anode means that there are high electric currents through the oxide films, which may lead to dielectric breakdown of the film [7]. Moreover in our experiments the thickness of the anodized layer is not uniform, so there are conditions in some weak points the potential drop to exceed the dielectric limit causing sparking [5]. The sparking causes micro-pits and spots along the grain boundaries [8]. As a result we observed micro-pits with about 2μm diameter in 30 min process at all voltages (Fig. 1 and Fig. 2a-2). This process is accompanied with increasing the local temperature up to several thousand degrees causing local melting [5], thus transforming pores into craters. Thermal stress of the anodized layer leads to cascading process of multiplication of weak points and consequently breakdown of the dielectric. As a result large number of craters is formed on the surface of pure titanium after anodization in 3h and 6h (Fig. 2).

As the grain boundaries characterizes with high degree of lattice disorder of the neighboring grains and condensation of vacancies [9], the diffusion of metal cation in these regions during anodization is higher. As a result oxide formations with different shape can be seen along the grain boundaries and in joints of three grains after short term anodization at all of the voltages (Fig. 3) which keep in

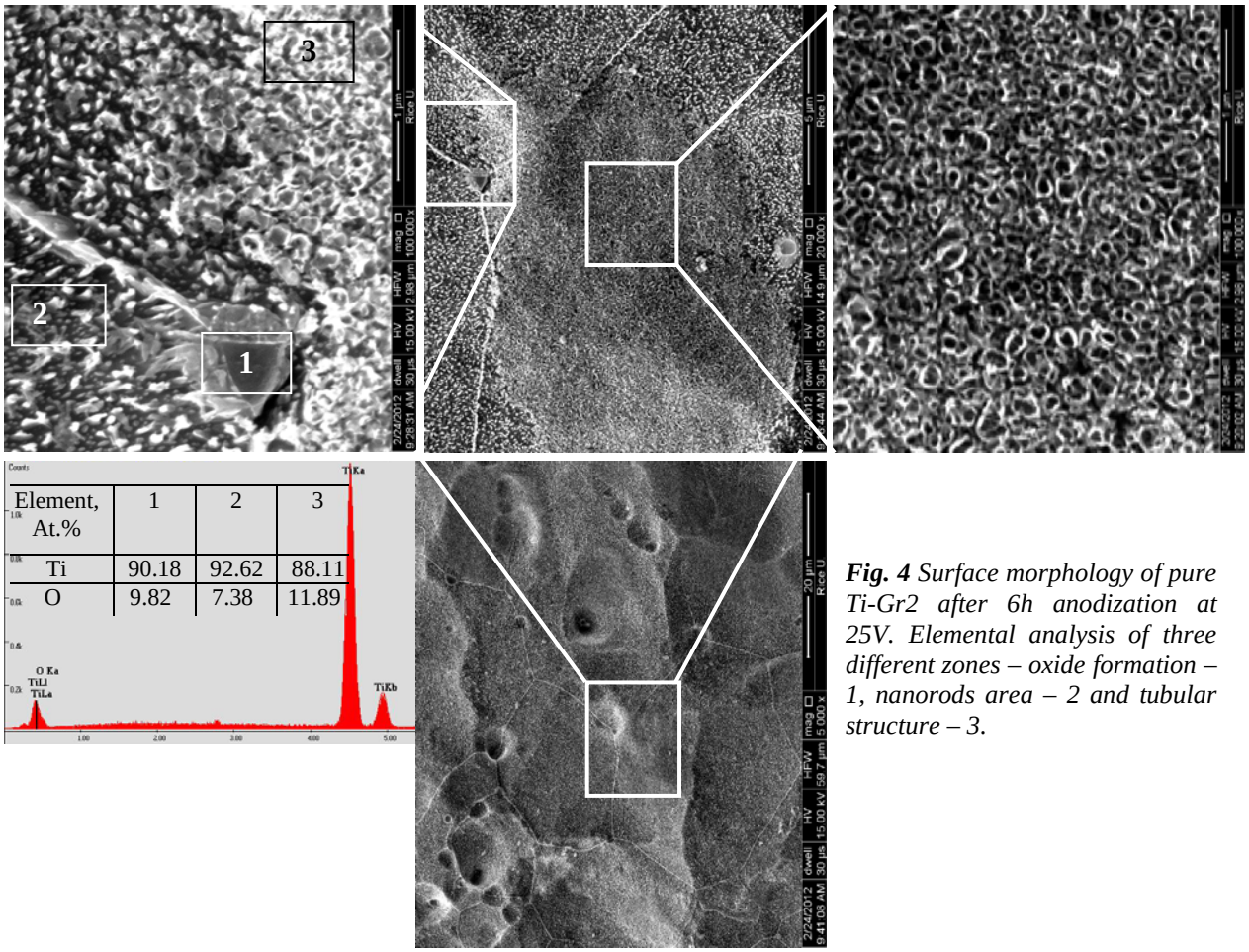


Fig. 4 *Surface morphology of pure Ti-Gr2 after 6h anodization at 25V. Elemental analysis of three different zones – oxide formation – 1, nanorods area – 2 and tubular structure – 3.*

time increase up to 7h. But, because of the high vacancies' accumulation, local decohesion of the oxide layer from the metal could occur thus weakening the anodized layer and creating conditions for dielectric breakdown. That is why the pores, growing further into craters, are mainly along the grain boundaries.

4. Conclusions

Samples' surface of pure titanium after anodization in water solution of HF acid at different regimes was investigated. Surface morphology is defined by the surface roughness before anodization, electrolyte type and process parameters – voltage and duration.

It was established that the surface of pure titanium after 3h-7h anodization at all voltages characterizes with large number of craters increasing the surface micro-roughness. At short-term processes only pores with diameter of about 2μm are observed. Increasing of time leads to increase of the number of pores and their diameter while their shape changes to crater-like with dimensions up to 25 μm (6h, 30 V).

Different oxide nanostructures are observed depending on the regimes used. After short-term anodization in lower voltages (16 V and 20 V) titanium surface is covered with nanodots, nanorods and nanoflakes. Increasing the voltage up to 25 V leads to originating of nano-tubular structure in some areas and sponge-like nano-structure at 30 V and 40 V. Increasing of the process duration leads to increase the proportion of nanotubes and sponge-like structure to that of nanorods up to 60-70%/40-30% (6h, 25V) and 60%/40% (6h, 25V) accordingly.

Surface morphology of pure titanium after anodization characterizes with higher micro-roughness and different morphology of the oxide layer which varies from nanodots,

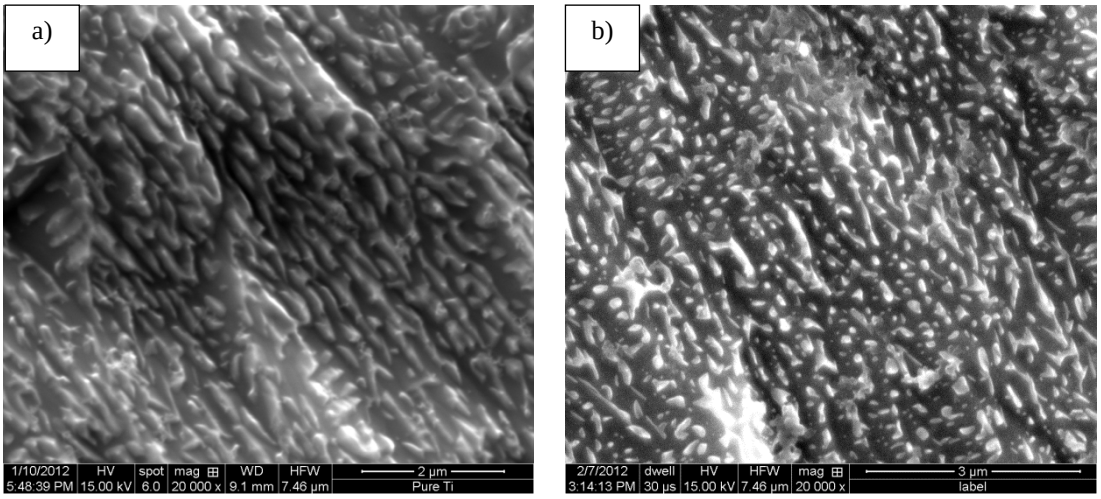


Fig. 5 *Surface of pure Ti-Gr2 after etching – a) and after subsequent 30 min anodization at 20V - b).*

nanorods and nanoflakes in lower voltages and short-term processes to nanotubes/nanorods and sponge-like/nanorods with different ratio in higher voltages and long-term anodization.

5. Acknowledgements

The present work is supported by the Fulbright grant for 2011-2012 year. It was done with colleagues of Prof. Pulickel Ajayan's group in MEMS Department of Rice University, Houston, USA.

6. References

1.Balazic M., J.Kopac, Review: titanium and titanium alloy applications in medicine, *Int. J. Nano and Biomaterials*, **1**, No.1, 2007, 3-34;

2.T.Ueno, N.Tsukimura, M.Yamada, T.Ogawa, *Enhanced bone-integration of alkali- and heat-treated nanopolymorphic titanium in micro-to-nanoscale hierarchy*, Biomaterials, 32 (2011), 7297-7308;

3.L.Zhao, Sh.Mei, P.K.Chu, Y.Zhang, Zh.Wu, *The influence of hierarchical hybrid micro/nano-textured titanium surface with titania nanotubes on osteoblast functions* , Biomaterials 31 (2010) 5072e5082;

4.G.K. Mor, O.K.Varghese, M. Paulose, N. Mukherjee, C.A. Grimes, *Fabrication of tapered, conical-shaped titania nanotubes*, J. Mater. Res., Vol.18, No11, Nov 2003, 2588-2593;

5.*Surface engineered surgical tools and medical devices*, J.Jackson; W.Ahmed, (Eds.), Springer, 2007, XXIV, 592p.;

6.Dikova Ts.D., *Influence of Technological Parameters on Titanium Nanotubes Formation*, Recourse Saving Technologies for Production and Pressure Shaping of Materials and Mchine Building, No1 (14) 2013, *p.150-160*, http://resource-saving.snu.edu.ua/PDF/E_COPY_2013/statti/dikova.pdf;

7.Kowalski D., Kim D., Schmuki P., *TiO_2 nanotubes, nanochannels and mesosponge: Self-organized formation and applications*, Nano Today (2013) 8, 235-264;

8.Park Tae-Eon, Choe Han-Cheol, Brantley W.A., *Bioactivity evaluation of porous TiO_2 surface formed on titanium in mixed electrolyte by spark anodization*, Surf. Coat. Tech. 235 (2013) 706-713;

9.Macdonald D.D., *On the formation of voids in anodic oxide films on aluminum*, J. Electrochem Soc. (1993), Vol 140, issue 3, L27-L30.

USER EVALUATIONS: APPLYING A COST-BENEFIT APPROACH TO HUMAN COMPUTER INTERACTIONS

Dr. Katz A.

Shamoon College of Engineering, Ashdod, Israel

adis@sce.ac.il

Abstract. *This study suggests a framework that analyzes individual preferences towards interactive systems by modeling users' evaluations of the cognitive costs and the benefits of using the systems. A graphical cost-benefit approach, which was originally applied in the area of system analysis and design to help decision-makers select computer systems for organizations, is applied in the area of human-computer interactions (HCI) to predict users' preferences of alternative application designs. We tie the HCI design methodology of personas to the cost-benefit model. Currently, we mainly propose the applicability of the original model into the field of HCI, and suggest a series of studies that will show that a user's preference can be predicted using the model. Initial results from a study on a backpack purchasing website already supports the relevance of the original model in HCI and indeed encourages further research to examine the model's applicability.*

KEYWORDS: HUMAN-COMPUTER INTERACTION, COST-BENEFIT, USER EVALUATIONS, PERSONAS.

1 Introduction

Cost and benefit considerations play an important role in many areas of our lives. A cost-benefit lens was previously used to explain different phenomena related to how people act in different tasks or contexts (e.g. [1], [2] and [3]). In this research we present a cost benefit approach to predict users' evaluations and preferences of interactive applications. We follow a previous cost-benefit approach that is applied in the area of systems analysis and design in the feasibility stage of selecting the optimal computer system among alternative proposals [4, 5]. While the original model refers to the costs of purchasing or developing a system for organizations in monetary terms, the current research is concerned with costs in terms of an individual's perceptions of the cognitive resources he or she needs to consume when using a system, such as effort and time spent. While the original model refers to the overall benefit of the system to the organization, which is derived from a list of relevant criteria (e.g. quality of the development team, reliability of the hardware, business processes and customer service improvements, etc.), the current research is concerned with the benefits that a user predicts he or she would achieve during or after using a system. The original model deals with organizational goals, but a system must fulfill also personal goals. Our framework takes the original model of cost-benefit considerations a step further from a macro-level (organizational) perspective to one that is micro-level (individual and cognitive).

Indeed, monetary costs are important when choosing among alternative systems, but we are more interested in user perceptions of the cognitive costs involved in using a system for a certain goal. Therefore, we consciously leave financial considerations out of the scope of this study; but of course we cannot ignore the fact that financial constrains can tip the balance and determine which system will be finally selected. Our scope is most relevant to situations in which system use is voluntary, such as choosing among different websites, different mobile applications or different versions of a system.

Every system action has costs and benefits that may be perceived differently depending on the user or the circumstances [6]. Users personal characteristics (traits), together with his or her current usage situation (state) such as motivation or current context, are important factors to affect the cost-benefit comparison process.

Previous theories have already studied the acceptance and use of technologies, and among them are the well-known TAM (technology acceptance model; [7]), and its extensions TAM3 [8] and UTAUT (unified theory of acceptance and use of technology; [9, 10]) models. While these models encompass a wide scope of vital antecedent determinants important for system acceptance, in this study we narrow our focus to looking at user preferences through a cost-benefit lens, and therefore we incorporate certain variables from these models that play an important role in users' cost and benefit considerations.

Using an application can lead to positive outcomes, such as reaching a high level of task performance or having a pleasant engagement with the application, but also can lead to less desirable outcomes, such as perceiving a high level of cognitive load, or spending a lot of time and effort on the expense of other tasks. It is reasonable to expect that users, if given a choice, would prefer applications with high benefits and low costs. Since many applications require the devotion of many user resources to reach

desirable outcomes, it is most interesting to know how much cost a user would invest to achieve a certain benefit, or in the terms of the original model, what is the weight distribution of costs and benefits [4, 5]. Previous studies had already looked at the impacts of cognitive costs and benefits on technology usage [6], [11]. While they measured cognitive effort as an objective variable (e.g. number of clicks or text entries), we measure costs and benefits in subjective terms since costs that may be perceived high by one individual may be perceived low by the other. The same can be said about benefits. In addition, the current context of use determines the user's momentary goals and motivations; affecting the cost that the user will be willing to invest to achieve them.

We integrate the well known user-centered design (UCD) method of personas, developed by Cooper [12], in the original cost-benefit model to show that the model is able to predict user preferences of systems or interactive modes. Since personas represent a cluster of users that share similar behaviors, attitudes, needs and desires, it is reasonable to believe that these characteristics and motivations affect their evaluations of the costs and the benefits of using a certain interactive computerized system.

2 Means for solving the problem

We intend to demonstrate the applicablility of the cost-benefit model is in the field of HCI by conducting a series of studies, and we are currently testing the model with different decision support systems (DSS) for product customization by online customers such as a backpack purchasing application, a cake purchasing application, and a trip planning application.

In each study, we design experimental prototypes that are different versions for a system or an application, varing in terms of cognitive costs (e.g. effort) and benefits (e.g. utility). We expose our participants to the different designs, and collect their evaluations by measuring the perceived costs and benefits of the different prototypes on Likert scales.

We classify participants to certain persona types, based on the relative importance they give to cost versus benefit (also derived from user's ratings on Likert scales).

For each participant, according to the original graphical cost-benefit technique [5] and based on his or her cost and benefit evaluations, we graphically draw graph lines for each application. As we explain below, we predict that the graphs will follow the same pattern at the individual user level, as the one at the organizational context level. We describe the process of creating the graphs in the following section.

3 Method

We are currently conducting a series of studies to test and to demonstrate the applicablility of the cost-benefit model is in the field of HCI, in the context of decision support systems (DSS) for product customization by online customers. In the current paper we describe and demonstrate our methodology using a backpack perchasing application.

In our initial study we used two backpack purchasing applications that represent decision support systems (DSS) for product customization by online customers. We designed the two applications so that they would differ in the levels of cognitive complexity (a cost factor) and utility (a benefit factor). Application 1, hereafter the "choose" app, proposes the user a list of 21 preset backpack designs, to choose among them and application 2, hereafter the "design" app, enables the user to design a backpack 'from scratch' by interacting graphically with objects such as colors, text, and images. The basic distinction between the applications was adopted from a previous study [13]. For the specific design we used print screens from an existing website of bag customization (http://www.makecustombags.com/).

In terms of cognitive costs, the difference between the choose and the design applications is in cognitive resources consumed: while the choose app is a system for purchasing a backpack in minimal time and effort, the design app is relatively more complex since it involves more actions (object manipulations) and is more time consuming. In terms of benefits, the choose app is relatively low on utility, since a user can only select a backpack from a limited predefined set of designs. On the other hand, the design app is a system of higher utility, which allows the user with means to experiment with various combinations of objects until he reaches a satisfactory customized (user "tailored") backpack design, therefore optimal to meet his specific aesthetic desires. Figure 1 presents print screens of the backpack applications.

Choose app	Design app

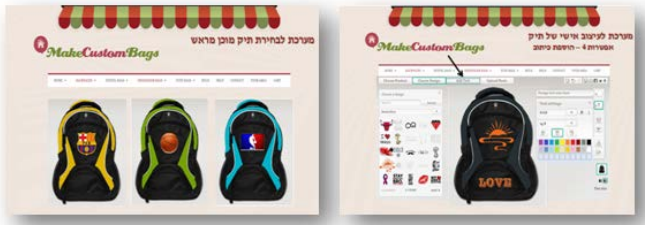


Fig. 1. The backpack purchasing applications

Following the original cost–benefit approach, the overall cost and benefit of each application can be calculated for each user according to his or her perceptions and then graphically presented on two vertical axes, one for the cost and the other for the benefit. In the original cost-benefit model, the cost values of the alternative computer systems are transformed onto a normalized-cost scale (using various transformation methods) to enable a comparison between two variables that are measured differently; costs are measured in monetary terms whereas the benefits are measured in subjective terms. However, this transformation is not required in the case of cost-benefit considerations of users that select a system among alternative designs, since perceived aspects that reflect cognitive costs can be measured on the same type of scales (e.g. Likert scales) as the perceived aspects that reflect benefits.

We exposed participants to each application, and afterwards we conducted a survey to capture their evaluations of the costs and the benefits. We follow the graph creation process of the original cost–benefit approach [4, 5], but made adjustments to HCI, to focus on user perceptions and interaction preferences of systems through a

cost-benefit lens. While in system analysis and design, the costs and the benefits of each alternative system are defined for a certain organization at the feasibility stage by IS experts (using different methods such as normalized-cost scales), we calculate the overall cost and the overall benefit of an application separately for each user by the average of his or her ratings on Likert scales that measure variables borrowed from TAM and its extensions (TAM3 and UTAUT) such as perceived ease of use and perceived usefulness (reflecting cost and benefit, respectively). We marked the overall cost and the overall benefit on the designated vertical axis and then we drew a connection line between the two marked values to graphically form a line for each alternative application. The horizontal axis is the weights scale that expresses the relative importance of costs and benefits, also derived from user's ratings on Likert scales

Using the personas method, we demonstrate how different types of users are positioned on the cost-benefit weight (relative importance) axis. When purchasing a backpack, some individuals are highly motivated to have the "perfect" backpack and would be willing to spend a lot of time and effort to create it, and on the other hand, others may be willing to settle for a "good enough" backpack, by investing a relatively small effort to have it. Accordingly, we designed two respectively personas, Dana and Ronen, who have personal characteristics and motivations that are relevant to the task of backpack purchasing. As presented in figure 2, for each user, each application can be positioned on a cost-benefit graph, according to its overall cost and overall benefit perceptions. Figure 2a demonstrates a possible graph predicted for a user represented by Dana that we expect to be positioned at any point on the weight axis to the right of the intersection with a preference to the design app. Figure 2b demonstrates a possible graph predicted for a user represented by Ronen, expected to be positioned at any point on the weight axis to the left of the intersection with a preference to the choose app.

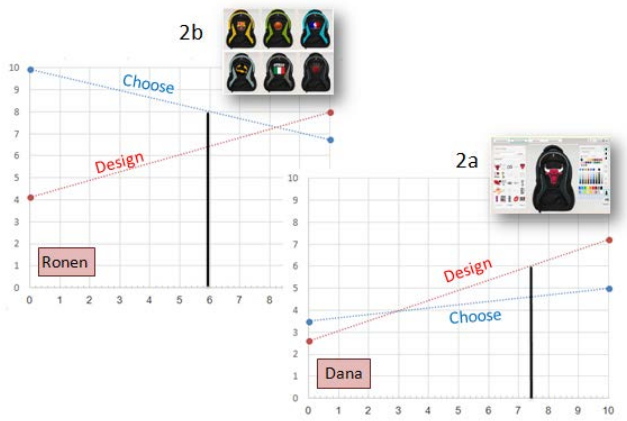


Fig. 2**.** Cost-benefit graphs for backpack applications including personas

2a example for the persona Dana; **2b** example for persona Ronen

As aforementioned, in each of our series of studies we expose participants to alternative applications and according to their ratings on the previously mentioned Likert scales we draw a cost-benefit graph for each user on the vertical axes. Using additional Likert scales that capture the relative importance of costs and benefits, we position each user on the horizontal weights axis. At the end of the survey, we also ask them to choose among the applications which one they prefer. We expect to receive graphs that are similar to the original cost–benefit approach, showing that users prefer applications that are designed to meet their needs and current motivations. In other words, and following the original cost-benefit model, we predict that the location of a participant user on the horizontal weight axis (cost-benefit relative importance) will be somewhere in the range where the maximum values on the vertical axis belongs to the exact application that he or she preferred. This will prove the model is suitable for the field of HCI.

4 Results and discussion

The backpack study was the first in a series of planned studies, which initially examined the feasibility of the cost-benefit model in HCI. Sixty 3rd and 4th year industrial engineering & management students from an academic engineering college in Israel participated in the study, as part of an HCI course; user computer interface design. There were 25 male and 35 female, with the average age of 26.

Table 1 summarizes the results, and shows that a significant majority of the participants had a preference to the design application. Also, results show, that female participants preferred the design application more than male.

Table 1**.** Backpack study results – application preferences

	Female	Male	Overall	
Design	31	13	44	73.3%
Choose	4	10	14	23.3%
Indifferent	0	2	2	3.33%
	35	25	60	

Our main objective was to test the feasibility of the cost-benefit model in HCI. In 47 cases, which are 78.3%, the graphs behaved as expected; in other words, the location of the majority of participations on the weight axis was somewhere in the range where the maximum values on the vertical axis belonged to the application that they preferred. This strongly supports our idea that the cost-benefit model can effectively predict which application would be preferred by a user, according to his characteristics, needs and current motives.

Though our initial results show that the cost-benefit model can be successfully adjusted to the area of HCI and applied to explain and predict user preferences of applications or choices between different versions of an application, a limitation of the current study is that the cost and benefit perceptions are based on non-interactive evaluations. While the backpack study involved simply presenting the applications to the participants using mockup prototypes, we plan to continue to empirically test the applicability of the cost-benefit model in the field of HCI in future studies that are designed to involve working prototypes and therefore will have users evaluating the systems after conducting certain tasks using them. These studies will test the model's applicability more precisely, since interactive user judgments of a system are based on more tangible and realistic experiences.

5 Conclusion

Understanding how users choose among systems is important theoretically and practically. In our series of experiments, the theoretical objective is to test whether the 'macro-level' cost-benefit approach for selecting alternative systems for organizations can be applied to the 'micro-level' of predicting individual users' acceptance of alternative applications. Modeling the cost-benefit considerations underlying user preferences can set a bridge between IS system acceptance models to HCI system acceptance models. Specifically, we intended to show that the relation between cost–benefit considerations and the user's traits and state, reflected in personas, can be presented graphically. Practically, the model can improve the prediction of user preferences with respect to certain personal characteristics and motives, which emphasize the relative importance given by the user to the cognitive costs during system use versus the perceived benefits of using it.

Acknowledgments. We wish to thank Lital Almugrabi and Gal Avioz for their contributions in designing the backpack application prototypes, and for all their help in conducting the backpack study.

6 References

1. Weick, K., Sutcliffe, K. H.: Managing the Unexpected: Assuring High Performance in an Age of Complexity. Jossey-Bass, San Francisco, CA. (2001)
2. Majchrzak, A., Malhotra, A., John, R.: Perceived Individual Collaboration Know-how Development through Information Technology-enabled Contextualization: Evidence from Distributed Teams, Information Systems Research. 16 (1), 9–27, (2005)
3. Katz, A., Te'eni, D.: The Contingent Impact of Contextualization on Computer-Mediated Collaboration, Organizational Science, 18, 261-279, (2007)
4. Shoval P., Lugasi Y.: Models for Computer System Evaluation and Selection, Information & Management, 12(3), 117-129, (1987)
5. Shoval P., Lugasi Y.: Computer-Systems Selection - the Graphical Cost-Benefit Approach, Information & Management, 15(3), 163-172, (1988)
6. Hui, B., Gustafson, S., Irani, P., Boutilier, C. The Need for an Interaction Cost Model. In Proc. of Advanced Visual Interfaces (AVI), pp. 145–148, (2008)
7. Davis, F. D.: Perceived Usefulness, Perceived Ease of Use and User Acceptance of Information Technology, MIS Quarterly, 13(3), 319-339, (1989)
8. Venkatesh, V., Morris, M. G., Davis, G. B., Davis, F. D.: User Acceptance of Information Technology: Toward a Unified View, MIS Quarterly, 27(3), 425–478, (2003)
9. Venkatesh, V., Bala, H.: Technology Acceptance Model 3 and a Research Agenda on Interventions, Decision Science, 39 (2), 273-315, (2008)
10. Venkatesh, V., Thong, J. Y. L., Xu, X,: Consumer Acceptance and Use of Information Technology: Extending the Unified Theory of Acceptance and Use of Technology, MIS Quarterly, 36 (1), 157–178, (2012)
11. Whitworth, B., Li, J.: Social Feedback and Social Bookmark Usage, in Proc. IADIS international conference ICT, Society and Human Beings Volume, 61-68, (2013)
12. Cooper, A.: The Inmates are Running the Asylum. Sams Publishing, Indianapolis, IN, (1999)
13. Kamis, A, Koufaris M, Stern T.: Using an Attribute-based Decision Support System for User-customized Products Online: an Experimental Investigation, MIS Quarterly, 32(1), 159-177, (2008)

PRODUCTION OF ALUMINA NANOPARTICLES (AL_2O_3) USING PULSED LASER ABLATION TECHNIQUE IN ETHANOL SOLUTION

Ph.D. Adel K. M.

Mechanical Engineering Department, College of Engineering, University of Diyala , Iraq

Email: adel_alkayali@yahoo.com

Abstract: *Pulsed Laser Ablation in Liquid (PLAL) has become an increasingly important technique for metals production and metal oxides nanoparticles (NPs). This technique has its many advantages compared with other conventional techniques (physical and chemical). This work was devoted for production of alumina (Al_2O_3) nanoparticles via PLAL technique from a solid alumina target immersed in ethanol at different values of laser fluences in order to study the effect of laser fluences on the optical properties and structure of Al_2O_3 nanoparticles. The controllability of particle size and size distribution is shown in this paper to be dependent upon laser fluences and it proved that the ablation at lower fluence led to the creation of smaller nanoparticles, smaller aggregates of nanoparticles, and a lower concentration of nanoparticles in contrast an increase of fluence leads to the formation of larger nanoparticles and most of these NPs were aggregated. The produces NPs were characterized by mean of many tests such as UV-visible (UV-Vis.), Atomic Force Microscope (AFM) and Scanning Electron Microscope (SEM).*

KEYWORDS: *ALUMINA NANOPARTICLES, PULSED LASER ABLATION TECHNIQUE, ETHANOL SOLUTION.*

1. INTRODUCTION

The properties and behavior of materials at nano levels differ greatly when compared to micro levels. Also these nanoparticles show great differences of their outstanding properties such as physical, chemical, optical and electronic properties from the bulk material of which they are made [1].

PLAL represents one of the most important, effective and simple technique for preparing metal, metal oxide nanoparticles. PLAL has many advantages compared with other conventional physical and chemical methods like purity, stability of the fabricated nanoparticle colloids, and do not require a vacuum chamber. It is the most flexible and promising technique because of its ability to control NPs size by optimizing the laser parameters, Also this technique provides the possibility of generating a large variety of NPs those are free of both surface-active substances and counter ions [2-4].

In general, the produced NPs through PLAL technique pass through three fundamental steps. Firstly plasma generates due to extreme heating during the interaction of laser with matter. Secondly the plasma, containing vapor of target atoms expands adiabatically, this leads to quick cooling of the plume region and hence to the formation of nanoparticles clusters. Finally after plasma extinguishing the formed nanoparticles clusters encounter and interact with the solvent and surfactant molecules in the surrounding solution, typically about a few microseconds, all these steps take place and nanoparticles are synthesized [5, 6].

Laser ablation in liquid media has been occurred either in nanosecond (ns) or femtosecond (fs) laser pulses. Femtosecond laser ablation (FLA) is one of the best methods to generate free nanoparticles with unique properties such narrower size distribution and with reduced porosity. FLA can be considered as isochoric process since the irradiation of laser pulse causes local heating in short time and it lasts before expansion of metal takes place [3].

Alumina or aluminum oxide one of important metal oxides has many interesting properties such as high hardness, high stability, high insulation, and transparency. Thus, because of these properties, it can be used in various applications e.g. fire retard, catalyst, insulator, surface coating, composite materials, thermal protections etc [7].

Many researchers direct their researches towards studying the effect of laser parameters on reducing particles sizes and collides stabilities. Co-workers later Tsuji have shown that the formation efficiencies and size of particles were changed with power of laser pulses. Recently, Sajti and co-workers found that laser ablation in water yields a greater material removal rate than in air [8].

In this work, alumina nanoparticles were produced by using pulsed laser ablation technique and study the effect of laser fluences on the size and size distribution of NPs in ethanol environment, size and morphology of the nanoparticles were investigated by AFM and SEM., their optical properties were examined by using UV-visible spectroscopy.

2. EXPERIMENTAL WORK

The experimental arrangement for the production of colloidal solution of nanoparticles by using pulsed laser ablation in aqueous media were carried out with a pulsed Ti/Sapphire laser beam (Quadronix IntenC laser) Kocaeli University - Laser Technologies Research and Application Center. The laser operates at 1 kHz repetition rate with a pulse width of ≤130 fs at 2.5 mJ/pulse maximum laser beam output.

Figure 1 shows the schematic diagram of PLAL experiment setup for synthesis colloidal solution of alumina NPs. The experiments of producing alumina NP were done at 90 min exposure time at 800 nm wavelength, 10 Hz pulse repetition rate and 130 fs pulse duration at different values of fluences. This laser beam is focused via a 100 mm focal length focusing lens to a minimum spot size at a solid alumina target (purity 99.99%). The alumina target was fixed by a fixture inside the flask and immersed at 10 mm depth in the solution inside the flask. A well designed and fabricated rotator mechanism used to rotate the flask in order to maintain continuous changing of the focused laser spot position at the target. A magnetic stirrer rotator was placed in the solution rotates at 600 r.p.m. to ensure uniform irradiation on target and the movement of solution that can enhance ablated particles diffusion also to disperse the produced NPs. Laser power was measured via a power meter type Newport 841-PE, the measurement was obtained at two locations very near to the final stage of the laser apparatus and before the focusing lens to evaluate the losses of the power in the beam delivery unit. Before starting the experiment the alumina target was cleaned by ultrasonic cleaning device type EMAG 50 HC then wiped with acetone and ethanol solvents. Ethanol was used as a wet environment. A number of tests were done to characterize the produced alumina NPs at different values of laser fluences, before doing the tests the sample was placed in the ultrasonic cleaner to ensure the homogeneity of the NPs solution. UV-visible extinction spectrum of the colloidal solutions was recorded using a spectrophotometer type Varian Cary-50 UV-Visible. NPs Size, morphology and distribution were examined by SEM imaging device type Tescan VEGA series and AFM test type AA3000 Scanning Probe Microscope is most popular model.

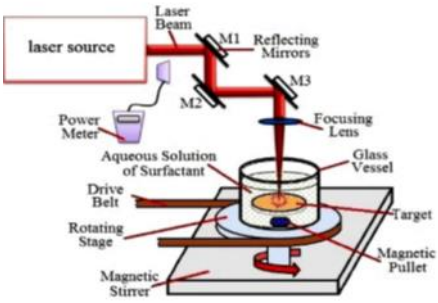


Fig.1 *Mapping Experimental set up of femtosecond laser ablation method [9].*

3. RESULTS AND DISCUSSION

Table 1 shows the effect of laser fluences and the effect of ablation medium on domain particle size and UV-Visible absorption peak wavelength(nm) in ethanol by using femtosecond laser (λ=800 nm mJ/pulse, τ =130 fs ,P.R.R =1KHz) for Al_2O_3 NPs.

Table 1 *Shows the effect of laser fluences and the effect of ablation medium on domian size and UV-Visible absorption peak wavelength(nm) by using femtosecond laser (λ=800 nm mJ/pulse, τ =130 fs ,P.R.R =1KHz) for Al2O3 NPs.*

Sample Code	Ablation medium	Fluences J/cm^2	Domain size of NPs	UV-Visible Absorption peak wave length (nm)
L1	Ethanol	0.83	80	213
L2	Ethanol	1.04	140	238

Laser fluence, plays an important role in ablated particle`s shape, size, structure, phase, and ablation efficiency, the laser ablation of the alumina rod was performed in Ethanol at two fluences 0.83 J/cm^2 and 1.04 J/cm^2 corresponding in samples L1 &L2. Ethanol provides a relatively inert environment for the production of nanoparticles. Nanoparticles produced from ablation of Al_2O_3 in ethanol are primarily alumina species. SEM analysis of the nanoparticles produced in ethanol showed a lack of aggregation as shown in Figure 2.

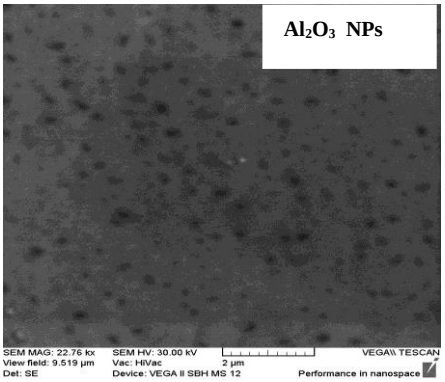


Fig. 2 *SEM image of nanoparticles formed from ablation of Al2O3 in Ethanol at 0.83J/cm^2 laser fluence.*

Figure 3 shows an AFM images of an area at a distance of ~ 500 nm from the edge of an ablated crater for samples L1& L2, It can be seen the average size and the shape of nanoparticles differ between these two samples.

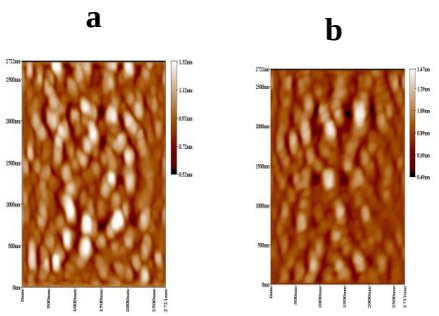


Fig. 3 *AFM images of Al_2O_3 NPs produced in water solution at a. 0.83 and b. 1.04 J/cm^2 laser fluences.*

Figure 4 shows a histogram of nanoparticles produced by ablation at 0.83 J/cm^2 and 1.04 J/cm^2 laser fluences in ethanol media. The histogram was normalized to represent the particles have a size ranging from 10-170 nm depending on the laser fluences. From figure 4 the dominant sizes of the particles obtained from 0.83 and 1.04 J/cm^2 is 80 and 140 nm, respectively. At 0.83 J /cm^2 of laser fluences offered the smallest dominant particle size, whereas that of the 1.04 J /cm^2 yielded the largest size.

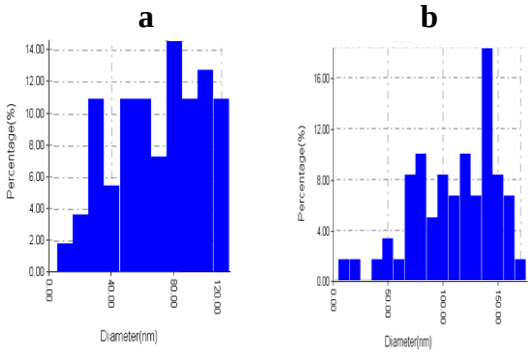


Fig. 4 *Histogram of nanoparticles formed by ablation Al_2O_3 in ethanol at: a. 0.83 and b. 1.04 J/cm2 laser fluences.*

During laser ablation of alumina in ethanol small bubbles can be observed in the solution and by increasing fluence results in more alumina being ejected from the rod, thus these bubbles created from ablation is larger. A larger bubble would have a larger volume for interaction, then allowing for longer times of nucleation and easy to form larger nanoparticle a superheated bubble expands until it reaches a critical volume, and after that collapses. The ablation event causes many bubbles to be ejected normal to the surface of the rod but the collapse is not proficient by all bubbles, as there are some that reach the surface. Based upon these results, the bubbles that survive to reach the surface contain a mixture of volatile gases such as H_2, CO, CO_2, as well as small hydrocarbon species. The gases are formed as a direct result of the high energy from the laser irradiation, which is sufficient to break the carbon-hydrogen bonds. During collapse, confined species are subjected to extremely high pressures, which may contribute to the formation of the nanoparticles. The collapse of the bubble also effectively binds solvent molecules to the nanoparticles.

These ethanol molecules form a shell which prevents the nanoparticle from undergoing further reaction. Therefore the solvent molecules surrounding the particles and serve to protect the formed nanoparticles from oxidation [10-12].

Also increasing fluence results in a shift in the size distribution to larger sizes. The shift is due to the presence of more particles at larger sizes, because too high laser fluences, may cause a coalescence or melt of the adjacent particles, which may be not suitable for some applications requiring individual particles. Nanoparticles greater than 100 nm were found at two fluence in this case; these nanoparticles have been excluded from the histogram and calculated averages to provide more accurate representation of the dominant species. The average size of samples L1 &L2 is about 85 nm &110 nm respectively.

Figure 5 shows the absorption spectra of alumina nanoparticles in Ethanol. The absorption spectra of the particles synthesized showed a strong absorption in the UV range with the maximum absorbance at around 213 nm in sample L1 and 238 nm in sample L2. As mentioned above the difference in the absorbance belongs to the difference in the concentration of nanoparticles in suspension thus the concentration of NPs in sample L1 more than NPs concentration in sample L2.

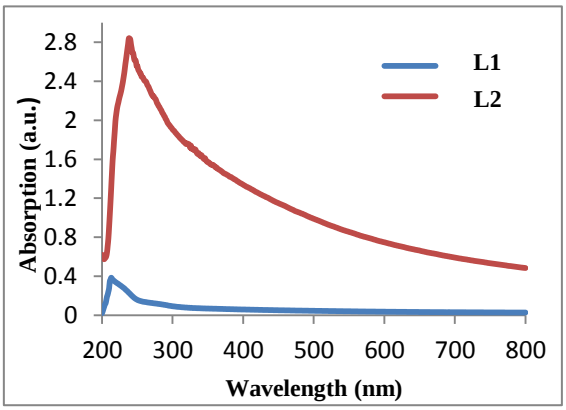


Fig. 5 *Shows the absorption spectra of Al_2O_3NPs in ethanol at two different fluences.*

4. Conclusions

In summary, the present research work has successfully demonstrated that alumina nanoparticles with a size of less than 100 nm can be easily produced via laser ablation in ethanol solution with less oxide cladding and different nanostructures formation at different values of laser fluences. The results indicate that lower laser flounces results in higher ablation efficiency and finer spherical nanoparticles in contrast an increase of fluence leads to the formation of larger nanoparticles and most of these NPs were aggregated. However, too high fluences may cause a coalescence or melt of the adjacent particles, which may be not suitable for some applications requiring individual particles and too low energy may have problems with a large fragment of alumina that did not ionized by the laser beam.

This convenient production strategy can be applied as a general approach that Al_2O_3 NPs have attracted significant interest of materials scientists and physicists due to their special properties and have attained a great importance in several technological applications such as industrial applications.

Acknowledgement

This work was supported by Kocaeli University - Laser Technologies Research and Application Center (LATARUM) in Turkey and Laser Institute for Postgraduate Studies, Baghdad University, Ministry of Higher Education and Science Research, Iraq.

References

[1]. Piriyawong V., V. Thongpool , P. Asanithi, P. Limsuwan, "Effect of Laser Pulse Energy on the Formation of Alumina Nanoparticles Synthesized by Laser Ablation in Water" , Surface Science Direct, 32, pp. 1107-1112, 2012.

[2]. Liu1 Z., Y Yuan, S Khan, A Abdolvand, DWhitehead, M Schmidt and L Li, "Generation of Metal-Oxide Nanoparticles using Continuous-Wave Fibre Laser Ablation in Liquid", Journal Micromech. Microeng., 19, pp. 1-7, 2009.

[3]. Krishna G. i, S. Hamad, S. Sreedhar, P. Tewari, S. Venugopal, "Fabrication and characterization of aluminum nanostructures and nanoparticles obtained using femtosecond ablation technique", Chemical Physics letters, 530, pp. 93–97, 2012.

[4]. Viau G., V. Collière, G.A. Shafeev, "Internal structure of nanoparticles of Al generated by laser ablation in liquid ethanol", Chemical Physics Letters, 501, pp. 419-422, 2011.

[5]. Baladi A., "Effect of laser wavelength and ablation time on pulsed laser ablation synthesis of Al nanoparticles in ethanol", International Journal of Modern Physics: Conference Series Vol. 5, pp. 58–65, 2012.

[6]. Arash B., Rasoul S., "Investigation of different liquid media and ablation times on pulsed laser ablation synthesis of aluminum nanoparticles", Applied Surface Science, 256, pp. 7559–7564, 2010.

[7]. Lukić, I · Krstić, J · Jovanović, D. Skala, "Alumina/silica supported K2CO3 as a catalyst for biodiesel synthesis from sunflower oil", Journal Bioresource Technology, 2009.

[8]. Al-Mamun S., Nakajima R., Zhu X., Ishigaki T., "Generation of alumina nanoparticles by a nanosecond laser-induced liquid plasma in water", Optics Express, 17, pp. 12650-12659, 2009.

[9]. Suha I. Alnassar, Adel K. M., Zainab F. M., "Study the Effect of Sodium Dodecyl Sulfate Surfactant Solution on the Production of Zirconia (ZrO2) Nanoparticles Synthesized by Laser Ablation Technique", Second International Conference on Advanced Manufacturing and Automation (INCAMA'13) 28th to 30th March, 2013.

[10]. Justin S.G., "Formation and characterization of nanoparticles via laser ablation solution", M.Sc. Thesis submitted to Pennsylvania State University, the Graduate School, Department of Chemistry, 2007.

[11]. Yavas O., A. Schilling, J. Bischof, J. Boneberg, P. Leiderer, "Bubble nucleation and pressure generation during laser cleaning of surfaces", Applied Physics/Materials Science and Processing, 64, pp. 331-339, 1997.

[12]. Schilling A., O. Yavas¸, J. Bischof, J. Boneberg, and P. Leiderera, "Absolute pressure measurements on a nanosecond time scale using surface plasmons", Applied Physical Letters 69, pp. 4159-4161, 1996.

COMPARISON BETWEEN PROJECT MANAGEMENT AND SOFTWARE PROJECT MANAGEMENT

M.Sc. Ivanova Milka

Faculty of Mechanical Engineering – Technical University of Sofia, Bulgaria

milkachr@tu-sofia.bg

Abstract: *Software project management encompasses the knowledge, techniques and tools necessary to manage the development of software products. Software project management remains different from project management in other more established fields for a number of reasons. Software is "brain product" only, unconstrained by the laws of physics or by the limits of manufacturing processes. In the report discusses topics that managers need to create a plan for software development using effective estimation of size and to execute the plan with attention to productivity and quality.*

In the report they have understand the concept of project management, software project management

Keywords: SOFTWARE, PROJECT MANAGEMENT, SOFTWARE PROJECT MANAGEMENT, PLANNING, ORGANIZING, MONITORING, ADJUSTING

Introduction

Small and fairly simple software projects need project management. What differs among the various software projects is in the degree of management efforts. A large and complex software project would require some sophisticated project management skills and considerable effort, along with tools to aid the management tasks. The key is to strike a balance between lean project management and excessive project management, never letting it become too meager or too overbearing.

Many software engineering confuse software project management with the software engineering process and development life cycle. Software project management follows a management process to ensure that the appropriate software engineering process is implemented, but it is not itself a software engineering process. Figure 1 depicts the high-level flow of a software project management process and the four major sets of activities (known as POMA) that are involved [2], [4]:

- Project **P**lanning,
- Project **O**rganizing,
- Project **M**onitoring
- Project **A**djusting.

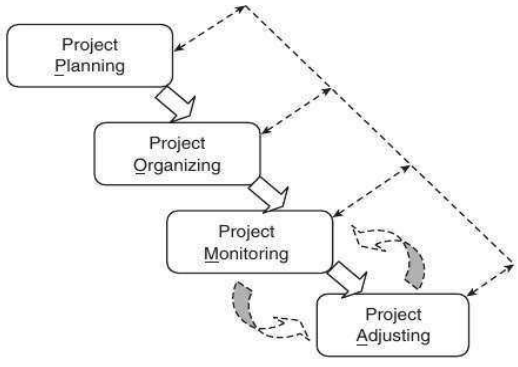


Figure 1 *Software project management process*

These four activities of POMA may sometimes overlap. Most of the major portions of the activities are performed in sequence, a flow depicted by the large arrows in the figure. Project management ensures that the following goals are met:

- The end results satisfy the customer's need;
- All the desired product/project attributes (quality, security, productivity, cost, etc.) are met;
- Target milestones are met along the way;
- Team members are operating effectively and with high morale;
- Required tools and other resources are available and effectively utilized.

It is important to remember that a project manager cannot do this alone but has to work through the team members to accomplish these management targets.

Planning

Planning is a natural first phase of any project. The success and failure of the project rides heavily on the results of proper planning. So many software projects tend to rush and minimize this phase citing schedule and cost constraints. Even with a well-planned project, it is not unusual to still see many changes and modifications. Some will use this reason to develop a poor plan or even totally skip planning. Having a well-conceived and documented plan, however, will help facilitate the anticipated modifications that often occur in a software project.

During the early planning phase, the answers to the following questions will contribute to the formulation of a project plan:

- What is the nature of the software project, who is sponsoring the project, and who are the users?
- What are the needed requirements and what are the desired requirements?
- What are the deliverables of the project?
- What are the constraints of the project (schedule, cost, etc.)?
- What are the known risks of the project?

Notice that these are very close to the same questions asked during the requirements gathering and analysis activities. Software engineering's requirements methodologies and process provide the directions on how to perform information gathering and analysis. Project management must ensure that there are qualified resources, proven methodology, and sample time set aside to perform the tasks related to answering these questions. Sometimes customers and users are asked to fund these activities separately; other times the software project organization will sponsor the activities as costs of doing business and fold them into the cost of the total project.

Sophisticated organizations realize the importance of this planning phase and are willing to pay for part of the activities.

Once the basic project requirements are understood, the rest of the project planning activities are much easier to perform and complete. The following activities are the major parts of project planning:

- Ensure that the requirements of the project are accurately understood and specified;
- Estimate the work effort, the schedule, and the needed resources/cost of the project;
- Define and establish measurable goals for the project;
- Determine the project resource allocations of people, process, tools, and facilities;
- Identify and analyze the project risks.

One of the most difficult tasks during this phase is defining realistic and measurable goals. We are used to making grand claims about software products-superior quality, easy to use, easy to maintain. We also like to claim that we have the most efficient and productive team members or most effective methodology. Unless these claims are well defined and measurable, they cannot serve as project goals because there will be no way of monitoring them. As happens in requirements gathering and analysis, a project manager will not be defining these goals alone. It usually is, and should be, a team effort. The success of a project is determined by whether the jointly planned and agreed to goals are achieved. Therefore, the project team members should all understand these goals and measurements. A goal or definition must be measurable so that as we are monitoring the project we can ascertain if the product will achieve the high quality expected.

This goal specification provides us with ways to measure the progress toward the final attainment of a goal. We сал quantitatively count the number of total functional requirements, the number of tested functional requirements, the number and severity of problems found during the test, and the number and severity of problems remaining at product release time. With these we can determine whether we have achieved the quality goal.

The goal of meeting project schedule should be stated with more than just a single date. It must be divided into multiple elements that can be measured along the way and the goals need to be quantitatively measurable and monitored throughout the project. Nonmeasurable goals are often said to be nonmanageable.

Another part of planning activities is the identification and analysis of risk items. There are very few projects with no risk. Software projects are fraught with cost overruns and schedule delays. Risk management thus becomes an integral part of software project management, and all risks must be considered during the planning phase. Risk management itself is composed of three major components: identification, p prioritization and mitigation

How do we identify risks? Some fertile areas to look for risks include new methodology, requirements new to the group, special skills and resource shortage, aggressive schedule, and tight funding. It is important to consider all possible items that might have a negative impact on the project Of course, such a list may be huge and impossible to work with, so it will be necessary to prioritize the risks and perhaps decide to consider and track only the high-priority problems. After a prioritized list of risks is agreed on, the planning process must include an activity set to mitigate these prioritized risks and to take some action. Hoping that some external force will magically appear and reduce the risks would be foolishly optimistic. A plan to mitigate these risks must thus be included during the project planning phase.

The activities in a project planning phase all contribute to developing an overall project plan. Depending on the projects, some project plans may be quick and short while others may be very extensive and lengthy. The content of a project plan [3] must include the following basic items:

- Brief description of the project requirements and deliverables;
- Set of project estimations:
  - ✓ Work effort
  - ✓ Needed resources
  - ✓ Schedule
- Set of project goals to be achieved;
- Set of assumptions and risks.

The plan may be expanded to include a discussion of the problems to be resolved, differentiating between those problems that must be fixed and those that it would be nice to fix. A user and customer profile may be included.

Although it is true that there will always be many unknowns during the planning stage, the more thorough the project planning phase is, the higher the chance that project will be successful. This does not mean that there will be no change to the project or to the plan. Even the best planned project will face some changes as the earlier unknowns become dearer. There will also be some justifiable change of heart as the project progresses. All project managers and project team members should be prepared for such changes.

Organizing

Once a project plan has been formulated or even before it has been completed, the organizing activities must be initiated. For example, as soon as we have the estimated resources planned, hiring and placement may begin. Table 1 shows how some of the planning and organizing activities may be paired and overlapped.

Table 1 Planning & Organizing Activities

Planning	Organizing
Project content & deliverables	
Project tasks & schedule	Set up tracking mechanisms of tasks and schedules
Project resources	Acquire, hire and prepare resources such as people, tools and processes
Project goals & measurement	Establish mechanism to measure and track the goals
Project risks	Establish mechanism to list, track and assign risk mitigation tasks

As soon as a specific planning activity such as risk planning is complete, we can establish the mechanism for tracking and mitigating the risks. The project manager does not need to wait for every planning activity to be finished before starting the organizing phase. The organizing phase requires more than broadband management skills.

Because software development and maintenance projects are more human intensive than most of the projects in other industries, it is vital that the project manager pay special attention to the personnel requirements and ensure that there is an organizational structure built in a timely manner and based on the project plan. Having a great plan and not being able to execute it due to a lack of, or a wrong grouping of, personnel is not always openly acknowledged because issues with people, organizations, and skill sets are often the most uncomfortable and emotional items to discuss.

During the organizing phase, other resources such as toots, education, and methodologies need to be scheduled, and preparations need to be made so that they are available at the correct time. Even though the plan may contain the appropriate financing for the resources, this is the phase when all problems related to procurement or financing of resources are rooted out and resolved.

In addition, all the mechanisms required for monitoring the project need to be defined and set up. In particular, the project goals that will be tracked during the monitoring phase need to be revisited, and all modifications to them should be made at this time.

Monitoring

After the project plan is set and organized, the project still cannot be expected to just coast to a successful completion by itself. No matter how thoroughly the plan is prepared and how carefully the project is organized, the process is never perfect. Inevitably, some part of what was planned and organized will face a change.

There are three main components involved in project monitoring:

- Collection of project information
- Analysis and evaluation of the collected data
- Presentation and communication of the information

The monitoring mechanism must collect relevant information pertaining to the project. The first question is what constitutes relevant information. At a minimum, the planned and stated project goals must be monitored. The second question is how the information will be collected. These two issues should have been addressed during the planning and the organizing phases. Data collection comes in two modes. Some data are gathered through regular and formal project review meetings. In these reviews, preestablished project information must be available and presented without exception. If any exception does occur, it should be viewed as a potential problem and will deserve at least a quick look by the project manager. Other data are collected through informal channels such as management walk around a process of informal socializing that should be a natural part of the manager's behavior. In today's global economy and distributed software development, the collection of data through indirect and informal channels is becoming increasingly difficult in spite of the advances in technology. Direct human contact is a costly proposition for geographically distributed organizations. As a result, many managers will cut on travel expenses and opt to spend on equipment or some other directly visible item. Software project managers need to be especially sensitive to this because the software industry is still a human-intensive business.

The information collected through the regular and formal project review meetings are analyzed in a variety of ways. Most project managers will attempt to perform the analysis themselves. In large and complex projects that involve several organizations and a long time frame, there may need to be a small staff group that performs the data analysis with established techniques such as the following:

- Data trend analysis and control charts
- Data correlation and regression analysis
- Moving averages and data smoothing
- General model building for both interpolating and extrapolating purposes

The collected and analyzed information must be communicated, reported, and acted upon. Otherwise, the entire monitoring process may be construed as nothing more than a superfluous bureaucratic exercise. Information reporting requires different presentation styles and awareness of the fact that the way some information is presented and visualized can certainly sway the receivers of the information. For example, we all love to see the revenue chart showing a curve that goes upward from left to right. The following are some of the more popular ways to visualize and report this information: Pie charts (to show proportion of different categories), Histogram (to show relative frequencies of different data value range in bar chart form), Pareto diagram (modified histogram – to show data in ascending or descending order), Time chart (to show the values of data trough time), Control chart (modified time chart – to show the values of data trough time in relationship to acceptable bounds) and Kiviat diagram (to show multiple metrics) [1].

Based on the monitored information, the project manager and the team would then collectively make decisions on whether the observations indicate a need for a change.

Adjusting

Making adjustments is a crucial step in project management because the chance that a project requires no change is very small. If the monitoring process indicates any need for adjustment, then the project management team must take timely actions. The areas that need change may be many and varied. However, the most likely instruments for adjustment that are available to the project management are the following:

- Resources
- Schedule
- Project content

The resources are directly under the control of the project management. For the most part, projects are usually in need of more resources. When more resources are added to the projects, the timing of such additions is very important. Adding human resources to rescue schedules may often result in the reverse effect. New employees may slow down the existing, experienced workers on the project because of the amount of time the experienced people would have to take away from their assigned work to explain and bring the new person on board. Introducing a new tool or a new process at the wrong time can produce the reverse effects of elongating the time and cost.

In contrast, there are times when resources are reduced. An example of human resource addition and reduction that often happens in a software project would be temporary testers who are brought on board to perform well-planned and scripted tests but are released after the testing has been completed. This is a planned increase and decrease of human resources. The more familiar cases are the nonplanned situations where a schedule crunch or an unexpected change in project content forces the project team to consider adjustments in resources. Assuming the schedule crunch means that the schedule must be maintained but other parameters may change and then adding resources is one possible solution and must be seriously considered. There are times when a crucial human resource may drop off from the project. Then the project management team must consider the possibilities of adjusting either the schedule or the project content or both. Doing nothing and just asking the remaining people to bear the brunt may only work once or only for a short period of time. For the most part, the project management team must consider some actions against the schedule or against the project content when there is a resource change.

Another scenario is that a schedule needs to be kept intact or even shortened but lost resources cannot be replaced or added quickly enough. That leaves only the option of a reduction of project content, Reducing project content late in the project cycle, much like adding human resources, is not trivial. A designed and coded functional area that has some level of coupling to other parts of the software cannot easily be taken out without careful consideration of the other interrelated areas. The time and effort spent in reducing the project content in order to keep or shorten a schedule may in fact create additional work and increase the schedule. In the event that more skilled resources can be added very quickly and in time, then that may be a better solution than reducing project content. There are times when customers flatly ask for a schedule reduction

due to increased competition, or when the upper management of a software development organization may request an earlier product release than planned due to unplanned external events. In such cases, a change in schedule will affect and most likely require adjustments to resources or to product content or both. Again, schedule changes are often unplanned and require that an appropriate adjustment is made quickly.

Often there are also changes in project content that occur after the project requirements are set and the project is organized to start. Inevitably, it is the customer or the user who asks for a change or an addition. Sometimes it is just human error or the result of seeing some prototype function and having a better understanding. We have already discussed possible effects of late reduction of the project contents. Additions or changes to project content are also time sensitive. In any case, most of the changes in project content would require an adjustment in either schedule or resources or both.

These three parameters - resources, schedule, and project content, are often the three key factors that project managers focus on during the monitoring and the adjusting phases. Changing one usually affects the other two. Notice that another familiar attribute in software engineering, software quality, has not been brought into the adjustment and trade-off discussion. This is because software quality level, once agreed upon, should be tracked but should rarely be an element offered in the adjustment and trade-offs of the software project. Software engineers and management should be extremely careful not to trade quality for schedule or for other parameters

Summary

We first introduced the four POMA phases of software project management: (1) planning, (2) organizing, (3} monitoring, and (4) adjusting. POMA is shown to be sequential at the macro level. However, the phases may overlap and may actually iterate among themselves, especially between the monitoring and adjustment phases. The complex and time-consuming planning phase is the key to project success. The monitoring phase is also important, and all projects must be monitored until the end. When necessary, the project manager must take actions and make the appropriate adjustments.

Project monitoring involves the ongoing comparison between what is planned and what is actual. Based on this observation, project managers would have to decide on whether any action, or adjustment, needs to be taken. Earned value management is introduced as a viable technique for monitoring the project effort and project schedule. This process essentially compares the planned or estimated project task efforts against those project task efforts that were actually expended. We have explained the need for setting goals and tracking the goals as part of project management, in order to accomplish those tasks, measurement is needed.

Literature:

1. Chank N. Mathematical Foundation, IEEE, 2012
2. Murray D., N. Sanford, Software Engineering Project Management, University of London, 2012
3. Sommerville I, Software Engineering, Pearson Edition, 2007
4. Tsui F., O. Karam, B. Bernal, Software Engineering, Jones & Bartlett Learning, 2010.

THERMOMECHANICAL STRENGTHENING AND STABILITY OF AUSTENITIC Cr18Ni10N STEEL

ТЕРМОМЕХАНИЧЕСКОЕ УПРОЧНЕНИЕ И СТАБИЛЬНОСТЬ АУСТЕНИТНОЙ СТАЛИ Х18АН10

D.Sc. Kaputkina L.M., D.Sc. Svyazhin A.G., D.Sc. Kaputkin D.E., PhD Smarygina I.V., PhD Kindop V.E.
National University of Science and Technology "MISIS", Moscow, Russia
E-mail: smarygina.inga@yandex.ru

Abstract: *The hardening and austenite stability as a result of nitrogen alloying steel type of Cr18Ni10 in the temperature range, which is usual for the application of such steels as corrosion-resistant structural heat-resistant and/or cryogenic ones was studied. It is shown that the nitrogen alloying is perspective for strengthening and increasing of stability of austenitic stainless steels. Additional strengthening due to the preliminary cold or warm deformation hardening increases a tendency to the martensite formation under load, which limits the operating temperature of these steels. High-strength non-magnetic nitrogen-alloyed steels on the base of Cr18Ni10 steels containing up to 0.22 % of nitrogen are suitable for cryogenic application of non-deformed articles only. Otherwise, a strain-induced martensite will always form in them at temperatures below -70 °C. High strength, ductility and toughness of these steels can be achieved simultaneously only as a result of the TRIP-effect or fine-grained structure formation.*

KEYWORDS: AUSTENITIC STEEL, CRYOGENIC STEEL, CORROSION RESISTANCE, HEAT RESISTANCE, ALLOYING BY NITROGEN, THERMAL STABILITY, THERMOMECHANICAL STRENGTHENING.

1. Introduction

Alloying by the nitrogen, using in the past years, is effective for stability, strength and corrosion resistance of austenitic steels [1–7].

Nitrogen-alloyed stable chrome-nickel and chrome-manganese austenitic steels often are strengthened by a cold plastic deformation and ageing.

The nitrogen reduces the temperature of the start of the martensite transformation during cooling, but it can increase the tendency to the formation of deformation-induced martensite due to the stack fault energy reducing.

The thermomechanical treatment is effective for nitrogen-containing austenitic steels and the range of controlled parameters for such steels can be extended.

Alloying steels with nitrogen increases resistance to local corrosion and intergranular corrosion [6, 7]. However, corrosion resistance sensitive to the structural state of steels, so when thermo-mechanical hardening of nitrogen-containing steels is also a need for a clear choice of regulated parameters of structures and more strict observance of technology of smelting and processing.

Thus, due to changes in the processes of structure formation with the adding to the steel even a small amount of nitrogen, it is necessary to strictly control the chemical composition, to adjust such parameters of thermal and thermomechanical treatment as temperature, degree of deformation, duration and conditions of subsequent cooling and aging, depending on the applications of the steel. In particular, it is necessary to take into account the specific temperature of formation and dissolution of nitrides, which can be estimated by thermodynamic calculations, for example, using phase diagrams. The change in the stability of austenite under and without loading can be evaluated only experimentally.

The aim of this work was to study both strengthening and stability of austenite resulted from the nitrogen alloying of Cr18Ni10-type steel in the temperature range usual for the application of such steels as structural corrosion-resistant heat-resistant and/or cryogenic.

2. Material and Experiment

Steels of Cr18Ni10-type with content of nitrogen varied from usual for contaminants (less than 0.01 %) to 0.22 % for specially alloyed by the nitrogen with application of traditional technologies of melt of corrosion-resistant chrome-nickel ones were studied. Chemical composition of steels is given in the Table 1.

Investigated steel were received and pre-processed in the following way. Steel 1 (Cr18Ni10Ti) was industrial melting and hot rolled.

Nitrogen-alloyed steels were produced in laboratory conditions using component of the charge of various purity by impurities. Steels 2 and 3 (Cr18Ni10N) were melted in the induction furnace from nitrogen-free steel of similar chemical composition with addition of pure charge components to the required composition. Steel 4 (Cr18Ni10N) was produced from pure materials: technical iron, electrolytic nickel, electrolytic manganese, pure chrome, nitrogenized ferrochrome, granulated aluminum in vacuum induction furnace. Ingots with the weight of 12.5 kg were forged in the temperature range 1160–820°C up to the general deformation of 80 % and cooled by air.

The final treatments were: 1) quenching on solid solution from the temperature of 1050 °C in the water or in the air; 2) high-temperature thermomechanical treatment, including hot multipass longitudinal rolling at the temperature 1070 °C with degrees of compression ε=35, 50 and 80 %, and the cooling from the temperature of rolling finish in the water or in the air.

The structure, phase composition and mechanical properties of steels after different schemes of heat and thermomechanical treatments, as well as their mechanical behavior in conditions of hot and warm deformation were studied.

Qualitative analysis of the microstructure was carried out using optical microscopy. Phase composition and the lattice period of austenite was studied using x-ray analysis.

Vickers hardness, mechanical properties (both tensile and impact bending tests) was is measured defined for all steels at room

Table 1. Chemical composition of investigated steels

No.	Steel	Chemical composition, wt. %								
		C	Cr	Ni	Mn	Mo	S	P	Al	N
1	Cr18Ni10Ti	0.10	17.7	9.5	1.19	0.10	0.007	0.027	0.11	<0.01
2	Cr18Ni10N (N=0.135 %)	0.05	18.0	10.3	1.04	–	0.015	0.023	0.10	0.135
3	Cr18Ni10N (N=0.186 %)	0.05	18.1	9.6	0.82	<0.10	0.018	0.025	0.12	0.186
4	Cr18Ni10N (impurity free, N=0.220 %)	0.007	19.1	9.3	1.42	0.012	0.004	0.002	0.035	0.220

* – base is Fe.

temperature (+20 °C), and for steel 4 (Cr18Ni10N) at the temperature -163 °C too. Samples in the initial state and after mechanical testing were studied for the presence of ferromagnetic phase using ferritometer.

3. Results and Discussion

All investigated steels are austenitic at the room temperature: they are non-magnetic and α-phases are not discovered using X-ray method. This fact consequents to their position on Shaeffler diagram (fig. 1).

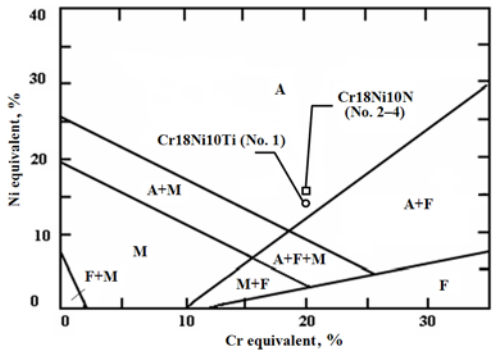


Fig. 1. *Positions of studied steels on Shaeffler diagram*

A formula taking into account only the actual chemical composition [8]:

$$M_S = 500 - 25(Ni + 0{,}8Cr + 1{,}2Mn - 8) - 12{,}5Mo - , \quad (1)$$
$$- 29{,}4Ti - 35Nb - 32{,}6Cu - 254(C + N)$$

evaluates the temperature of the martensite transformation (Table 2). Values M_S are in the range of +23 °C (steel 1 (Cr18Ni10Ti)) to -15 °C (steel 4 (Cr18Ni10N)).

Table 2. Evaluated temperatures M_S and M_{d30}

No.	Steel	M_S, °C	M_{d30}, °C
1	Cr18Ni10Ti	23	-1
2	Cr18Ni10N (N=0.135 %)	-14	-54
3	Cr18Ni10N (N=0.186 %)	-7	-66
4	Cr18Ni10N (impurity free, N=0.220 %)	-15	-71

Fig. 2 presents polythermal section of phase diagram for alloys with the content of alloying elements corresponding to steels (Table 1), and the nitrogen content from 0 to 1 %. The diagram was built by the Thermo-Calc program on the basis of the thermodynamic database TCFE6. It is seen that the temperatures of hot processing and heating for quenching correspond to the austenitic region. So, after the complete dissolution of excess phases neither δ-ferrite nor martensite in the studied steels should not be.

Mechanical properties of the studied steels are given in Table 3. Hardness values in all the investigated steels are similar and typical for austenitic steels.

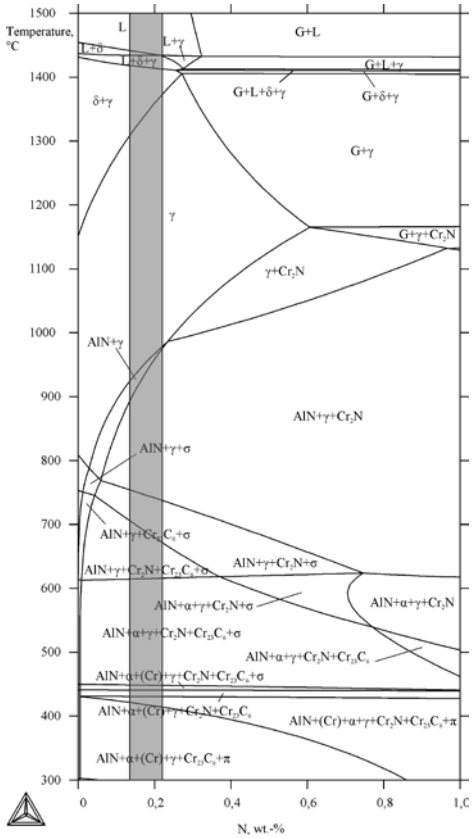


Fig. 2. *Phase diagram for steels Cr18Ni10N (steels 2, 3, and 4)*

When the tensile tests at 20 °C all nitrogen-containing steels discovered a behavior typical for austenitic ones as a stable high-plastic materials. Deformation curves are smooth, without a serration, except steel 4 (Cr18Ni10N). The deformation pattern of this steel demonstrated high plasticity and hardly noticeable aliasing (with a small amount of peaks) in the deformation range of 30–40 %. After the test samples of this steel were poor magnetic (Table 4). That is connected with formation of a small number of deformation-induced martensite (α-martensite). Other steels in the field of uniform deformation and after tensile up to failure at room temperature remained non-magnetic. After the tensile test at -163 °C the steel 4 (Cr18Ni10N) was strongly magnetic (see table 4), suggesting a relatively large part of the α-martensite.

The strength of steels increases according to the nitrogen content in steels 1–4 (Table 3), and the resistance to the small plastic deformation YS increases more actively. Characteristics of strength at the temperature -163 °C are, naturally, higher than at room temperature.

Evaluation of the tendency to formation of deformation-induced martensite is carried out through the M_{d30} temperature at which 50 % of martensite formed under the influence of 30 %

Table 3. Mechanical properties of the investigated steels

No.	Steel	Processing	T_{test}, °C	HV, MPa	UTS, MPa	YS, MPa	El_U/El*, %	RA, %	KCU (KCV), MJ/m^2
1	Cr18Ni10Ti	hardening, air	+20	210	515	230	47	51	(2.2)
		HTMT 80 %, air	+20	310	700	440	26	54	(0.9)
2	Cr18Ni10N (N=0.135 %)	hardening, water	+20	255	530	315	29	63	(2.2)
		HTMT 50 %, water	+20	260	670	370	42	71	(1.9)
3	Cr18Ni10N (N=0.186 %)	hardening, water	+20	240	715	355	25	67	(1.7)
		HTMT 50 %, water	+20	255	690	345	27	74	(1.3)
4	Cr18Ni10N (impurity free, N=0.220 %)	HTMT 35 %, water	+20	240	750	400	63/44	84	3.9
			-163	–	1065	645	39/31	78	2.5

* – El_U – uniform elongation, El – total elongation.

Table 4. Assessments of stability of austenite at mechanical tests of steel 4 (Cr18Ni10N)

T_{test}, °C	Tensile test			Tests for impact bend		
	El_U*, %	magnetization during the uniform deformation	magnetization in the neck	magnetization away from the area of destruction	magnetization in the field of fracture	mass part of austenite**, %
+20	44	poor magnetic	poor magnetic	non-magnetic	non-magnetic	100
-163	31	strongly magnetic	strongly magnetic	weakly magnetic	medium magnetic	96

* – designation corresponds to table 3; ** – the part of austenite in the non-deformed samples was measured by x-ray analysis

deformation, according to the equation of T. Gladman, J. Hammond, F. Marsh [9]:

$$M_{d30} = 497 - 462(C+N) - 9{,}2Si - 8{,}1Mn - 13{,}7Cr - 20Ni - 18{,}5Mo \quad (2)$$

This equation, in general, reflect the influence of the composition of the steel (see table 2) after final processing for solid solution. Real data may be different, because here, as in the evaluation of M_S points, also not taken into account any differences in the structural state of the steels or conditions of deformation. M_S of steels can be decreased by grinding the grain down to 10 microns in preprocessing. This preprocessing don't significantly effect on M_{d30} [10].

All steel under tension at room temperature have high characteristics of plasticity: El is from 26 to 63 %; reduction of area RA is from 51 to 84 % (see Table 3). The clean steel 4 (Cr18Ni10N) with the highest content of nitrogen among the steels demonstrate higher plasticity, minimal stability during deformation and the highest strength. It is possible to note that quite high plasticity of the steel at temperature -163 °C El=39 %, RA=78 % is resulted from the TRIP-effect.

On the diagrams of deformation during testing at the temperature -163 °C of steel 4 (Cr18Ni10N) appeared aliasing was also found under strain over 10 %.

Intensive formation of deformation-induced martensite in nitrogen-containing steels of the Cr18Ni10N-type leads to their strong deformation hardening and retaining high plasticity provides high level of relations UTS/YS.

Tests at room and low temperatures showed good reproducibility of results and a very small spread of absolute values of all characteristics of strength and plasticity, which reflects the stability of the mechanical behavior of all investigated steels.

The results of impact tests showed naturally high values and for steels with nitrogen at room temperature: $KCU_{+20°C}$=1,7–3,9 MJ/m^2; maximum value of impact strength is for steel 4 (Cr18Ni10N).

The impact strength at the test temperature -163 °C for steel 4 (Cr18Ni10N) is also quite high: 2.5 MJ/m^2. In the area of plastic deformation and fracture of this steel 4 (Cr18Ni10N) α-martensite was found: alloy became magnetic near the zone of destruction (see Table 4). This suggests that even at such high speed of loading (~10 m/s) quite big plastic deformation takes place due to the the TRIP-effect.

The final structure and properties of strongly hot-deformed austenite are the only determined by the conditions of hot deformation and cooling cycle in thermo-mechanical processing.

The warm deformation of austenitic steels was carried out at the temperature of maximum effect of aging – 410 °C. The maximal hardening thus achieved when processing scheme was hot deformation → warm deformation. So the warm deformation of steel 2 (Cr18Ni10N) at 410 °C by the compression up the true reduction e = 0,08 with the speed of 0.01 s^{-1} in vacuum after the hot compression at temperature 1050°C up e=0.27 with the speed of 1 s^{-1} and rapid cooling to of 410 °C leads to additional strengthening on near 170 MPa. Resistance to deformation at e=0.08 (close to the steady-state stage) reached 436 MPa.

Patterns of warm deformation have normal view, explicit serration not revealed. The average value of austenitic grain during warm deformation does not change. Resistance to warm deformation is defined by both a composition of steel and hot-deformed structure of austenite, i.e. it depends from the modes hot deformation of each steel. The addition of nitrogen significantly increases the resistance to the small (YS) and large (UTS) degrees of warm deformation. The small grain increases the effect of increasing the resistance to large deformations.

All steel remained austenitic after cooling to room temperature. Their hardness noticeably increased. For example, for steel 2 (Cr18Ni10N) it increased up to 260 HV compared to 245 HV for hot-deformed and 200 HV for the non-deformed state.

4. Conclusion

Alloying of austenitic stainless steels, used as heat-resistant and cryogenic, by nitrogen is perspective for strengthening and increasing of stability.

Both strength and thermal stability of austenite increase with increasing of the nitrogen content. Additional strengthening due to the preliminary cold or warm hammering, usually used for austenitic steels, increases the tendency to the formation of martensite under load, especially near and below M_S. This effect limits the working temperature of these steels.

High strength non-magnetic nitrogen-containing Cr18Ni10N-based steels with the nitrogen concentration not more then 0.22 % are applicable as cryogenic for non-deforming products. Otherwise, the deformation-induced martensite will form at temperatures below -70 °C. High strength, ductility and toughness (especially in the case of the raised cleanliness of detrimental impurities) for these steels can be achieved only through the TRIP-effect or grain refining.

5. References

1. Solntsev, Y.P. Cold-resistant steels and alloys. St. Petersburg, Khimizdat, 2005, 480 p. (in Russian)
2. Solntsev, Y.P., B.S. Ermakov, O.I. Sleptsov. Materials for low temperature and cryogenic: Encyclopedic reference, St. Petersburg, Khimizdat, 2008, 768 p. (in Russian)
3. Chymosin, F.F. Stainless steel. Moscow, Metallurgy, 1967, 800 p. (in Russian)
4. Svyazhin, A.G., L.M. Kaputkina, V.G. Prokoshkina, Effect of nitrogen on structure and properties of thermomechanically strengthened steels. – In: Proceed. 10th Int. Conf. on High Nitrogen Steels, Moscow, MISiS, 2009, pp. 77–82.
5. Svyazhin, A.G., J. Siwka, L.M. Kaputkina, High-nitrogen steels – The current state and development trends. – In: Proceed. Int. Conf. Advanced Steels, China, Beijing, Metallurgical Industry Press, 2010, pp. 352–356.
6. Speidel, M.O., H.J. Speidel, Commercial low-nickel and high nitrogen steels. – In: Proceed. 10th Int. Conf. on High Nitrogen Steels, Moscow, MISiS, 2009, pp. 121–128.
7. Mushnikova, S.Yu., Yu.L. Legostaev, A.A. Harkov and other. An investigation on the influence of nitrogen on austenitic steel pitting resistance. – Issues of material science, 2 (38), 2004, pp. 126–135. (in Russian)
8. Birman, S.R. Economically alloyed maraging steel. Moscow, Metallurgy, 1974, 208 p. (in Russian)
9. Pickering, F.B. Physical Metallurgy and the Design of Steels. London, Applied Science Publisher Ltd., 1978, 104 p.
10. Matsuoka, Y., T. Iwasaki, N. Nakada and other. Effect of grain size on thermal and mechanical stability of austenite in metastable austenitic stainless steel. – ISIJ International, 53 (7), 2013, pp. 1224–1230.

The work was done in the framework of project № 11.1943.2014 to the competitive part of the state job institutions, subordinate to the Ministry of education and science, in the field of scientific activities in 2014–2016.

IN-SITU STRESS-STRAIN TESTING OF STEELS IN CO_2-CONTAINING SALINE SOLUTIONS

Prof. Dr.-Ing. Pfennig A.[1], Trenner S.[1], Wolf M. [1], Bork C.-P. [2]
HTW University of Applied Sciences - Berlin, Germany[1]
BAM Federal Institute for Materials Research and Testing - Berlin, Germany[2]

anja.pfennig@htw-berlin.de

Abstract: *In CCS environment (carbon capture and storage) pipes and in geothermal power plants the materials used in pumps are loaded cyclically and exposed constantly to the highly corrosive hot thermal water. The lifetime reduction of AISI630 (X5CrNiCuNb16-4, 1.4542) is demonstrated in in-situ-laboratory experiments (T=60 °C, geothermal brine: Stuttgart Aquifer flow rate: 9 l/h, CO2). S-N plots, micrographic-, phase-, fractographic- and surface analysis were applied to obtain sustainable information on the corrosion fatigue behavior.*

Keywords: CORROSION FATIGUE, HIGH CYCLE FATIGUE, STEEL, CCS, CO_2-STORAGE, GEOTHERMAL ENERGY

1. Introduction

Materials in geothermal power plants are loaded cyclically under pressure and exposed constantly to the highly corrosive hot thermal water (up to ca. 200 °C, ca. 100 bar, ca. 20 % salinity of the geothermal water) where fluid properties may differ strongly [1]. This leads to corrosion fatigue and thus inevitably to the reduction of the lifetime of these components. The influence of frequency, temperature and chloride concentration on the corrosion fatigue behaviour is very well known in literature [2]. In general corrosion processes with or without applied mechanical stress are enhanced, especially in steels with low chromium content [3], with the presence of chloride [4], hydrogen sulfide (H_2S) [5] and CO2 [6]. The endurance limit [7] will decrease with increasing temperature, increasing mechanical load and decreasing pH for high alloyed steels. But increasing chromium content of steels as well as internal compressive stress in surface regions will increase the endurance limit [8].

This work was carried out to assess the influence of corrosive media on the mechanical behaviour of stainless steels such as AISI630 (X5CrNiCuNb16-4, 1.4542) in geothermal energy production.

2. Corrosion Chamber for Corrosion Fatigue Testing

The objective was to simulate in-situ conditions (temperature up to 100 °C, corrosive environment) of a material exposed to dynamic mechanical stress and corrosive gas- saturated saline aquifer environment, such as components in geothermal power plant. Highlight is the corrosion chamber fixed directly onto the sample leaving the resonant testing machine unaffected (figure 1). During mechanical stress-strain tests a magnetically driven gear pump (3) constantly pumps the corrosive media from the reservoir (4) to the corrosion-and temperature-resistant corrosion chamber (1) surrounding the test specimen (2). Heating is realized by two independent heating elements (5,6). The ratio of sample surface to volume of the corrosive media after DIN 50905 Part 1 (10 ml/cm²) is greater than required. The connecting of the chamber onto the specimen via clamping collar creates a force-fit process ensuring enough force to the corrosion chamber at high frequencies to keep it firmly on the test specimen (figure 2). The corrosion chamber is sealed in the area of restraint over 0-rings made of Viton. In order not to impede the change in length occurring during the experiment, the corrosion chamber has a membrane as a motion-compensating element.

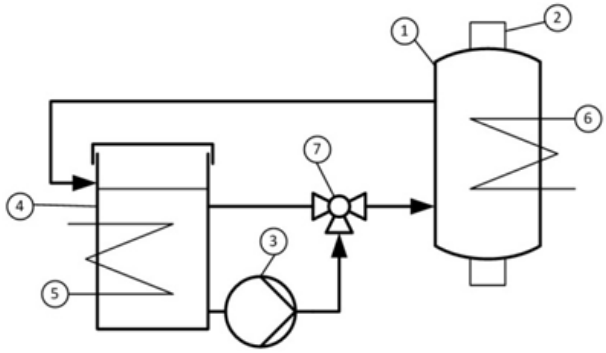


Figure 1: *Schematic set-up of operating corrosion chamber for in-situ corrosion fatigue testing*



Figure 2: *Experimental set-up: corrosion chamber applied to resonance testing machine*

The corrosion chamber is also equipped with measurement technique to gain electrochemical data during the mechanical tests. For measurement of the electrochemical potential a sensor (figure 2) is placed in the chamber. The sensor which is used is a silver-silver chloride electrode. Because of its method of construction this electrode is shock resistant and hence optimized for use inside the corrosion chamber under cyclically load. The silver wire (position 1) is fixed in a channel made of Teflon (position 2).



Figure 3: *Silver-silver chloride sensor optimized for the* corrosion chamber

3. Dynamic in-situ corrosion experiments at ambient pressure (HCF)

The corrosion fatigue strength of stainless steel with 16% chromium (1.4542, hardened and tempered with martensitic microstructure, surface roughness Rz=4) is examined in dynamic stress-strain tests (R=-1, ~30 Hz) in CO_2-saturated aquifer (Stuttgart Aquifer [9]) at 60 °C. Without corrosive environment the fatigue strength of the material (theoretically an infinite number of load cycles without failure) is and has a relatively smooth slope. The decrease of the fatigue limit line of 1.4542 samples with increasing number of cycles (Wöhler-exponent of k = 3,59) is much larger in corrosive environment than in air (tensile strength in air: 1078 MPa, largest number of cycles in corrosive environment (0,6 x 10^7 at 200 MPa). As for 1.4034 [9] no typical fatigue strength of 1.4542 exists as shown in a log-log plot (figure 4). The coefficient of correlation r2 = 0.33 from the regression is so small that doubt on the hypothesis of a (linear) relationship of the considered variables exist. In addition, the scattering range TN = 1:34,4 is disproportionately large.

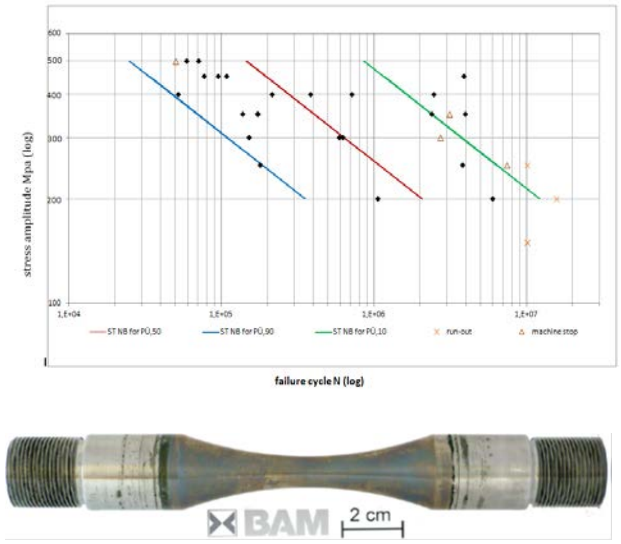


Figure 5: S-N-curve, corrosion chamber, sample and fracture surface 1.4542 exposed to flowing saline aquifer [10] and CO_2.

Generally multiple cracks are found throughout the entire sample area and not only within the sample area that is mechanically loaded highest. Once the crack opens he crack-flank surfaces corrode continuously during cyclic load (figure 5). Crack propagation is then perpendicular to the direction of load. Localized corrosion (pits: 0.1 mm deep and 0.2 mm diameter) is accompanied with cracks, but not necessarily identified as the cause of crack initiation and failure under mechanical load.



Figure 4: *Sample Surface after Testing.*

4. Conclusion

- A highly flexible corrosion chamber allowing for electrochemical testing, O2-partial pressure or gas partial pressure measurement was designed to support stress-strain loaded corrosion fatigue experiments by enabling an in-situ corrosive environment which may be used up to 100 °C at ambient pressure.
- The corrosion fatigue behaviour of AISI630 (X5CrNiCuNb16-4, 1.4542) is described by statistical crack initiation but characteristic crack propagation and fracture surfaces for one stress amplitude. A typical fatigue strength of the S-N-curve does not exist under CCS corrosive conditions. The fatigue strength of the material in non-corrosive conditions of under cyclic rotation of 620 MPa is reduced significantly due to corrosion. Note, that cyclic rotation does not accurately compare to compression-tension testing and that reference measurements are due in future experiments.

5. Acknowledgement

This work was supported by the FNK (Fachkonferenz für wissenschaftlichliche Nachwuchskräfte) of the Applied University of Berlin, HTW and by IMPACT (EU-Project EFRE 20072013 2/21).

7. Literature

[1] L.B. Giese et al: Geochemie der Formationsfluide der Bohrung E Groß Schönebeck 3/90, STR02/14, Geothermie Report 02-1 (2001) 145 - 169

[2] J.P. Thomas and R.P. Wei, Corrosion fatigue crack growth of steels in aqueous solutions I: Experimental results and modeling the effects of frequency and temperature, Material Science and Engineering, A159 (1992) 205-221

[3] L.J. Mu, W.Z. Zhao, Investigation on carbon dioxide corrosion behavior of HP13Cr110 stainless steel in simulated stratum water, Corrosion Science 52 (2010) 82-89

[4] Ya.B. Unigovski, G. Lothongkum, E.M Gutman, D. Alush, R. Cohen, Low-cycle fatigue behaviour of 316L-type stainless stell in chloride solutions, Corrosion Science 51 (2009) 3014-3120

[5] C.M. Holtam, D.P.Baxter, I.A. Ashcroft, R.C.Thomsen, Effect of crack depth on fatigue crack growth rates for a C-Mn pipeline steel in a sour environment, International Journal of Fatigue 32 (2010) 288-296

[6] I. Thorbjörnsson, Corrosion fatigue testing of eight different steels in an Icelandic geothermal environment, Materials and Design Vol.16 No. 2 (1995) 97-102

[7] E. Roeder, H.-J.Bassler, M.Huber und J. Vollmar, Schwingungsrisskorrosionsverhalten des austenitischen Stahles X6CrNiMoTi 17 12 2 in 3%iger NaCl-Lösung unter Umlaufbiegebelastung, Werkstoffe und Korrosion 43 (1992) 426-431

[8] R. Ebara, Corrosion fatigue crack initiation behaviour of stainless steels, Procedia Engineering 2 (2010) 1297-1306

[9] A. Pfennig, R. Wiegand, M. Wolf, C.-P. Bork, Corrosion and corrosion fatigue of AISI 420C (X46Cr13) at 60 °C in CO2-saturated artificial geothermal brine, Corrosion Science 68 (2013) 134–143

[10] A. Förster, B. Norden, K. Zinck-Jørgensen, P. Frykman, J. Kulenkampff, E. Spangenberg, J. Erzinger, M. Zimmer, J. Kopp, G. Borm, C. Juhlin, C. Cosma, S. Hurter, 2006, Baseline characterization of the CO2SINK geological storage site at Ketzin, Germany: Environmental Geosciences, V. 13, No. 3 (September 2006), pp. 145-161.

ROBUST BI-CRITERIA APPROACH TO OPTIMIZE THE COMPOSITION AND PROPERTIES OF TITANIUM ALLOY

Nikolay Tontchev Yordan Kalev
University of Transport – Sofia, tontchev@vtu.bg

Abstract: *The numerical experiment has proved the ability to improve the quality of titanium alloys. Mathematical models suitable for forecasting and optimization have been derived. The approach of Taguchi applied has lead to a desired result, to separate variables Xi for the examined parameters that do not influence significantly on the final result. With this limit, the numerical optimization for maximum search has been conducted with each chemical composition. That allows improving it.*

Keywords: METALLURGICAL DESIGN, TENSILE PROPERTIES, COMPOSITION-PROCESSING-PROPERTY CORRELATION, OPTIMIZATION OF THE COMPOSITION

1. Introduction

Titan and its alloys was originally intended for use in military and defense industry, but over time they are becoming more common in peaceful areas – the economy, civil aviation, medicine and marine studies, sports and automotive industry. [1]

Thanks to the development of large lean production titan became more accessible and cost-effective material. Its high performance coupled with modern technological and industrial advances have opened vast opportunities for use in transport machinebuilding.

Very small quantities of the concentration of alloying elements and their combinations may result in significant changes in the physical and mechanical properties of the alloys. This fact determines the need to seek the most appropriate for the specific concentrations of alloying elements. Probably the most famous center for research in the field of modeling and regression analysis of super-alloys is the one in the University of Cambridge UK [2-4]

The traditional alloy-development strategy consists of producing numerous samples with varying composition and set of the elements, the processing mode included, to define an alloy with optimal properties [5].

The approach resulted in high costs of experimentation [6].

This is the reason that the methods of directed search and the 'trial and error' method reside the lowest level in the hierarchy of methods.

An alternative effective approach is to use data from past experience worked to a statistical model – based on a large amount of data associated by composition, processing and properties.

This research is part of series of approaches and methodologies that at the stage of generating the decision do not use the knowledge gained in the field of metallurgy. The proposal has the potential to predict the mechanical properties of alloys, like in [7], using prior information of data linking composition, processing and properties. The cited monograph explores the iron-based alloys, thus confirming the thesis for evaluation of these alloys numerically and experimentally. This methodology is the way to design alloys at a predetermined database.

Not only does each element strengthen alloys through more than one mechanism, but sometimes two or three elements can combine together to influence the strength.

In addition, the realization of strengthening effects of these elements strongly relies on the processing conditions.

2. Formulation of the problem

The ambition consists in building an approach and validation techniques to determine the trade-offs in meeting specific requirements are the properties of titanium alloys. For these specific properties there are indicated the possible combinations of alloying elements for different types of heat treatment. Regression and neural models are designed for the properties and optimization is performed for the composition and the processing parameters for a large database with more than 300 monitorings of different titanium alloys.

The creation of mathematical models to analyze the objects of metallurgical process under examination is an important stage. These models contribute to improve the set of properties and the final product quality. It is confirmed that it is possible to meet the requirements of the current market by implementation of such models. The wide range of problems, which Taguchi method has been applied to, is shown in [7].

The core of Taguchi approach consists of the method for reducing the influence of factors called noise (disturbing) that impair the quality parameters of the product/process. It is where the radical difference from the traditional technique of quality, which provides identification of existing sources and conduction of measurements that are often costly due to their control. The parametric design of Taguchi ensures non-sensitivity to noise along the way to the proper selection of certain parameters called controllable factors.

The aim of this paper is to present a robust approach for determining the influence of alloying elements on the properties of iron-based alloys that ensures better results than the input ones used to obtain a mathematical model.

The statistical analysis presented in this article is based on of data collected during the real production process described in [8]

The ranges of change of the used alloying elements of ferrous alloys are listed in Table 1.

Input parameters – Alloyng components		**Al [%]**	**Mo [%]**	**Sn [%]**	**Zr [%]**	**Cr [%]**	**Fe [%]**	**V [%]**	**Si [%]**	**O [%]**
min		0,00	0,00	0,00	0,00	0,00	0,15	0,00	0,00	0,05
max		8,00	15,00	11,00	11,00	11,00	5,00	15,00	0,50	0,25
mean		4,13	3,11	1,46	1,92	1,24	0,49	3,29	0,03	0,12
St. Dev.		2,14	4,25	2,08	2,54	2,77	0,75	4,62	0,08	0,02
Number of data pairs containing this element at output parameters	**Rp_{02}**	277								
	E	252								

Table 1 *Minimum and maximum values of alloying components*

Heat treatment

№	Heat treatment
1.	Without heat treatment
2.	Annealing (β)
3.	Annealing (α + β)
4.	Annealing (α)
5.	Solution treatment (β)
6.	Solution treatment (α + β)
7.	Solution treatment
8.	(β) + ageing
9.	Solution treatment
10.	(α + β) + ageing
11.	Duplex annealing

Table 2*. Heat treatments used in the database*

3. General description of the approach

The analysis presented in this paper is related to the analysis of mechanical properties of titanium specimens described by the following parameters: yield strength, *Rp02* [MPa] and relative elongation E [%]. The limitations connected with these parameters are due to Ti alloys grade characteristics and customer's specifications. However, the main problem is that these parameters cannot be under direct observation during the manufacturing process, so any limitations associated with them cannot be clearly defined in the optimization model. That means that we must develop models linking the final mechanical properties of the specimen/sample of the alloys chemical composition as well as the parameters of the production process.

The regression analysis allows describing the relation between the variables of input and output, without going into the phenomenon nature during the process.

The regression models presented below have been created based on the data collected during the industrial production process.

The statistical analysis described in this section is based on a data set of 300 records extracted from the whole database.

The Least Squares method, LS is used to estimate the regression parameters. The estimated models of parameters Rp_{02} , E obtained in the examinations are given below.

In respect to the problem under examination, nonlinear regression dependencies have been identified for each of the mechanical properties of titanium alloys. The regression dependencies are of the following kind:

$$f_i(x) = b_{00}^i + \sum_{j=1}^{10} b_{j0}^i x_j + \sum_{j=1}^{10} b_{jj}^i x_j^2 + \sum_{j=1}^{10} \sum_{l=j+1}^{10} b_{jl} x_j x_l$$

Here b_{ij} are the regression model parameters. The coefficients in equations are defined in Table 2. The models can be used for prediction if the check-up $F > F(0.5, \nu_1, \nu_2)$ described in details has been made. .

No	Coef	Rp_{02} [MPa]		No	Coef	Rp_{02} [MPa]	
1	C_0	396.2381	20.93544	**36**	$X_4 X_5$	9.379346	-0.01963
2	X_1	-32.0791	1.38401	**37**	$X_4 X_6$	15.51388	-0.37177
3	X_2	112.122	-7.84864	**38**	$X_4 X_7$	-10.5601	0.331122
4	X_3	78.1541	-0.16339	**39**	$X_4 X_8$	-16.6893	1.854779
5	X_4	130.7104	10.20102	**40**	$X_4 X_9$	-2.24882	-0.20250
6	X_5	-68.973	-6.45484	**41**	$X_4 X_{10}$	-48.3878	-2.56518
7	X_6	-730.192	21.26902	**42**	$X_5 X_6$	-2587.76	2.647485
8	X_7	-298.681	21.50194	**43**	$X_5 X_7$	44.56953	-0.80710
9	X_8	-3.12209	5.387568	**44**	$X_5 X_8$	-82.9475	-0.31884
10	X_9	-198.672	-31.7729	**45**	$X_5 X_9$	-6.13139	0.313483
11	X_{10}	-54.3129	2.672808	**46**	$X_5 X_{10}$	745.7955	-4.73098
13	$X_1 X_2$	-4.43718	-0.01702	**47**	$X_6 X_7$	-8.27673	-0.77459
14	$X_1 X_3$	-1.97432	-0.09657	**48**	$X_6 X_8$	263.0571	-9.12352
15	$X_1 X_5$	3.394209	-0.09768	**49**	$X_6 X_9$	-1.48548	-0.09670
16	$X_1 X_6$	7.171607	-0.03038	**50**	$X_6 X_{10}$	833.1564	-14.9056
17	$X_1 X_7$	2.889379	-0.17456	**51**	$X_7 X_8$	-87.6232	2.552293
18	$X_1 X_8$	9.00349	-0.19287	**52**	$X_7 X_9$	-16.70463	-0.32755
19	$X_1 X_9$	-1.1397	-0.05656	**53**	$X_7 X_{10}$	990.25321	-34.7130
20	$X_1 X_{10}$	-160.918	1.594115	**54**	$X_8 X_9$	-223.4617	2.604354
21	$X_2 X_3$	20.43437	0.487606	**55**	$X_8 X_{10}$	0	0
22	$X_2 X_4$	20.43437	0.487606	**56**	$X_9 X_{10}$	-585.6379	-0.988713
23	$X_2 X_5$	28.43656	-1.36517	**57**	X_1^2	84.742546	-3.812744
24	$X_2 X_6$	-18.7498	1.221792	**58**	X_2^2	6.993687	-0.133356
25	$X_2 X_7$	57.55664	-2.47272	**59**	X_3^2	-13.60908	0.8324983
26	$X_2 X_8$	21.12227	-0.48067	**60**	X_4^2	-6.65281	0.0710407
27	$X_2 X_9$	4.359865	-0.31536	**61**	X_5^2	-.168734	-0.20634
28	$X_2 X_{10}$	-164.874	14.12199	**62**	X_6^2	6.283372	0.0988364
29	$X_3 X_4$	443.6655	-0.54792	**63**	X_7^2	38.88832	-0.777694
30	$X_3 X_5$	-3.52382	-0.35718	**64**	X_8^2	71.03410	-6.386223
31	$X_3 X_6$	14.67915	0.115228	**65**	X_9^2	13.38640	-0.417462
32	$X_3 X_7$	48.49843	-0.50207	**66**	X_{10}^2	-549.354	-48.96597
33	$X_3 X_8$	78.61216	0.752812	**R**		0.7071	0.7312
34	$X_3 X_9$	-16.0990	-0.30255	**F cal**		3.246	3.467
35	$X_3 X_{10}$	366.2553	2.326692	**F tabl**		1.37	1.37

Table 2 *Coefficients of regression models of the examined target parameters*

By Taguchi methodology (Khosrow Dehnad, 1989) an experiment modeled on orthogonal matrices developed by him is carried out. The experiment can be accomplished in two ways by:

- a real experiment leading to obtaining results for processing;
- a numerical experiment with the presence of adequate regression models.

The availability of the described model coefficients, which can be used to predict, give a possibility to make a numerical experiment involving Taguchi method. The noise matrix is selected from orthogonal matrix I (27,13) with 27 rows and 13 columns developed by Taguchi [7]. The matrix is worked out with factors at three levels.

Specifically for the data of the experiment, eight of columns are used since the regression models are obtained on the basis of eight variables. In the matrix X_1 corresponds to parameter heat treatment, X_2 corresponds to aluminum , X_3 corresponds to molybdenum, X_4 corresponds to tin, X_5 - corresponds to zirconium, X_6 corresponds to chromium, X_7 corresponds to iron, X_8 corresponds to vanadium, X_9 corresponds to silicon and X_{10} corresponds to oxygen.

The methodology proposed is implemented for yield strength Rp_{02} and relative elongation E. To take out the models of these two target functions, 277 measurements that form the data matrix Rp_{02} (277, 10 +1), and - E (252, 10+1) have been used. Here the added column "1" is for the output target function Rp_{02} or E stored compactly in the matrix.

To optimize the computing process, the scheme, which having been processed for the particular case takes the following kind, is selected.

In numerical experiments that use models based on the chemical composition the noise can be expressed only in the change of the respective components. It is assumed to express noise Δ in the following way $\Delta_i = \frac{\overline{x}_i}{k}$ where further calculations are made for k equal to 100.

Here $\overline{x}_i$ is the mean value of relevant variable "i".

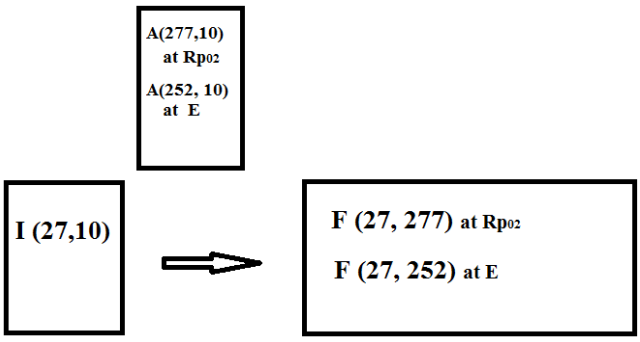


Fig. 1. *Organizing experiments with parametric planning with matrices I, A and F*

For level "1" of I (27,10) noise is subtracted from relevant x_i taking the value of $x_i - \Delta_i$. With level "2" no correction is applied, the value of x_i is preserved. With level "3" noise is added to relevant x_i taking the value of $x_i + \Delta_i$. In numerical experiments where models based on chemical composition are used, noise can be expressed only in the change of the respective components.

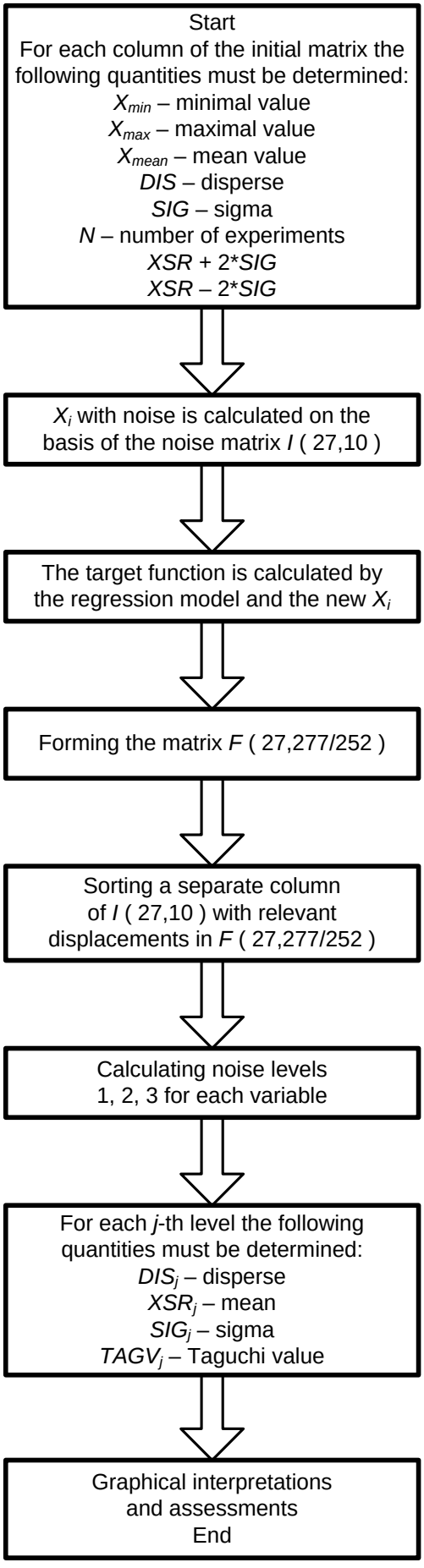


Fig. 2 *Computational algorithm*

Noise Δ is assumed to be expressed as follows $\Delta_i = \frac{\overline{x}_i}{k}$, where the further calculations are made for k equal to 100. Here $\overline{x}_i$ is the average value of the respective variable "i". In level "1" I (27,10) noise is subtracted from respective x_i taking the value of $x_i - \Delta_i$. In level "2" no correction is applied, the value of x_i is preserved. In level "3" noise is added to respective x_i taking the value of $x_i + \Delta_i$.

Thus, noise is expressed in the change of chemical composition. The calculation process is organized as follows:

A row of matrix I (27,10) is taken (for example, row 1 - I (1,10)). In this row level "1" is assigned for each x_i, i.e. noise will be taken out from each value x_i.

Thus F (1,1) of the matrix F (27,277) at Rp_{02} (F(27, 252) at E) is obtained from the first row of A (277,10). The same rule is applied to the rest of the series F (277,10) /F (252,10)/ and it forms F (27,277) /F (27,252)/.

It is continued with the next row of matrix I (27,10) performing the following sequence. Each row of matrix I (27,10) forms a relevant row of matrix F (27,277) /F (27,252)/.

Calculations are performed according to the following algorithm.

If we take the first column of matrix I (27,10) relevant to X_1, it is seen that the first nine rows correspond to level "1" of noise, the second nine lines correspond to level "2" and the third nine rows correspond to level "3" of noise. This makes possible to use the values of the first nine rows of matrix F (27,277) / F (27,252) / to calculate level "1", to use the second nine rows to calculate level of "2" and the third nine rows for calculation at level "3" for X_1. For other columns from 2 to 10 it is necessary to sort in ascending order Xi from I (27,10). After sorting the column obtains the kind of the first column. If changes are made with sorting, they are reflected also in matrix F (27,277) / F (27,252) /– fig.1.

After sorting of the respective variable, calculations for different levels can be made. It is continued with the next matrix row I (27,10) performing the following sequence. Each row of matrix I (27,8) forms a corresponding row of matrix F (27,277) / F (27,252) /. If we take the first column of matrix I (27,10) corresponding to the X_1 , it is seen that the first nine rows correspond to noise level "1" of noise, the second nine rows correspond to level "2" and the third nine rows correspond to noise level "3". That allows using the values of the first nine rows of matrix F (27,277) /F (27,252) / to calculate level "1", the second nine rows to calculate level "2" and the third nine rows to calculate level "3" for X_1. For the rest columns from 2 to 10 it is necessary to sort by ascending order of Xi of I(27,10). After sorting the column takes the kind of the first column. With sorting, if shifts are made, they are reflected in matrix F (27,277) /F (27,252)/. After sorting the corresponding variable it is possible to make calculations for different levels.

Variable	Input parameters	Noise level	
		R_{p02}	E
X_1	№ HT	1	2
X_2	Al	1	1
X_3	Mo	1	1
X_4	Sn	2	3
X_5	Zr	3	1
X_6	Cr	1	1
X_7	Fe	3	2
X_8	V	1	3
X_9	Si	3	3
X_{10}	O	3	1

Table 3 *Levels of noise factors for the research parameters*

After the analysis of assessments of the respective graphics for yield strength (R_{p02}) and relative elongation (E), the generalization of the solution is shown in Table3.

The conclusion that can be made on the boundary of yield strength R_{p02} based on the results in the table is that tin do not significantly affect the ultimate outcome within the range of variation examined. Zirconium, iron, silicon and oxygen influence significantly on R_{p02} as it is expected that these elements will change in direction to increase of their values. Aluminum, chromium, molybdenum, vanadium in direction to decrease of their values.

4. Search of optimal composition

As the experiment is numerical, it is possible to perform numerical optimization with the mathematical models obtained as the values of X_i are remained to change within the limits defined by the output data (Table 3).

From the performed Taguchi analysis (presented as a summary in Table 3) for the research quantity Rp 02 it is evident that the maximum of X4 (Zr) occurs at level 2; this means that X4 (Zr) must be maintained at a constant level. It is clear from the output data described in Table 1 that this parameter takes values in the range $0 \le X4 \le 11.0$.

Different methods for numerical optimization are described in [9]. The simplex method of Nelder and Mead with a deformable polyhedron has been selected for the purpose. It is a method of direct searching extremes, so it is suitable for the case of ravine surface of the target function.

After fixing X4 in the cited range optimization is applied to the rest of the parameters with in the range from Table 1. The values of the optimized parameters are shown in Table. 4. An increase in X4 leads to increasing the extremum value for Rp 02.

For elongation E the performed Taguchi analysis suggested fixing two variables X1 and X7.

Three cases were formed:

-Parameter X1 takes values in the range $1 \le X_1 \le 8$ as X_7 remains constant with a value of 0.15;

-Parameter X1 takes values in the range $1 \le X_1 \le 8$ as X_7 remains constant with a value of 2;

-Parameter X1 takes values in the range $1 \le X_1 \le 8$ as X_7 remains constant with a value of 1.

After optimization with the method of Nelder and Mead for various combinations of X_1 and X_7 it was clear that the increase of X1 leads to an increase of the extremum of E for each of the three cases. The obtained values are bigger than the biggest quantity in the output data in three cases.

This circumstance guarantees an improvement of these indicators.

An interesting result is obtained if model Rp 02 is calculated for the extrema values of E in the cases with fixed X_1 and X_7 – Table 4.

Parameters		Rp_{02}	
X_1	X_7	calculated F	F max data
1	0.15	868.8	945
0	1.0	2451.3	945
0	2.0	2627.5	945

Table 4. Optimal *parameters*

This indicates that there is a case where an increase in E leads to an increase of Rp 02 and this leads to the requirement for implementing an improvement of both of these criteria simultaneously, which proved that the task is feasible and executed..

Conclusion

The numerical experiment has proved the ability to improve the quality of Ti alloys of a certain class. Mathematical models suitable for forecasting and optimization have been derived. The approach of Taguchi applied has lead to a desired result, to separate variables Xi for the examined parameters that do not influence significantly on the final result. With this limit, the numerical optimization for maximum search has been conducted with each chemical composition. That allows improving it. Relative elongation A turned to be less variable index and yield strength Rp_{02} requires caution with extreme selecting. The decision of bi-criteria problem set has been defined thus proving that the Taguchi approach is applicable to a similar class of problems.

References

1. **Listopad, D.A**., World titanium market and its prospects / Listopad, D.A., V.P. Ivashchenko, I.F. Chervonyi // Theory and practice of metallurgy, 2010, № 5-6, pp. 16-21

2. **Bhadeshia H.K.D.H**., “Neural networks in materials science”, ISIJ International, 39 (1999), 966-979.

3. **Fujii, MacKay, D. J. C. and Bhadeshia, H. K. D. H.**, "Bayesian neural Network Analysis of Fatigue Crack Growth Rate in Nickel-Base Superalloys”, ISIJ International, Vol. 36, 1996, pp. 1373-1382.

4. **Jones, J. , MacKay, D. J. C.**, "Neural Network Modeling of the Mechanical Properties of Nickel Base Superalloys", 8th Int. Symposium on Superalloys, Seven Springs, PA, eds. R. D. Kissinger et al., published by TMS, 1996, pp. 417-424.

5. **Campbell C.E., G.B. Olson**, “System design of high performance stainless steels I, Conceptual and computational design”, Journal of Computer-Aided Materials Design 2001, 7:145-17

6. **Vitos L., P.A. Korzhavyi and B. Johansson**, "Stainless steel optimization from quantum mechanical calculations", Nature Materials 2003, 2:25-28

7. **Tontchev N**. Materials Science, Effective solutions and Technological variants, 2014/3/3, LAMBERT Academic Publishing

8. **Malinov, S, Sha, McKeown, J.J.**: Modelling and Correlation between Processing Parameters and Properties of Titanium Alloys using Artificial Neural Network. Computational Material Science 21, 375--394 (2001)

9. **Vuchkov, I., & Stoyanov, S.** (1980). Mathematical modeling and optimization of process units. Sofia: Engineering, (In Bulgarian).

ANALYSIS OF THE APPROACHES FOR IMPROVEMENT OF THE ENERGY EFFICIENCY OF ELECTRIC RESISTANCE FURNACES

АНАЛИЗ ПОДХОДОВ ДЛЯ УЛУЧШЕНИЯ ЭНЕРГЕТИЧЕСКОЙ ЭФФЕКТИВНОСТИ ЭЛЕКТРИЧЕСКИХ ПЕЧЕЙ СОПРОТИВЛЕНИЯ

Assoc. Prof. eng. Ph.D Borislav Dimitrov [1], Asisst. Prof. eng. Ognyan Zhekov [2], Electrcal Engeneering Faculti [1], Mechanical Engeneering Faculti [2], Technical University of Varna, Bulgaria

Abstraks: *Chamber electric resistance furnaces (CRF), used for performing of various heating processes, are powerful consumers of electric power. During their operation, different deviations from the original construction may appear and defects, such as: defects in the insulation and the gaskets, deformations of the body, and others. They result in increased thermal flow, running from the chamber to the ambience, increased thermal losses and, as a whole, increased electric power losses. This problem is of special concern in view of current energy efficiency criteria and its solution is sought in the following directions: analysis of the energy efficiency of the furnaces at the stage of their design; analysis of the reconstruction and repair works due to worn-out equipment, consisting in replacement of thermal insulation in order to decrease the losses.*

KEYWORDS: CHAMBER ELECTRIC RESISTANCE FURNACES, THERMAL LOSSES, ELECTRIC POWER LOSSES, ANALYSIS OF THE ENERGY EFFICIENCY, DECREASE THE LOSSES, IMPROVEMENT OF THE ENERGY EFFICIENCY.

1. Introduction

The analysis of the options for improvement of the energy efficiency of industrial chamber electric resistance furnaces (CRF) was carried out in two directions:

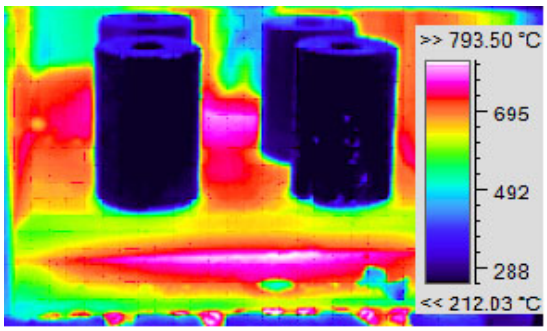
- *Design of new CRF*. The established methods for designing [1] are graph-analytical, based on criterial dependencies (Bi, Fo, Sk etc.). With them, table or graphical dependencies are used, which makes them hard to use and insufficiently precise. Moreover, the end result is directed towards obtaining mass-geometrical characteristics of the furnace and determining the required materials. With these methods, there is no information about the running thermal processes, the distribution of thermal energy in the insulation and in the charge being treated, the distribution of thermal flows, etc. This indicates that design methodologies need certain modifications in direction of applying mathematical modeling methods at the stage of designing. Although this approach is also widely used, its application in direction of energy efficiency analysis should be discussed in more details.
- *Reconstruction of worn-out CRF*. The issue of increasing energy efficiency by repair works is also of current concern. The defects occurring in the process of thermal equipment operation result in increased losses and decreased efficiency, respectively.

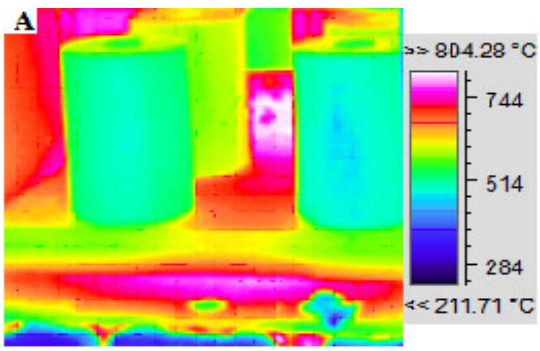
The purpose of this study is to analyze the opportunities for energy efficiency assessment and improvement at both stages: designing of new facilities and reconstruction of ones already in operation.

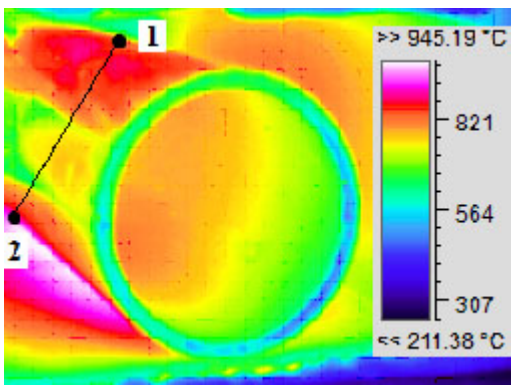
The analysis is based on specific examples for application of mathematical modeling and simulation in order to carry out energy analysis of the equipment and assessment of the energy efficiency at the design stage. Experimental studies are presented, conducted with furnace equipment, identifying the need for repair works. A description is given of the procedure to follow when carrying out repair works and the efficiency is assessed.

2. Analisis

Mathematical modeling of CRF makes it possible to determine the distribution of temperature in the working space and in the insulation as well as the distribution of thermal flows. The latter are divided into a summary thermal flow of losses and a useful flow, directed towards the charge being treated. Fig.1 shows the experimental results obtained by help of thermo chamber: (A) start and end of a heating process realized through positioning of heated details in a heated furnace; (B) distribution of the temperature along the surface of a pipe; (C) a sample transitional process achieved by computational procedure.







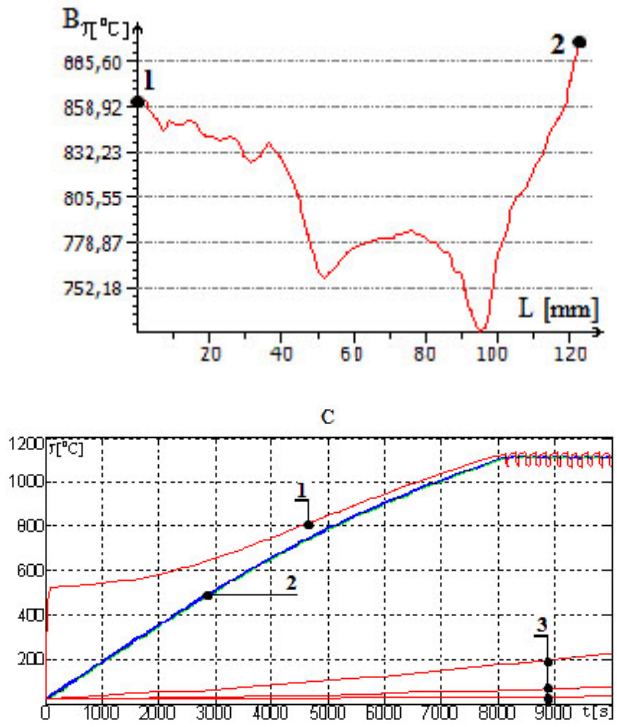


***Fig.1**. Thermal equipment. A: distribution of the temperature while details are heated – start and end of the heating process; B: distribution of the temperature along the surface of the heated pipe and along the diameter 1-2; C: sample transitional process of heating: 1 – heater; 2 – heated detail; 3 – temperature in the insulation of the furnace.*

The studies presented here show that the temperature in the working space is not uniform during the transitional process; it depends on a number of factors: construction of the furnace; condition of the insulation during operation; regulation of the heating process through the furnace controls; thermal characteristics of the heated details, etc. This shows that these factors must be accounted for as early as at the design stage by use of modeling, where the goal is to achieve a uniform temperature field with minimal losses.

A modification of the design methodologies requires introduction of a software realization of mathematical modeling for assessment of the CRF energy efficiency in relation to the technological mode [2,3,4,6]. Depending on the mode, it is possible, through simulation based on a mathematical model, to obtain optimal (towards an accepted criterion) mode parameters of the process. In order to specify the total quantity of thermal energy, lost during the transitional process, it is necessary to calculate, through the simulation procedure, the thermal flows and the respective powers. It is on that basis that the efficiency factor is determined for a specific mode under specific conditions. The efficiency factor serves as a criterion when designing a new furnace and also on assessing the efficiency performance of an existing facility.

The quantity of heat $Q_{ak,i}$ stored in the thermal insulation is determined by the attained transitional temperature τ_i depending on the duration of the process [1,5]:

$$Q_{ak,i} = c_i . m_i . (\tau_i - \tau_{o,c}) \qquad (1)$$

Where: $c_i.,m_i$ - characteristics of the medium, specific thermal capacity or mass, respectively; $\tau_{o,c}$ - ambient temperature;

The equation of the useful quantity of heat is of identical structure (1); it registers the thermal characteristics of the heated detail and its temperature τ_i. The installed electric power capacity P_{in} is different depending on the mode, but it is assumed to be independent of the temperature, and the power is calculated accordingly:

$$Q_{el} = P_{in} . \sum_{i=1}^{n} \Delta t_{w,i} \qquad (2)$$

The efficiency factor η is obtained as dependent of the mode, or the duration of the process, respectively:

$$\eta = \frac{Q_{el} - Q_z}{Q_{el}} = 1 - \frac{Q_z}{Q_{el}} \qquad (3)$$

The main point in the modification of the methodology consists in affording the opportunity to analyze the distribution of thermal energy in the individual elements of the *furnace & heated charge* system. This enables accounting for the energy characteristics of an electrothermal unit as early as at the design stage.

Fig.2 (A) graph 1 presents the efficiency factor as starting from the maximum and decreasing along with the temperature being established. The start of the process is shown in graph 2(A). In the same figure (B), graphs 5,6 show the accumulated energy in one of the walls, in the two layers of CRF, whereas graphs 1,2,3,4 show the accumulated energy in the surface layer, the second, third and the center of the body, respectively. The energy analysis is presented graphically (C) by graph 2: total losses, obtained from the sum of graph 3: losses to the ambient medium and graph 4: losses in the walls. The total power (graph 1) is the sum of the total losses and the energy in the body (graph 5).

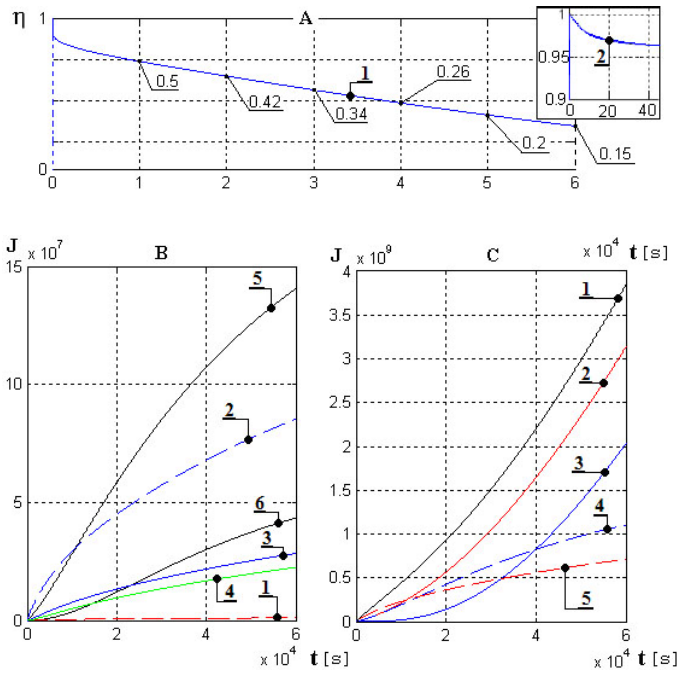


***Fig.2** Energy analysis of CRF in uncontrollable mode. A- 1,2 – efficiency factor, B – accumulated energy in one side of the furnace layers (5,6) and the body (1,2,3,4); C – 1 total losses, 2 – summary losses in the walls of CRF and the ambient medium, 3 – losses to the ambient medium, 4 – losses in the walls of the furnace, 5 – energy accumulated in the body.*

The controlling process for the same CRF model is shown in Fig.2, where the values remain the same. Graphs 2(A) and 5(B) show a trend towards establishing the values, i.e. with the establishing of the temperature, the thermal energy in the body is also established.

The data from the model and experiment, having been repeatedly ascertained, show the following dependency: the efficiency factor is greater with similar sizes of the *chamber & detail* system, and it decreases along with the increase of the size difference (a small body being heated in a large chamber). Thus the energy analysis can be used to set criteria for the geometric sizing of the system, i.e. CRF can be used for details of random sizes with sufficient results.

The issue of finding out the efficiency factor of the *furnace & detail* system is connected to a specific setting and mode of operation. For example, the energy analysis when simulating the heating of an empty furnace aims at determining the losses through the walls to the ambient medium, but the calculation of the efficiency factor must start after the detail has been placed in the working chamber. Another feature of the energy sizing is the case in which the heaters are turned off when the process has been established. The disconnection of the electric power supply leads to incorrect accounting of the efficiency factor, which necessitates the inclusion of extra conditions in the simulation process to discontinue its calculation.

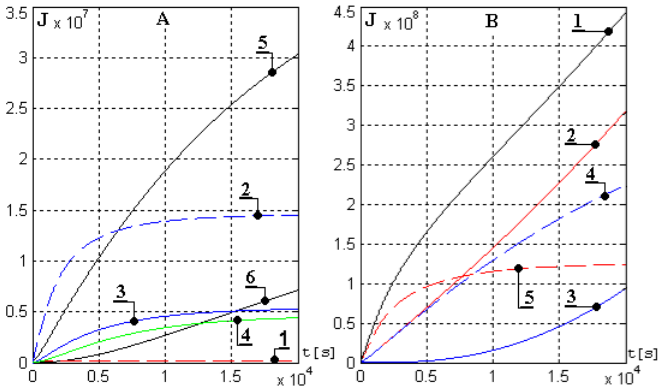


Fig.3 *Energy analysis of CRF in controllable mode. A – accumulated energy in one side of the layers of the furnace (5,6) and the body (1,2,3,4); B – 1 total losses, 2 – summary losses in the walls of CRF and ambient medium, 3 – losses to the ambient medium, 4 – losses in the walls of the furnace, 5 – energy accumulated in the body.*

The methodology for assessment of the CRF condition and the necessary repair activities, has the following sequence [2,3,4]:

1. **Measurement and analysis of the consumed electric power per working cycle.** The control over the consumed electric power offers the possibility to determine the condition of the furnace and its wearing-out during operation. The consumption for one heating cycle, detected to be larger than the nominal one with a certain technological process, is determined by the increased losses through the insulation as a result of defects. This indicates that a thorough inspection is needed, including, in particular, measuring the temperature along the furnace body.

2. **Inspection of the furnace in operative mode through thermographic measurements.** The measurements with an IR thermographic chamber are meant to determine the distribution of the temperature field in all main constructive elements of the furnace. The measurement is supposed to afford a possibility to determine the condition of the insulation and to detect zones on the body where the temperature is increased due to defects, etc.

3. **Analysis of the obtained results.** The analysis of the obtained results is supposed to summarize the condition of the inspected facility. It requires that a full list be made of the detected defects, areas of increased temperature on the body, condition of the gasket elements, etc. It is at this stage that an expert assessment should be given about the technical resources needed for the repair works.

4. **Economic analysis and determining of the necessary repair activities.** The economic analysis is based on the results obtained so far and is intended to determine the volume of the required repair activities. The purpose is to make an economic validation, through which a decision to be taken by choosing among the following options: partial repair, thorough repair, complete replacement of the furnace**.**

The results from the reconstruction of the furnace equipment, conducted by use of the suggested methodology, are shown in Fig.4: A – defects in the insulation causing increased temperature in the furnace body; B – furnaces reconstructed by use of new thermoinsulating and fireproof materials. Measurements show that the defects in the insulation increase the losses and lead to deformation of the temperature field in the furnace chamber, increased financial costs and low-quality production.

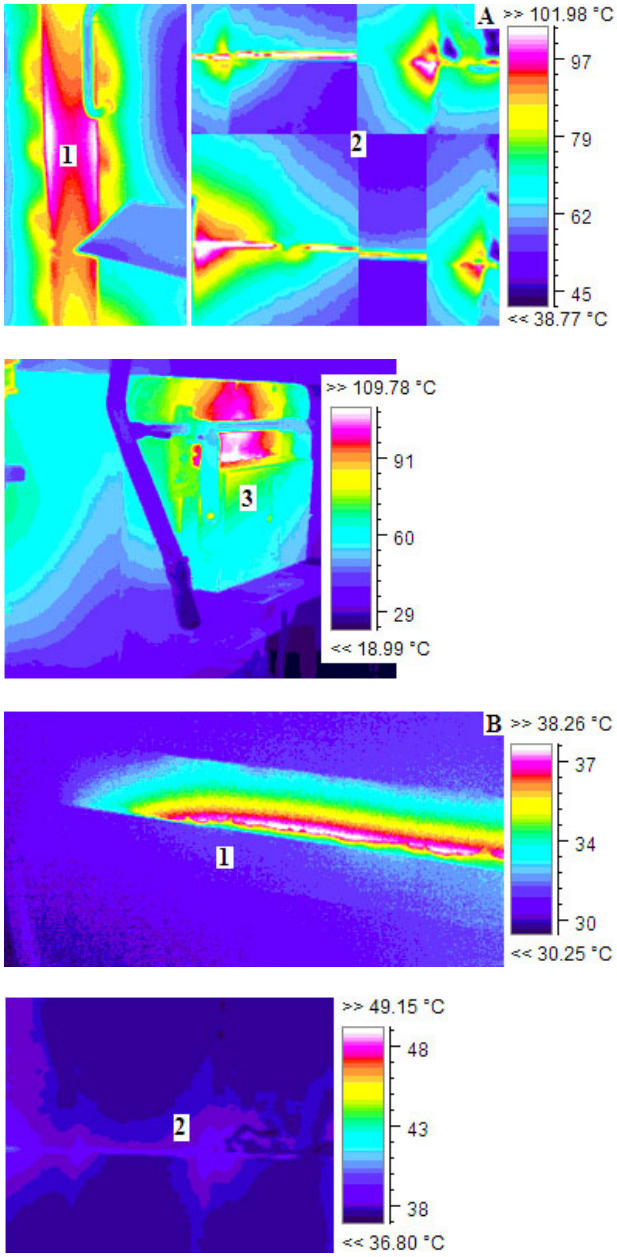


Fig.4 *Measurements by thermochamber showing: A – furnaces subject to reconstruction due to increased temperature on their surface; B – reconstructed equipment.*

3. Conclusion

The modification of the methodologies for CRF design suggested here is based on the modeling and analysis of the furnaces. From the verification of its application and the solutions of practical problems in designing, it can be concluded that it is suitable for application with:

- Design of new devices meeting the criteria specified in the project. It is possible to design furnaces of general application or specialized furnaces for specific needs.
- Analysis of the existing thermal equipment for the purposes of repair, complete reconstruction, insulation replacement, optimization, etc.
- The design methodology features the following advantages:
- It shortens the operative time and eliminates the probability of occasional errors when using the ERF models; the designer is relieved from the main part of calculating work.
- The preciseness of work is increased. The need for work with graphs and taking criteria into account is eliminated by the realized approach – working with a model made up of a system of DE and realization through numerical methods.
- The operation methodology is all-inclusive, i.e. though one model and calculation procedure, the parameters are determined of the ERF being designed: distribution of the temperature in the chamber and the insulation, temporal parameters of the transitional process, analysis of the parameters of the controls, energy analysis, optimization of the construction.
- The project has a potential of wide application – it can be used in the operation of the thermal unit. It would be appropriate to include the models thus created in the passport of the furnace so as to serve for assessment of the required technological processes. The same can be used by non-professionals as well.

Used literature

1. Тахрилов Хр, Димитров Б, **Проектиране, моделиране и оптимизация на електросъпротивителни пещи**. ТУ-Варна 2010
2. Dimitrov B., H. B. Nenov, A. Marinov, **Comparative analysis between methodologies and their software realizations applied to modeling and simulation of industrial thermal processes**. The 36-th International ICT Convention – MIPRO 2013, pages: 1129-1133.
3. Tahrilov Hr, B. Dimitrov, S. Benev, **Methodology for determining the need of reconstruction for resistive heater furnaces in order to increase their energy efficiency**. Third international Scientific congress – 50-th Anniversary Technical University of Varna, Part 3, pages: 149-154.
4. Dimitrov B., I. Yachev, **Study of high-temperature chamber-type electric resistance furnace and attainment of uniform temperature field**. International Conference on Applied and Theoretical Electricity – University of Craiova ICATE
5. Lienhard J. **A heat transfer textbook**, third edition, Phlogiston press, Cambridge Massachusetts, 2003

www.matlab.com

CREATING AND RESEARCHING SUSTAINABLE DESIGN OF CORRUGATED CARDBOARD FURNITURE WITH ADVANCED TECHNOLOGICAL MEANS

СЪЗДАВАНЕ И ИЗСЛЕДВАНЕ УСТОЙЧИВИЯ ДИЗАЙН НА ГОФРИРАНИ КАРТОНЕНИ МЕБЕЛИ СЪС СЪВРЕМЕННИ ТЕХНОЛОГИЧНИ СРЕДСТВА

Phd Tihomir Dovramadjiev, Prof. Phd Plamen Bratanov, Phd Kremena Cankova, Phd Ginka Jecheva
Mechanical Engineering Faculty, Industrial Design Department - Technical University of Varna, Bulgaria.

tihomir.dovramadjiev@gmail.com, plamenbratanov@abv.bg, kremenacankova@abv.bg, ginkaaa@yahoo.com

Abstract: *Furniture made of corrugated cardboard is environmentally friendly, cheap and allow a construction of complex geometry in design and ergonomics of wide application. They may have functional value, art direction, etc. The application of advanced technological means which support the design process of furniture made of cardboard allows optimization of the complete process of creating a sustainable design.*

Keywords: SUSTAINABLE, DESIGN, 3D, CARDBOARD, FURNITURE, SOLIDWORKS

1. Problem discussion

Furniture made of cardboard are ecologically clean, cheap and allow a construction of design with complex geometry of design, ergonomics and wide application in various aspects of daily life, interior and exterior. They may have functional value and art direction. For furniture made of cardboard new and/or already recycled materials can be used that contribute to the saving of timber (environmental and green protection), water saving (up to 99%), energy (up to 50%) and removal of waste (up to 90%) [1 - 3]. A very important point is the usefulness of the cardboard material referring to the environment and the advantage which is its quality to hold carbon emissions in the bulk structure. In order the relationship between cardboard material, its own volume and the level of carbon to be precisely examined it is necessary to use advanced technological means of Dassault System SolidWorks Sustainable [4, 5]. It allows analyzing the ecological impact on the environment of already constructed in SolidWorks CAD medium 3D models of furniture and optimizes their design compared to global environmental standards. Optimizing the process of creating furniture designs made from cardboard will help in improving the condition and quality of the production and optimization of the product life cycle [6 - 9]. The present work aims to explore the possibilities of direct advanced technological tools applied in the creation of sustainable furniture design made of cardboard and optimize the process.

2. Objective and research methodologies

The design of environmentally friendly furniture made of cardboard material is optimized by methods combining basic principles when constructing models through technological means, opportunities to study the quality of the material and market factors (Table 1).

Table 1. *Creation sustainable design of cardboard furniture*

CREATION SUSTAINABLE DESIGN OF CARDBOARD FURNITURE		
	PLM	SolidWorks Sustainable
Technological way of making cardboard furniture	CAD/CAM	Part, Assemblies and Drawings Design
Opportunities to study the quality of the material	CAE / empirical real tests	Database / in real time internet analysis
Factors	Optimization of the design criteria and standards	▪ Carbon footprint ▪ Water Eutrophication ▪ Air Acidification ▪ Total Energy Consumed
Market	▪ Environment ▪ Equity / Society ▪ Economy	▪ Material ▪ Production ▪ Transportation Distribution (LCA)

The design of furniture from cardboard passes through ESW cycle (Fig. 1). The stages of the process support the optimization design based on specific features separated by criteria which contribute to the precise design from the conceptual idea to the finished product and its quality evaluation by SolidWorks Sustainable technological mean.

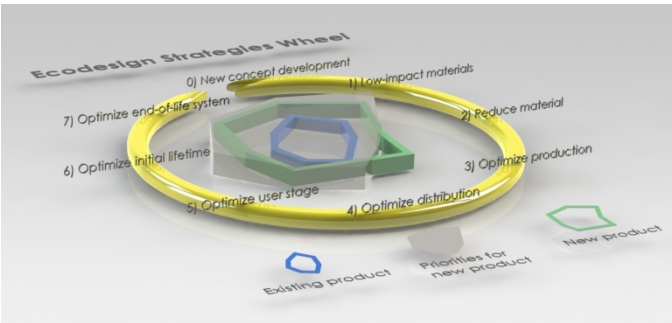
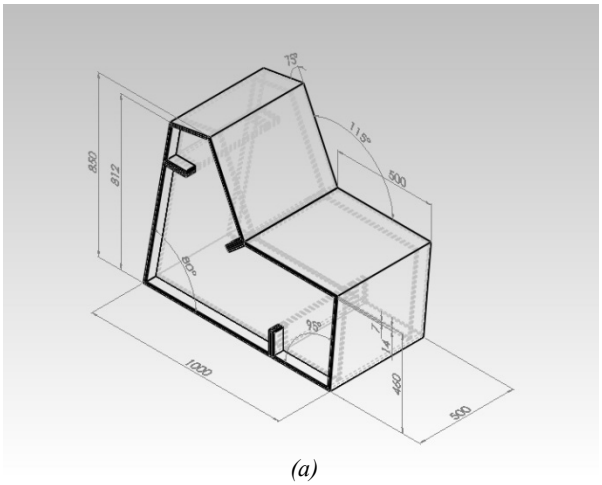
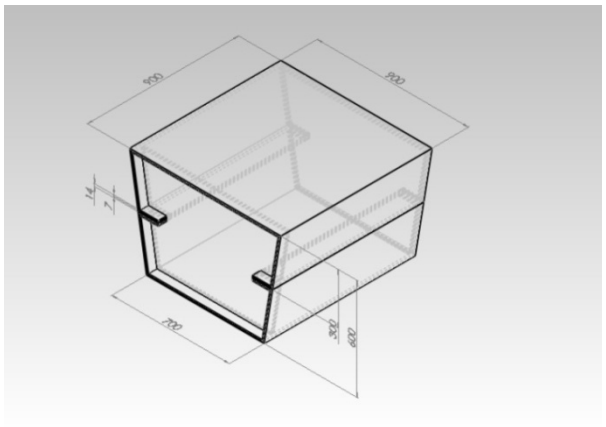


Fig.1. *Ecodesign Strategies Wheel [1, 4, 9]*

Using the methodology (Table 1) to create cardboard furniture and ESW cycle there have been developed variations of ergonomically streamlined design of interior and exterior furniture - chairs and table. Their design is fully optimized in terms of material and strength. Constructive appropriate options are selected of assembling in important areas providing stability. The thickness of a single sheet of cardboard is 7mm. The specific points, where are the supporting parts, are connected by three (7mm corrugated paper), providing the necessary reliability of the structure (Fig. 2).



(a)



(b)

Fig. 2. *Dimensions of the models (a) ECOSEAT and (b)ECOTABLE*

The concept of using eco furniture from cardboard implies the right atmosphere and setting. An exemplary application of the resulting patterns in the interior environment is shown in Fig. 3.



Fig. 3. *Models of interior cardboard furniture*

The sustainable design of the models is developed and optimized for the European region (Fig. 4).

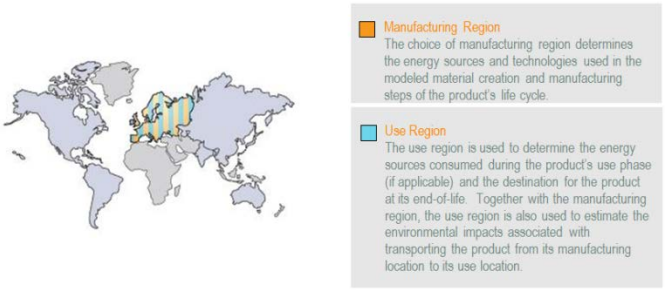


Fig.4. *Manufacturing and use region*

The information about transport, the sustainable design information, and environmental values of Carbon Footprint, Water Eutrophication, Air Acidification and Total Energy Consumed per unit model ecoseat and ecotable are shown in tables. 2 and 3.

Table 2. *Properties*

PROPERTIES	ECOSEAT	ECOTABLE
Material	Corrugated paper	Corrugated paper
Volume:	4.99E+7 mm^3	5.84E+7 mm^3
Surface Area:	1.46E+7 mm^2	1.70E+7 mm^2
Weight:	7792.13 g	9109.51 g
Primary Mode of Transportation:	Train	Train

Table 3. *Environmental impact*

ENVIRONMENTAL IMPACT	ECOSEAT	ECOTABLE
Carbon Footprint	3.50 kg CO_2	4.09 kg CO_2
Water Eutrophication	9.33E-3 kg PO_4	0.01 kg PO_4
Air Acidification	0.02 kg SO_2	0.03 kg SO_2
Total Energy Consumed	109.51 MJ	128.03 MJ

3. Conclusion

Integration of advanced technological means in creating the design of eco furniture from corrugated cardboard material is a very good sustainable solution. The modeling of the ESW full cycle support both optimization of the design of the developed products and qualitative analysis of environmental values. These are necessary conditions for the protection of ecological environment combined with modern, sleek and available at cost price of products widely used in both the interior and the exterior environment.

References

[1]. NCASI. Life cycle assessment of u.s. average corrugated product. Research Triangle Park, NC. USA, April 2014.

[2]. Planet Ark Environmental Foundation. Sydney, Austalia, 2014 .http://planetark.org/.

[3]. Corrugated Packaging Alliance (CPA). Corrugated Packaging Life-cycle Assessment. Summary Report. USA, 2010.

[4]. Guide to Sustainable Design using SolidWorks Sustainability. Dassault Systemes SolidWorks. USA, 2014.

[5]. Benjamin Tan. Green Design with SolidWorks. Dassault Systemes.

[6]. Oltikar, akhil manohar. Computer-Aided Engineering of Plywood Upholstered Furniture Frames. USA, 2000.

[7]. Michael Lee. Cardboard Chair Project. Research Report.

[8]. Greg Saul, Manfred Lau, Jun Mitani, Takeo Igarashi. SketchChair: An All-in-one Chair Design System for End Users. TEI'11, January 22–26, 2011, Funchal, Portugal.

[9]. Julija Jeganova. Product Life Cycle Design: Integrating Environmental Aspects into Product Design and Development Process at Alfa Laval. Lund University. Sweden, 20004.

NUMERICAL SIMULATION AND EXPERIMENTAL INVESTIGATION OF EQUAL-CHANNEL ANGULAR PRESSING OF POROUS POWDER BILLETS

Full Prof., Dr. Tech. Science Ryabicheva L., Ph.D Usatyuk D., Dyadichev A.
Department of Material Science – Volodymyr Dahl East Ukrainian National University, Lugansk, Ukraine

ryabic@gmail.com

Abstract: *The theoretical and experimental study of stress-strain state and density distribution into the billet at equal-channel angular pressing has been conducted. It has shown clearly that deformation zone takes a substantial volume with dramatic non-uniformity of stress-strain state after the first pass of equal-channel angular pressing at the backpressure of 90 MPa. The presence of turbulence zone that ensures structure fragmentation of material has established by microhardness indentation. A possibility of production of high-density billets after the second pass at the backpressure of 150 MPa with high mechanical properties and more uniform stress-strain state, free of loosening and cracks has presented.*

KEYWORDS: BILLET, STRESS, DEFORMATION, BACKPRESSURE, DENSITY, MICROHARDNESS, TURBULENCE ZONE.

1. Introduction

Different methods of severe plastic deformation, including equal-channel angular pressing (ECAP), are effective production techniques for materials with prescribed properties. It allows production of high-density powder materials with fine-grained structure, as a result of which their properties are changing qualitatively. Computer modelling of ECAP of various porosity powder billets without backpressure have observed in papers [1, 2]. Evolution of densification and deformation zones depending on physical and mechanical properties of material and deforming conditions has shown clearly. A part of sample moving onto a free surface does not compact properly and its density remains the same with initial billet at deforming without backpressure. It has established [3] that it is possible to obtain ultimate density of powder billets of high initial porosity by ECAP with backpressure.

The purpose of this work is further theoretical and experimental study of densification and plastic forming of porous powder billets after one and two ECAP passes with backpressure.

2. Mathematical model

Mathematical modelling of ECAP has been conducted using the fundamentals of plasticity theory of porous bodies where the plastic potential is described as a function of stress tensor components with the smooth, convex and closed surface corresponding to it into the stress space [4, 5]. This potential may be presented in the following way:

$$F=\frac{\tau^2}{\varphi}+(1+m)^2\frac{\left(p+\frac{m}{m+1}\bar{\rho}\sigma_s\sqrt{\psi}\right)^2}{\psi}-\bar{\rho}\sigma_s, \quad (1)$$

where $p=\frac{1}{3}\sigma_{ij}\delta_{ij}$ - is the hydrostatic pressure;

$\tau=\sqrt{(\sigma_{ij}-p\delta_{ij})(\sigma_{ij}-p\delta_{ij})}$ - is the intensity of shear stresses;

$\varphi=(1-\theta)^2$, $\psi=\frac{2}{3}\frac{(1-\theta)^2}{\theta}$ - are functions of porosity θ;

$\bar{\rho}=1-\theta$ - is the relative density.

m - is the parameter characterizing the degree of imperfection of the contacts in the powder preparation and defining different resistance of a porous body during its testing in tension and compression.

The rate of volume change as a result of plastic deformation may be expressed as follows [5]:

$$e\sim\frac{2(1+m)^2}{\psi}p+\frac{2m(1+m)\sigma_0}{\sqrt{\psi}}, \quad (2)$$

where σ_0 - is the flow stress of hard phase, which is a function of accumulated deformation ω and is determined by a hardening curve of powder material at uniaxial tension.

A flow stress of hard phase may be expressed as the function $\sigma=\sigma_0+K\omega^{0.5}$, where K - is the hardening coefficient. It was assumed that $K/\sigma_0=0.5$ during numerical simulation.

The rate of accumulating deformation in hard phase of porous body was determined on the basis of postulate of uniqueness of the dissipation function formulated by Skorokhod V.V. [6]:

$$\omega=\sqrt{1-\theta}\left(\frac{m}{1+m}\sqrt{\psi}e+\frac{\sqrt{(1+m)^2\gamma^2+e^2\psi}}{1+m}\right), \quad (3)$$

where γ - is the shape changing rate.

The value of accumulated deformation ω is renewed by solving of the following differential equation [5]:

$$\frac{d\omega}{dt}=W, \quad (4)$$

where W - is the equivalent strain rate defined as follows [5]:

$$W=\frac{1}{\sqrt{1-\Theta}}\sqrt{\psi e^2+\varphi\gamma^2}\ . \quad (5)$$

A finite element method presented as a series of procedures was implemented for determination of distributions of stress and strain intensity, as well as density. The first procedure is a triangulation of a plastic deformed body or transition from a continuum billet to its finite element counterpart. Such simulation requires implementation of extremal requirement for the functional [5]:

$$J(v_i(x))=\int_{\Omega}D(e_{ij}(V_i))d\Omega+\int_{\partial\Omega_p}p_iv_id(\partial\Omega), \quad (6)$$

where $D(e_{ij}(V_i))$ - is the dissipative function;

p_i - is the stress vector on the surface of investigated billet;

v_i - is the velocity vector on the surface of investigated billet.

The first integral in the functional (6) is the total rate of energy dissipation, the second integral is the power of external stresses.

The dissipation function $D\left(e_{ij}(V_i)\right)$ of plastically deforming porous body is described by the following expression [5]:

$$D\left(e_{ij}(V_i)\right)=\frac{\sqrt{\gamma^2\varphi+e^2\psi}}{\sqrt{1-\theta}}\tau_s+\frac{p_0e}{\sqrt{1-\theta}}, \quad (7)$$

where

(8) $V_i = v(x),\ e_{ij} = \frac{1}{2}\left(\frac{\partial v_i}{\partial x_j} + \frac{\partial v_j}{\partial x_i}\right),\ p_0 = -\sqrt{\frac{2}{3}}\tau_s\sqrt{\psi}\,\frac{m}{1+m}$,

τ_s - is the shear yield stress.

The dependences (1) - (8) were used for finite element analysis of ECAP of prismatic-shaped copper porous powder billet with section 15x15 mm, 59 mm in length, initial porosity 42% at temperature 20°C by using of QForm 5.1.3 program. The molybdenum disulfide is used as lubrication material. The visco-plastic material model was implemented for the billet: modulus of elasticity is 124000 MPa, Poisson's ratio 0.35, initial yield stress 100 MPa. The Levanov's exponential friction law was implemented for modelling of friction. Parts of die tool were presented as elasto-plastic bodies at isothermal conditions [4, 7, 8].

The essential advantage of the QForm 5.1.3 program is special simulation algorithm for deformation of sintered porous powder billets with initial porosity up to 30%. This algorithm ensures simultaneous calculation of the stress-strain state and distribution of density by the volume of billet for each step of deformation process. The initial data preparation procedure includes operations that are very similar to compact materials with adding of one variable for relative density [8].

Another substantial advantage of the Qform 5.1.3 is fully automatic generation of initial adopted finite element mesh with regular automatic remeshing during simulation process. At the same time the automatic remeshing algorithm allows finite element simulation of forming operations of porous billets with substantial non-uniformity of stress-strain state, because it generates finer mesh in areas of high solution gradients and surface curvature [8].

Finite element modelling of different extrusion schemes performed by authors of papers [1-3, 9-11] has shown clearly possibilities of simulation of metal forming operations for billets with higher initial porosity by the results of mechanical testing of samples with given initial porosity and following multiplying of calculated relative density values by the coefficient of correction that is a quotient of real value of relative density of the billet divided by minimum permissible value for solver of the Qform 5.1.3 that is equal to 0.7 [8, 9].

Thereby, modelling included the following stages: construction of solid model of ECAP, development of mathematical model of deformed porous powder material by the results of uniaxial compression tests of samples with 42% initial porosity, generation of initial adopted finite element mesh from quadratic elements, determination of initial and boundaries conditions, solving of governing equations system, analysis of simulation results [8, 11].

In such case, the density of billet for each deformation step may be determined by the following expression [12]:

(9) $$\rho_i = \frac{\rho_p \cdot h_k}{h_k + (s_i - s_{i-1})},$$

where ρ_p - is the pycnometric density of powder material;

h_k - is the final height of the billet;
s_i - is the displacement of punch at the end of *i* deformation step;
s_{i-1} - is the displacement of punch at the beginning of *i* deformation step.

Therefore, average density of the billet may be calculated by the formula [8, 13, 14]:

(10) $$\rho_{ave} = \sum_{i=1}^{n} \rho_i ,$$

where n - is the number of deformation steps.

The increment of relative density for the finite element *j* on *i* deformation step, while accounting of expressions (9) and (10), is determined in the following way:

(11) $$\Delta\bar{\rho}_{ij} = \frac{v_{ji}}{v_{ji} - v_{ji-1}},$$

where v_{ji} - is the volume of the finite element *j* at the end of *i* deformation step;
v_{ji-1} - is the volume of the finite element *j* at the beginning of *i* deformation step.

Consequently, the relative density value for the finite element *j* on *i* deformation step was calculated by the following expression:

(12) $$\bar{\rho}_{ij} = \bar{\rho}_{ij} + \Delta\bar{\rho}_{ij} .$$

The average value of relative density of porous powder billet on deformation step *i* during simulation of density distribution for set of finite elements into the volume of billet:

(13) $$\bar{\rho}_i = \sum_{j=1}^{N} \bar{\rho}_{ij} ,$$

where N - is the number of finite elements into the volume of billet.

The limitation on initial value of relative density set in program-solver may be overcome by implementing the coefficient of correction as follows:

(14) $$k_\rho = \frac{\bar{\rho}_{init}^{real}}{\bar{\rho}_{init}},$$

where $\bar{\rho}_{init}^{real}$ - is the initial value of relative density of porous powder billet;
$\bar{\rho}_{init}$ - is the minimum permissible value, limited by the solver.

A precision of simulation of porous powder billets compaction and other forming operations for production of powder parts is defined mostly by the discreteness of finite element discretization the volume of billet and may be increased while decreasing of characteristic dimension of finite element [13, 14].

3. Experimental investigation

The experimental investigation of ECAP has been conducted for verifying of simulation results. Prismatic-shaped with section 15x15 mm, 59 mm in length, initial porosity 42% obtained from electrolytic copper powder PMS-1 GOST 4960-75 by double-action pressing on the hydraulic press PD-476 (force 1600 kN). Sintering was carried out into synthesis gas medium (the gas composition is 72% H_2, 21% CO, 5.5% CO_2, 1.5% H_2O) in a stepwise mode. ECAP performed by the scheme presented on fig. 1 on the same hydraulic press.

The coordinate grid with the cell 3x3 mm was patterned on the billet before ECAP. The compacting pressure during the first pass was 890 MPa and 1330 MPa for the second pass. The value of backpressure assumed 90 MPa for the first pass and 150 MPa for the second pass.

Distributions of stress-strain parameters by sections 1, 2 and 3 (fig. 2) after the first and second passes are presented on fig. 3. The section 1 is from backpressure side and section 3 under the punch.

Simulation of ECAP has shown that stress-strain state after the first pass is characterized by substantial non-uniformity (fig. 3, a). Increasing of the intensity of stress has been observed in section 1 from bottom face to upper face with maximal value of 257 MPa into the deformation zone. It decreases dramatically on the upper face of billet. The same character of variation of stress intensity has been observed in the section 2 with a bit higher value into the deformation zone. The second deformation zone is formed under the punch in section 3 under the influence of friction forces similarly to closed-die upsetting: the intensity of stress has grown from the bottom to upper face. At the same time the intensity of stress under the punch was equal to 198 MPa.

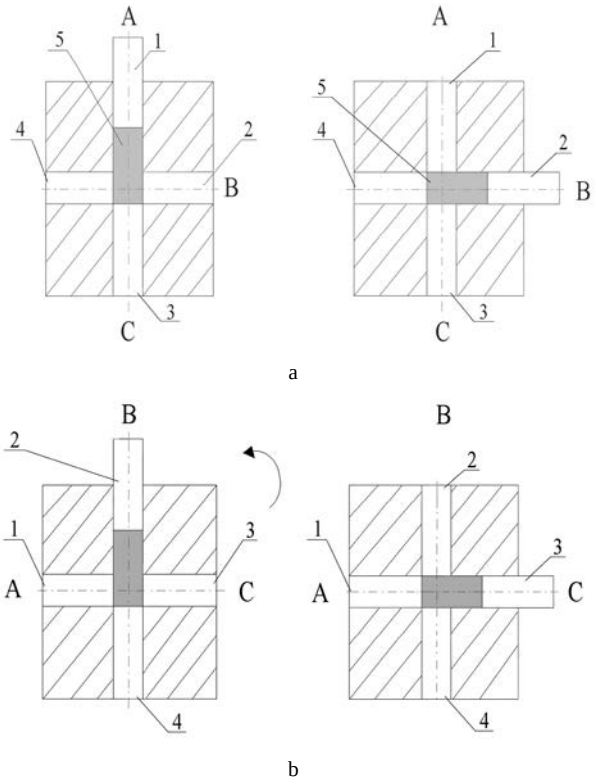


Fig. 1 *Scheme of equal-channel angular pressing: a – is the first pass; b – is the second pass.*

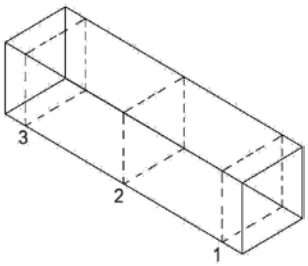


Fig. 2 *Sections of the billet.*

The second pass has been performed after rotation of the billet: section 1 was placed under the punch; section 3 – from the backpressure side, explanation remained the same. Decreasing the intensity of stress has been observed in section 1 from the bottom face to upper face. The deformation zone with maximal intensity of stress remained in section 2, but its size is smaller due to hardening of hard phase obtained during the first pass. Diminishing of stress intensity in section 3 under the punch has been observed (fig. 3, a).

Changing the intensity of deformation indicates that deformation zone almost fills the central part of billet, scoping the volume from the punch to backpressure side. In such case intensity of deformation grows to maximum value into the deformation zone and on the corner part of the upper face. The volume of the deformation zone after the second pass decreased, densification was minimal, deformation of powder particles has happened. Obviously, the volume changing rate of billet is lower than forming rate.

Experimentally verified distribution of deformation intensity is presented on fig. 4. The character and value of deformation intensity is similar to the picture obtained by numerical simulation. Loosening has appeared on upper face of the billet in section 1 that indicating of insufficient backpressure value. The billet has no loosening and cracks after the second pass while increasing of backpressure up to 150 MPa. The coordinate grid was substantially distorted. Formation of vortex has observed into the deformation zone that indicates intensity of high angle boundaries formation [7].

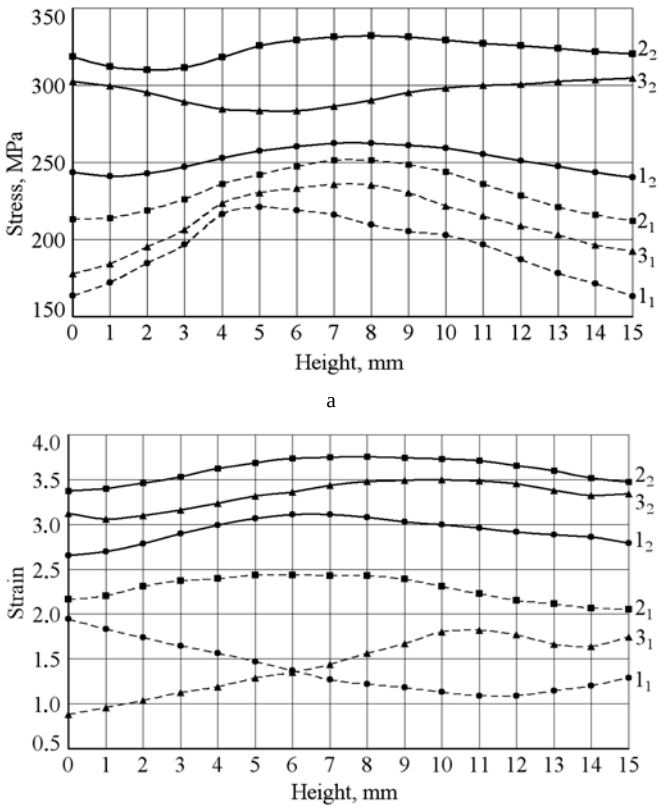


Fig. 3 *Distribution of the intensity of stress – a and deformation – b in sections 1, 2 and 3, obtained by numerical simulation: $1_1,2_1,3_1$ – after the first pass; $1_2,2_2,3_2$ – after the second pass.*

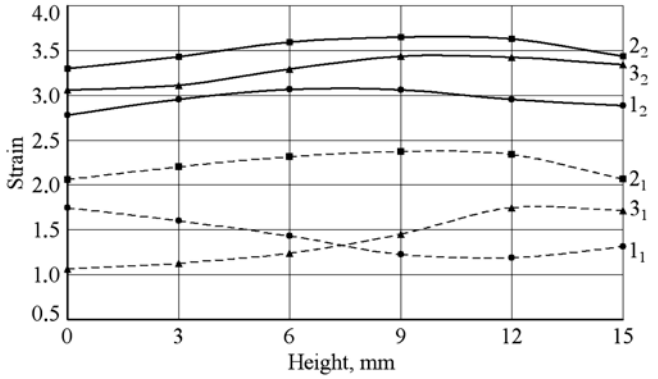


Fig. 4 *Distribution of the deformation intensity by the sections 1, 2 and 3 (experimental): $1_1,2_1,3_1$ – after the first pass; $1_2,2_2,3_2$ – after the second pass.*

Microhardness variation has been investigated by longitudinal section of the sample after the first and second passes for experimental estimation of stress state. A non-monotonic distribution of microhardness after the first pass has been observed. The microhardness level is growing by section of billet from outer faces to the centre while growing the intensity of deformation. The highest microhardness value 714 MPa that is corresponding to maximal intensity of deformation has measured into the deformation zone. The microhardness into zone from backpressure side was 480 MPa at deformation intensity 1.2 that is connected with development of loosening. Growing of microhardness has been observed after the second pass and variation of its values between the outer surface and centre of the billet drops substantially while increasing of accumulated deformation. The highest microhardness of 780 MPa was measures after the second pass into the deformation zone where formation of vortex field, connected with transversal flow of material in the plane normal to the deformation axis, has been observed. The highest intensity of deformation after the second pass was equal to 4.0, corresponding to main

microhardness growth into the middle zone and zone under the punch.

Distributions of relative density lengthwise of billets are presented on fig. 5. It has established that after the first pass of ECAP it is possible to distinguish three zones into the volume of billet: 1 – is the loosening zone appeared from the backpressure side; 2 – is the middle zone of maximal density; 3 – is the zone under the punch.

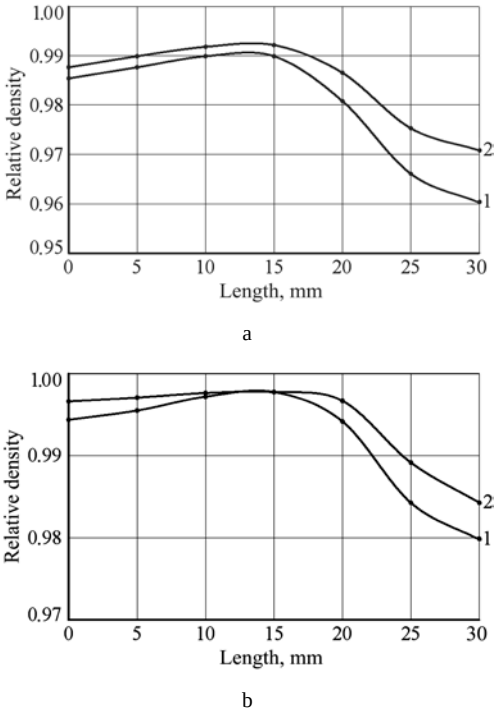


Fig. 5 Density distributions lengthwise of billets after ECAP: a – after the first pass; b – after the second pass: 1 – is the experimental dependence; 2 – is the dependence plotted by the results of numerical simulation.

The length of each zone was approximately 10 mm after the first pass, while depth of damage layer from the backpressure side was 0.4 mm.

The inhomogeneous distribution of relative density after the first pass is stipulated by non-uniformity of stress-strain state and effect of friction forces. The relative density that is almost equal to 1 has been observed after the second pass into zones 2 and 3 while decreasing from the backpressure side.

The relative error of determination of relative density by a finite element method with implementation of expressions (11) - (14) was 1.4-2.5 % that is quite sufficient for practical purposes.

4. Conclusions

Theoretical investigation and finite element simulation using the QForm 5.1.3 program verified by the results of laboratory experiments have shown clearly that density obtained into the volume of porous powder billet after the first pass of ECAP at the backpressure of 90 MPa was lower than density of compact material. The deformation zone fills large volume, scoping of three zones distinguished into the billet, at substantial non-uniformity of stress-strain state. The high-density billet with more uniform stress-strain state, free of loosening and cracks has been obtained after the second pass of ECAP at the backpressure of 150 MPa while contracting a size of the deformation zone. The presence of turbulence zone that ensures structure fragmentation and promotes to production of billets of powder materials with ultrafine-grained structure and high mechanical properties has been established by microhardness indentation.

5. References

1. Maydanyuk A. Equal-channel angular extrusion of porous billets: computer simulation and experimental study, The International congress and exhibition EURO PM 2010 proceedings, October 10-14, 2010, Florence, Vol. 3, pp. 1206–1212 (Maydanyuk, A., M. Shtern, G. Bagluck, L. Ryabicheva).

2. Maydanyuk A.P. Evolution of density distribution at equal-channel angular pressing of porous billets, Herald of the Volodymyr Dahl East Ukrainian National University, 2008, Issue 3, Vol. 2, pp. 213–216 (Maydanyuk, A.P., L.A. Ryabicheva, M.B. Shtern, G.A. Bagluck).

3. Ryabicheva L.A. Deformation behavior of porous powder billet during equal-channel angular pressing, Herald of the National Technical University «Kharkiv Polytechnical Institute», 2010, pp. 42–50 (Ryabicheva, L.A., V.V. Smolyak).

4. Favrot N. Modeling Sintering Deformations Occurring After Cold Compaction, Qualitative Methods for the Mechanics of Compaction, Proceedings of the International Workshop on Modeling of Metal Powder Forming Process, Grenoble, France, 21-23 July 1997, pp. 133 – 147 (Favrot, N., J. Besson, C. Colin, F. Delannay, Y. Bienvenu).

5. Shtern M.B. Phenomenological theories of powders pressing. Kiev, Naukova dumka, 1982. – 140 p (Shtern, M.B., G.G. Serdjuk, L.A. Maksimenko).

6. Skorokhod V.V. The rheological basics of sintering theory, Kyiv, Naukova Dumka, 1972. – 152 p (Skorokhod, V.V.).

7. Beygelzimer Ya.E. Some considerations concerning severe plastic deformations based on their similarity with vorticity, High Pressure Physics and Technics, 2008, Vol. 18, No 4, pp. 77–86 (Beygelzimer, Ya.E.).

8. Biba N. Material Forming Simulation Environment based on QForm3D Software System, Metal Forming 2008: Proceedings of the 12th International Conference on Metal Forming / Ed. by M.Pietrzyk et.al., Verlag Stahleisen GmbH., Poland, Krakow, 2008 (Biba, N., S. Stebunov).

9. Ryabicheva L.A Modeling of evolution of the deformation zone for different extrusion schemes, Gerald of the Moscow State University of Mechanical Engineering «MAMI», 2013, No. 1(15), pp. 120-124 (Ryabicheva, L.A, D.A. Usatyuk).

10. Ryabicheva L. Computer modeling of radial-direct extrusion of complex-shaped details // Journal of Computer and Information Technology, 2012. Vol. 2, No. 1, pp. 91–101 (Ryabicheva, L., D. Usatyuk, N. Beloshitskij).

11. Ryabicheva L. Computer Modelling of Radial-Direct Extrusion of Porous Powder Billets. Computational and Numerical Simulations: The book, INTECH Open Access Publisher, Croatia, 2014, Ch. 6, pp. 119–137 (Ryabicheva, L., D. Usatyuk), http://dx.doi.org/10.5772/57142.

12. Bragina I.Y. The study of the pressure effect on the compression of ZrO_2 powder with heating by electric current // Materials working by pressure, 2013, No. 3 (36), pp. 145–149.

13. Ryabicheva L. Mathematical Modelling of Structure Formation of Discrete Materials // Numerical Simulations, Applications, Examples and Theory: The book, INTECH Open Access Publisher, Croatia, 2011, pp. 377–400 (Ryabicheva, L., D. Usatyuk), http://dx.doi.org/10.5772/13193.

14. Wagoner R.H. Metal Forming Analysis. Cambridge University Press, 2001. – 376 p (Wagoner, R.H., J.L. Chenot).

PULSED DISCHARGE TECHNOLOGIES OF PROCESSING AND OBTAINMENT OF NEW MATERIALS
(Review)

РАЗРЯДНОИМПУЛЬСНЫЕ ТЕХНОЛОГИИ ОБРАБОТКИ И ПОЛУЧЕНИЯ НОВЫХ МАТЕРИАЛОВ
(Обзор)

Prof., Doctor of Science Sizonenko O., Prof., Doctor of Science Vovchenko A.
Ukraine, Mykolaiv, Institute of Pulse Processes and Technologies of NAS of Ukraine
E-mail: sizonenko43@rambler.ru

Abstract: *Review of pulses discharge technologies (PDT), in which pulses electric discharge in liquid is utilized, is given. PDT of processing and obtainment of new materials allows to impact both changes of geometrical size and the structure of objects in order to give it certain mechanical and physical properties. They are used in oil production, instrumentation, mechanical engineering, metallurgy, chemical industry, mining complex, and other.*

KEY WORDS*: ELECTRIC DISCHARGE IN LIQUID, SYNTHESIS, NANOMATERIALS, METAL-MATRIX COMPOSITES, SPARK PLASMA SINTERING*

1.Introduction

All variety of PDT using intense pulsed electric discharge (ED) in the liquid is reduced to the processes taking place at the explosive transformation of electrical energy into other forms of energy during the 1-100 ms. Therefore, methods of processing materials using electrical discharge in the liquid reasonably are related to a class of pulsed methods. Due to the high energy density (10^4 - 10^5 J/cm^3) in a limited volume of the discharge channel the pressure therein reaches 10^8 - 10^9 Pa and shock extension of the discharge channel is observed. As a result, powerful compression waves, acoustic fields, the complex cavitation (from micro to macroruptures) phenomena, electromagnetic and light radiation are generated in medium. The use of these factors of the ED is the basis of electric discharge methods for processing and obtainment of new materials. Technological equipment for ED treatment, regardless of the specific purpose and an object of processing, has identical block diagram and consists of the following main parts: [1] generator of pulse currents (GPC) with capacitive energy storage, discharge circuit, the discharge-processing unit, integrated control block for GPC and technological cycle.

2. Analysis and discussion

For analysis and discussion PDT, which are the most widely used for the processing and production of new materials, are presented.

2.1 PDT of intensification of filtration processes in porous materials – stimulation of oil wells [2].

The essence of this PDT is that in a borehole filled with liquid, using a high voltage pulse discharge such fators are aroused: electromagnetic and thermal fields; cyclic compressional waves with an amplitude of up to 50 MPa at the fron,; which are transformed into acoustic waves with the spectrum of frequencies from 10 Hz to 10 kHz; powerful hydrostreams (speed at the front of ~ 150 m/s) and volume microcavitation. A distinctive feature of PDT of oil wells stimulation is the ability of selective processing of local area of productive horizon. This PDT is eco-friendly, simple and reliable in operation with minimum energy consumption (power consumption of an electric downhole device no more than 2 kW).

This PDT promotes: the creation of non-additive (synergistic) effect in change (improvement) of the filtration characteristics of porous materials saturated with liquid with deep stratification (productive oil reservoirs), the removal of all types of deposits in the near-wellbore zone, prevention of the subsequent crystal growth of deposits and their sticking to the surface, contributing to the increase of processing effect time; development of existing cracks and the creation of new fracture channels; removal of contaminants from the pores; destruction of structural skeleton of oil inside the pores, enhancing its mobility by filtration (reduced yield stress, shear stress and dynamic viscosity); increase of the reservoir impact coverage by increasing penetrating filtration capacity of reactive compounds.

PDT can be implemented to improve the performance of production and injection wells during underground and major repairs; processing of bottom-hole zones of high strata, waxy crude oils and bitumen; provocation of influx into the well during development; provocation of influx from potentially productive layers of prospecting and exploration wells.

Electric discharge method of synergistic effect creation in improving the filtration properties of porous materials of deep stratification is adapted to porous materials of artificial origin - the regeneration of the filter elements[3].

2.2 PDT of electric hydro pulse processing (EHPP) of liquid and crystalizing metal [4].

The peculiarity of this technology is the fact of incompatibility of the physical parameters of the object (high temperature) and a liquid medium in which the ED can be realized. Therefore, in this PDT an electric discharge generator of elastic vibrations (EDGEV) is applied in the discharge-processing block, wherein the solid barrier (eg, membrane) placed at the boundary between two media, transforms ED in fluid into the elastic vibrations that affect the subject of the treatment (liquid metal) .

The essence of the EHPP method is to generate elastic vibrations by discharge in water filling EDGEV and to transmit these vibrations into the melt through the waveguide-radiator system (waveguide). Different modifications of EDGEV allow to realize electric discharge processes in wide range of electric parameters change: voltage from 1 up to 50 kV; current from 1 up to 30 kA; discharge pulses frequency from 1 up 16 Hz. Currently accumulated experience of EHPP of nonferrous metals and alloys of iron shows some positive effects resulting from treatment: reducing the inhomogeneity of chemical elements distribution; reduction of diffusion-movable oxygen and hydrogen; grinding and removal of nonmetallic inclusions; increase in fracture toughness, impact strength and formability of steels; intensification of the processes of degassing, refining and homogenization of the melt which creates conditions for a more homogeneous crystallization.

EHPP of melt in the ladle by EDGEV waveguide before casting applied to alloys based on Fe and Al increases the crystallization ability of the metal - a key factor in the formation of the solid metal properties. Efficiency of melt EHPP includes: the removal of free hydrogen by at least 30%; reducing the number of nonmetal inclusions by 15%; grinding macro and microstructure; lowering the threshold of cold brittleness at 20 ºC; reduction in variability of the mechanical properties by at least 15% (the casting of shipbuilding and general purpose steel); increase the wear resistance by not less than 50% (high-carbon alloy castings, operating under hydro wear); reduction of magnetic permeability in high-carbon alloys for electrical purposes by 4 – 10%; increase of the tightness of complex configuration aluminum alloys castings at high operating pressures; 10%; reduction of the harmful effects of iron impurities and structural heredity when remelting of secondary aluminum alloys.

2.3 PDT of intensification of materials volumetric deformation [5]

PDT of volumetric deformation of materials include PDT aimed directly at changing the shape of the processed material without significant destruction. Such PDT includes electrohydraulic stamping (EHS), press-fitting of tubes in heat exchangers, as well as electro-treatment of the welds.

EHS is based on realization of ED in working chamber and transmission of pressure, which arouses during discharge channel extension, to the processed blank directly or by die. In this case, the blank takes the desired shape by a special matrix.

he particular feature of the pulse-static deformation is that the energy of the electric discharge is not aimed at creating forces deforming part, but instead at agitation of waves of mechanical stresses and deformations in the material which, together with the static loading stresses cause plastic deformation of the parts. Static constituent of load creates elastic deformation of part, and pulsed constituent transforms it into plastic by means of elastic stresses relaxation. Such method of deformation significantly decreases the energy of pulse load and power consumption of used equipment. The same level of stress relaxation in the material and the amount of plastic deformation can be obtained both by increasing the impact pulse parameters and by achieving high stresses of elastic strain (up to the yield point) at the lower pulsed load.

Pulsed-static deforming creates favorable conditions for the relaxation of residual stresses in a formed or calibrated part.

Major advantages of EHS over conventional press stamping are: punching precision is improved because of the reduction of stresses, especially when processing most hardly-deformed metals; possibility of obtaining solid components of complex shapes in a single passage, whereas in conventional methods such parts require several passages and are performed welded; increase of materials deformation permissible degree; possibility of producing parts that are economically unviable, or impossible to produce by other methods; improved surface quality of stamped parts; greatly simplifies and reduces the cost of tooling, thereby reducing the time of preparation of manufacture.

2.4 PDT of destruction of durable nonmetallic objects consists in using forces from the shock wave generatedbya high voltage discharge in a liquid [6]. As well as in case of explosives use, in destructible object holes are performed, into which water is poured and electrode system is placed. When a high voltage from the GPC is applied to the electrode system, the discharge occurs in the discharge gap. This process is accompanied by extension of discharge channel, rise of pressure that can reach up to 10^9 Pa and formation of shock wave.

Destruction of soils, concrete and reinforced concrete objects occurs by creating cracks occurring in all directions around the hole, with subsequent separation of the solid pieces. Number of cracks, their depth and direction are determined by a grid of holes made in the object(the distance between the holes, location of the drill holes relative to each other, the depth of drill holes) and the structural features of breakable objects.

Installation is a mobile device that can be transported from one destructed object to another. PDT of durable objects destruction has several advantages over the use of explosives, namely: the possibility of controlling energy consumption during objects destruction; absence of brisance that excludes scattering of splinters; absence of harmful substances excretion during destruction; providing a predetermined aimed spalling.

2.5 PDT of cleaning the hulls of ships and fixed offshore platforms from biological fouling [7].

PDT of cleaning ship hulls allows cleaning siding afloat, without entering the vessel to the dock. This PDT is also used for cleaning fixed offshore platforms (FOP) from biological fouling. Technological unit (electrode) is mounted on the element of FOP support structure by divers, fixed on it with defined working gap relatively to fouling and then is connected to GPC. High voltage pulsed corona discharge in medium with high conductivity (sea water) creates pressure waves and high speed hydro streams that destroy biological fouling on support constructions of FOP. Electrodes are moved across processed surface in the longitudinal direction at a distance of 1500 mm. Then they are rotated by predetermined angle (from 30º to 6 º), and the electrodes are moved in the opposite direction. Then technological unit is relocated to new area and abovementioned operations are repeated. PDT of cleaning ship hulls and fixed offshore platforms from biological fouling provides the performance of at least 200 m^2/h; it is collapsible for staff; device is mobile, easy to operate. Device withstands the current standards of environmental control. Mechanisms and components of equipment have a high operational reliability and do not require frequent maintenance and replacement of consumables.

2.6 PDT of rods knockout and castings cleaning *[8]* is to use the power factors of high-voltage discharge in water between the special electrode and the surface of the casting. In this case the shock waves arise in fluid which destroy the rods and mixture baked-on to the casting, cleaning its surface. Destruction of material is possible when creating critical stress in it. Moreover, destruction efficiency depends only on the time during which this condition persists.

With regard to the factors of the electrical discharge in the liquid rods destruction occurs under the action of the stress waves generated by the shock waves, and due to the pressure of fluid flow generated by post-discharge processes. The role of each of these factors is determined by the physical properties of the material rods, characterized by their acoustic stiffness. Electrohydraulic devices are used for knockout of rods from steel, iron castings, castings of non-ferrous alloys. These devise can be used in a single, small-scale and commercial production. Their most appropriate application is knockout of rods from large and medium sized castings.

Advantages of PDT of rods knockout are that it provides high performance and efficiency, eliminates hard manual labor, and reduces dust in the air in foundries.

2.7 PDT of crushing and grinding of artificial materials [9, 10], obtained by chemical reduction and melting or by crystal growth. Such materials include fused silica, refractory carbides, metallurgical and monocrystalline silicon, superhard materials (diamonds, cubic boron nitride). PDT of crushing and grinding of artificial materials because of the action of the ED as a source of high energy density have the ability to control the process of disintegration and to produce a product with a given fractional composition while minimizing waste and

pollution of metal hardware, can significantly reduce the capital and energy costs and has small dimensions of the equipment.

2.8 PDT of carbon nanomaterials synthesis [11].

Under the influence of powerful electric discharge pulses in liquid hydrocarbons appears a region of high pressure and temperature, in which the destruction and decomposition of hydrocarbon molecules takes place The ultimate degradation products are carbon in the solid phase, and hydrogen as a gas. In this case, the carbon can be emitted in different allotropic forms. In the process of electrical discharge treatment the composition of the organic liquids does not change, but the decomposition of the molecules occurs to form a solid phase - hydrocarbon nanomaterials (HCNM), and hydrogen and gaseous hydrocarbons excrete. The dry powder output nonlinearly increases with the number of carbon atoms in the molecules of the organic liquid and linearly - with the increase in the specific energy input.

Electrical discharge treatment of organic liquids produces amorphous carbon, short-range order of which is determined by the degree of hybridization of carbon atoms and by molecular structure of the original liquid. Retaining the same degree of hybridization of carbon atoms after the discharge treatment is caused by the choice of single discharge energy and by and the ratio of the energy of C-C and C-H bond breaking the hydrocarbon molecules.

Obtained HCNM show hydrogen sorption, electrokinetic, magnetic, anti-friction and anti-wear properties. PDT of hydrocarbon nanomaterials synthesis by electric explosion and electric discharge treatment of condensed carbon-containing substances allow obtaining nanomaterials with different functional purpose:

- carbon nanomaterials, use of which as additives to the magnesium during the mechano-chemical synthesis leads to improved sorption kinetics of hydrogen and a significant decrease in hydrogenation temperature regimes;
- intelligent anti-friction and anti-wear carbon nanomaterials containing nanographite, amorphous carbon nanotubes and nanofibers, which are promising additives for motor oil, transmission fluid;
- nanocarbon materials with strong magnetic properties (the value of specific saturation magnetization reaches values close to typical ferromagnets - 57 $A \cdot m^2/kg$);
- carbon nanomaterials containing higher fullerenes and endometallfullerenes.

The advantages of hydrocarbon nanomaterials synthesis PDT are high performance, continuity and wastelessness of processes.

2.9. PDT of carbon nanomaterials (CNM) production by plasma-chemical synthesis from carbon-containing gases [12].

The essence of the PDT of nanocarbon synthesis from gas carbonaceous raw material is to obtain a nonequilibrium plasma under the action of pulsed high frequency discharges and due to the high temperature and pressure gradients. As a result of this method of synthesis carbon nanomaterials have a low bulk density (13.4 kg/m^3) and high specific surface area (SBET ~ 80 m^2/g). Composition of synthesis products obtained by a high-frequency discharge-pulse method of the carbon-containing gas (a mixture of propane, butane, acetylene) is essentially uniform, up to 90% of the particles have a similar form of granules with dimensions of the order of 15 to 35 nm, the yield of pure nanocarbon is up to 35 g/(kVt·h). Synthesis products are characterized by high content of chemically pure carbon up to 99%, confirming the possibility to eliminate the laborious cleaning operation. PDT produces virtually the entire spectrum of known allotropes of nanocarbon including carbine and graphene.

2.10 PDT of obtaining highly wear-resistant metal-matrix composites, dispersion-hardened by nanoparticles [13].

PDT of obtaining highly wear-resistant metal- dispersion-hardened composites is based on the ability to effectively use the latest methods of influence of highly concentrated energy flows on disperse systems – dispersion, activation and synthesis of polydisperse micro (from 10^{-5} to 10^{-7} m) and nanosized (from 10^{-7} to 10^{-9} m) composite powders with their subsequent consolidation by relatively low-temperature method of spark plasma sintering. Through the use of effects of necessary disperse phases excretion during a high-voltage ED impact on elementary powders and their mixtures heterogeneity of the blend may be artificially created and the rate of grain growth may be influenced by high-speed method of spark plasma sintering.

PDT of obtaining highly wear-resistant metal-matrix composites, dispersion-hardened by nanoparticles is directed upon obtaining highly wear-resistant composites of “carbide steel” type and new composites with metal binders for products of structural and instrumental purpose, working in conditions of friction and high loads, such as details of oil and gas pumps, parts of metallurgical and mining equipment, amenable to significant wear (guide rollers of wire rolling mill, etc).

Fundamentally new compositions of highly wear-resistant dispersion-hardened materials, based primarily on the domestic resource base, in particular – on iron, titanium, large reserves of which are located in Ukraine that provides a significant level of export replaceability of raw materials, are developed.

The advantages of PDT processing methods should include the increase of both strength and wear resistance of materials (by 30-60% or more) due to the fact that unlike conventional methods, the disperse reinforcement particles are not mechanically introduced into the powder mixture as an additional component in the blending of powders, but instead are generated by a reaction with an electric synthesis during ED processing of elemental powders and mixtures thereof in a hydrocarbon liquid. This provides not only a high degree of dispersion, but also significantly higher strength of adhesive bond between reinforcing microparticles and the base material.

Using a high-speed heating and lower maximum temperature holding time during spark plasma sintering of polydisperse micro and nanoscale composite powders produces compacts with higher relative density and a finer structure than when using conventional sintering techniques such as hot pressing and hot isostatic pressing.

In IPPT NASU an experimental system for spark plasma sintering "Gefest-10" [14], which is based on the direct passage o of output current with a peak value of 1 kA (superposition of direct and alternating current of high frequency (10 kHz) through the powder composition, was developed . Direct current heats evenly all section of the briquette, but due to the heat sink peripheral areas are cooled. The alternating current, due to skin effect, is partly displaced to the surface of specimens section, so it preferably carries out heating of the peripheral portion. This compensates for the effect of the heat sink and aligns the temperature conditions in the cross section.

Developed technological methods allow us to offer to market a simplified flow diagram for production of multifunctional materials, dispersion-hardened by nanoparticles, which can be used to significantly improve the wear resistance and heat resistance of tools for different purposes, and structural materials for reactor steels with high heat resistance characteristics, engines for different purposes, etc.

3. Conclusion

The analysis of PDT used in oil production, engineering, instrumentation, metallurgy, chemical industry, mining complexes, etc is performed in present review.

The use of high voltage electric discharge in different mediums allows to impact both changes of geometrical size and the structure of objects in order to give it certain mechanical and physical properties.

The Institute of Pulse Processes and Technologies of NAS of Ukraine designed and tested in the industry more than 40 different pulsed discharge technological processes: stimulation of oil wells; synthesis of hydrocarbon nanomaterials; removing rods from castings; crushing and grinding of materials; destruction of oversized and old foundations; regeneration of molding compounds; preparation of structured liquids; dispersion of mineral environments; activation of water and cement mortar; hardening of machine parts and stamping; fixing the pipe ends in the tube sheets of heat exchangers; calibration; compaction of the powder material; metal forming (rolling, drawing, extruding); processing of salt slag; intensification of the processes of casting and solidification of metals and alloys, etc.

Evolution of PDT and creation of new electric discharge devices is directed upon development of new pulsed technological processes for processing and obtainment of new materials.

4. References

1. **Малюшевский, П.П.** Основы разрядно-импульсной технологии / П.П. Малюшевский. – Киев: Наук, думка, 1983. –272 с.

2 **Сизоненко, О.Н**. Электроразрядное воздействие на структуру пористых материалов и динамику фильтрации в них углеводородных флюидов: Автореф. дисс. на соискание ученой степени д-ра техн. наук: спец. 05.02.01 «Материаловедение»/ О.Н. Сизоненко. – Киев, 2007. – 43 с.

3. **Пат. 97183 Україна, МПК(2011) B01D 41/00**. Спосіб електрогідроімпульсної регенерації пористого фільтроелемента / О.М. Сизоненко, Е.І. Тафтай, А.С. Торпаков, А.Д. Зайченко, Є.В. Липян; заявник і патентовласник ІІПТ НАН України. – № a2010 06095; заявл. 20.05.2010; опубл. 10.01.2012, Бюл. № 1. – 4 с.

4. **Грабовый В.М.** Научные и технологические основы электрогидроимпульсного воздействия на структуру и свойства отливок из сплавов на основе железа и алюминия: Автореф. дисс. на соискание ученой степени д-ра техн. наук: спец. 05.16.04 «Литейное производство»/ В.М. Грабовый. – Киев, 2007. – 42 с.

5. **Пат. 64899 Україна, МПК(2006) B21D 26/12.** Спосіб імпульсного електрогідравлічного штампування / М.В. Старков, С.В. Сокол, Л.І. Стрелковська; заявник і патентовласник ІІПТ НАН України. – № u2011 04241; заявл. 07.04.2011; опубл. 25.11.202011, Бюл. № 22. – 3 с.

6. **Пат. 79148 Україна, МПК(2006) E21C 37/18, B02C 19/18.** Спосіб електрогідроімпульсного руйнування міцних монолітних об`єктів під водою / О.І. Вовченко, І.С. Швець, В.С. Блінцов, А.Р. Різун, Ю.В. Голень, С.А. Яцюк; заявник і патентовласник ІІПТ НАН України. – № a2005 02999; заявл. 01.04.2005; опубл. 25.05.2007, Бюл. № 7. – 2 с.

7. **Пат. 84983 Україна, МПК(2006) B63B 59/00, B08B 3/10, H01M 4/00.** Спосіб електророзрядного очищення підводних металоконструкцій від біологічного обростання / О.І. Вовченко, М.А. Заблудовський, І.С. Швець, В.В Барліт, А.Р. Різун, Л.З. Богуславський, Ю.В. Голень; заявник і патентовласник ІІПТ НАН України. – № a2007 04322; заявл. 19.04.2007; опубл. 10.12.2008, Бюл. № 23. – 3 с.

8. **Пат. 75782 Україна, МПК(2006) B22D 29/00.** Спосіб очищення виливок точного лиття / Т.Д. Денисюк, А.Р. Різун, І.С. Швець, Ю.В. Голень; заявник і патентовласник ІІПТ НАН України. – № 2004 0705934; заявл. 19.07.2004; опубл. 15.05.2006, Бюл. № 5. – 3 с.

9. **Пат. 100268 Україна, МПК(2012) B02C 19/18, C01B 33/00.** Спосіб електророзрядного подрібнення металургійного кремнію / А.Р. Різун, Ю.В. Голень, Г.М. Морев, Г.П. Муштатний, В.Ю. Кононов, Т.Д. Денисюк, Л.О. Жекул, Н.І. Сиворижська, О.М. Рачков; заявник і патентовласник ІІПТ НАН України. – № a2010 15158; заявл. 16.12.2010; опубл. 10.12.2012, Бюл. № 23. – 5 с.

10.**Пат. 49909 Україна, МПК(2010) B24D 3/06, C01B 31/06.** Спосіб виготовлення мікропорошків надтвердого матеріалу / Г.П. Богатирьова, А.Л. Майстренко, О.М. Сизоненко, Н.О. Олійник, Г.Д. Ільницька, Г.А. Петасюк, Ю.В. Нестеренко, Е.І. Тафтай, А.С. Торпаков, Є.В. Липян; заявник і патентовласник ІІПТ НАН України та ІСМ ім. Бакуля НАН України – № 200913969; заявл. 30.12.2009; опубл. 11.05.2010, Бюл. № 9 – 5 с.

11.**Кускова Н.И.** Процессы взаимодействия мощного импульса тока с конденсированным веществом: Автореф. дисс. на соискание ученой степени д-ра техн. наук: спец.05.03.07 «Процессы физико-технической обработки»/ Н.И. Кускова. – Киев, 2007. – 37 с.

12.**Пат. 101891 Україна, МПК(2013) C01B 31/02, B82B 3/00.** Електророзрядний спосіб синтезу вуглецевих наноматеріалів / Л.З. Богуславський, Д.В. Вінниченко, Н.С. Назарова; заявник і патентовласник ІІПТ НАН України. – № a2011 12712; заявл. 31.10.11; опубл. 13.05.13, Бюл. № 9. – 6 с.

13.**Пат. 97890 Україна, МПК(2012) C01B 31/30, B01J 3/06, B22F 9/14, B82B 3/00.** Спосіб одержання карбідів металів перехідної групи / О.М. Сизоненко, Е.І. Тафтай, О.І. Райченко, Г.А. Баглюк, А.С. Торпаков, Є.В. Липян, А.Д. Зайченко; заявник і патентовласник ІІПТ НАН України. – № a2010 11723; заявл. 04.10.10; опубл. 26.03.12, Бюл. № 6. – 6 с.

14. **Пат. 101575 Україна, МПК(2006) B22F 3/14, B22F 3/105, B30B 15/02.** Пристрій для іскроплазмового спікання порошків / О.М. Сизоненко, А.І. Івлієв, О.І. Райченко, В.В. Литвинов, А.Д. Зайченко, С.Д. Конотоп; заявник і патентовласник ІІПТ НАН України. – № a2012 00957; заявл. 30.01.12; опубл. 10.04.13, Бюл. № 7. – 5 с.

THE ROLE OF SEVERE PLASTIC DEFORMATION IN THE FORMATION OF HIGH ELECTRICAL PROPERTIES OF ALUMINUM ALLOY

РОЛЬ ИПД ПРИ ФОРМИРОВАНИИ ПОВЫШЕННЫХ СВОЙСТВ ЭЛЕКТРОТЕХНИЧЕСКОГО АЛЮМИНИЕВОГО СПЛАВА

Prof. Raab G.I., PhD Stud. Fakhretdinova E.I.[+]
Ufa State Aviation Technical University, Ufa, Russia
[+]corresponding author, e-mail: yelka89@mail.ru

Abstract: *At present time there is considerable interest in extending the application area of low-alloy and rather inexpensive heat-hardenable aluminum Al-Mg-Si alloys in the automotive industry, aviation, construction and electrical engineering. In this regard, the topical problem is to enhance strength and electrical conductivity of such materials, which would subsequently reduce the weight of products made of structural and electrical Al-Mg-Si materials. Severe plastic deformation is one of the promising methods of obtaining a significant increase in properties. In this paper a new SPD method is investigated – Multi-ECAP-Conform, characterized by the fact that per one processing cycle the accumulation of true strain is provided up to e>2.5. In order to study the stress-strain state effect on the mechanical properties of the aluminum Al-Mg-Si alloy, mathematical and physical modeling with the modern software Deform-3D were applied, as long as the well-established techniques of assessment of materials mechanical characteristics after plastic processing. The obtained results demonstrate the adequacy of using mathematical and physical modeling to estimate the stress- strain state by Multi-ECAP-Conform.*

KEYWORDS*: ALUMINUM ALLOYS, SEVERE PLASTIC DEFORMATION METHODS, ULTRAFINEGRAINED STRUCTURE, MATHEMATICAL MODELING*

1. Introduction

Currently, there is a considerable interest in extending the range of application of low-alloy and relatively cheap thermally hardenable aluminum Al-Mg-Si alloys in automotive industry, aviation, construction and electrical engineering [1-3]. In this regard, the topical problem is to enhance mechanical properties of such materials, which would reduce dimensions and, hence, the weight of produced articles. One of the ways of increasing strength and other properties of aluminum alloys is severe plastic deformation (SPD), which makes it possible to produce an ultrafine-grained structure and achieve enhanced properties via several cycles of deformation combined with heat treatment [4]. The most advanced for commercial application techniques are ECAP-Conform and ECAP in parallel channels (ECAP-PC), which ensure the UFG structure formation via high-cycle processing in elongated and discrete billets with high metal utilization factor. But these techniques have disadvantages – the process duration (multi-cycle processing) and higher energy consumption. In order to remove the above shortcomings, we developed a new modification of ECAP-Conform (Multi) providing the enhanced – ~ 3 times – level of accumulated strain in one processing cycle. In this regard, a thorough study of the features of the new ECAP-Conform modification is required, including the investigation of the stress-strain state and its relationship with mechanical and functional properties of the aluminum Al-Mg-Si alloy.

2. Principle of Multi-ECAP-Conform processing

The main feature of Multi-ECAP-Conform is that in combines the advantages of a continuous process of ECAP-PC and ECAP-Conform resulting in a significant change of the deformation scheme at a pressing stage, as compared to other SPD methods. The process is implemented as follows: the metal billet 1 in the form of a rod is subjected to continuous angular pressing; it is fed to the input of a working channel formed between the rotating roll 2 with U-shaped engraving and a fixed limiting base (shoe) 3, surrounding the turning roll and covering a part of the groove length of. Via the roll 2 rotation and frictional forces appearing between the engraving and the billet 1, the billet is moved through the working channel in the direction towards the outlet in the shoe 3.

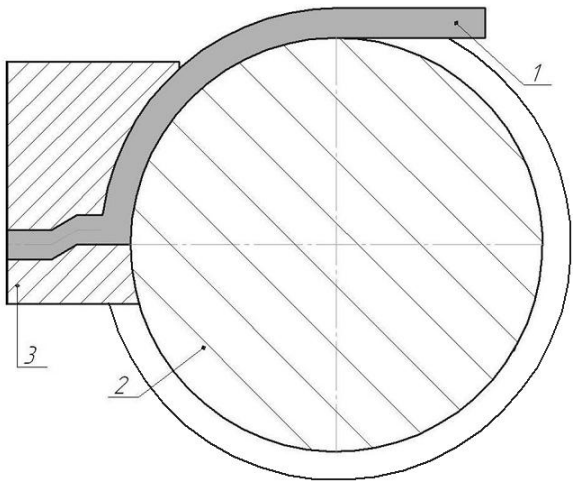


Fig. 1. *Scheme of Multi-ECAP-Conform:*
1 - billet, 2 - roll, 3 - limiting base

In this regard, the purpose of this work is to study the stress-strain state of the Multi-ECAP-Conform and the impact of this process on the mechanical and functional properties of aluminum Al-Mg-Si alloys.

3. The process modeling

The analysis of the proposed scheme was performed using mathematical modeling on software DEFORM-3D [6]. The material of the initial billet is aluminum (Al-6101), its size is 12x12 mm, the cross-section of the final product – wire rod – is 11x11 mm.

Conditions and assumptions used in modeling on software DEFORM-3D:

- The billet material in the initial state (before straining) is isotropic and has no initial stresses and strains;
- The billet temperature is assumed constant – 20 ºC, the deformation heating is disregarded;
- The tool is assumed absolutely rigid; geometry of the tool – 3D models – were previously created in KOMPAS 3D 11V and saved with the extension stl;
- The initial billet material is assumed ductile;

- The material taken for modeling AL 6101, the hardening curves were taken from the DeForm-3D library;
- The coefficient of friction (shear) between the rolls and the billet was taken equal to 0.5, between the die and the billet – 0.5 (recommended for use);
- The number of modeling steps - 620...1030, with a step of 1 s.
- The roll speed is 40 turns per minute.

Results of computer modeling show that compressive stresses dominate in the deformation sites – this affects the fabrication of defect-free semi-products in a positive way. At the output to the horizontal channel the area with tensile stresses is observed (Fig. 2). We should note that the tensile stresses do not exceed 100 MPa and are close to the alloy yield stress value at the temperature of straining.

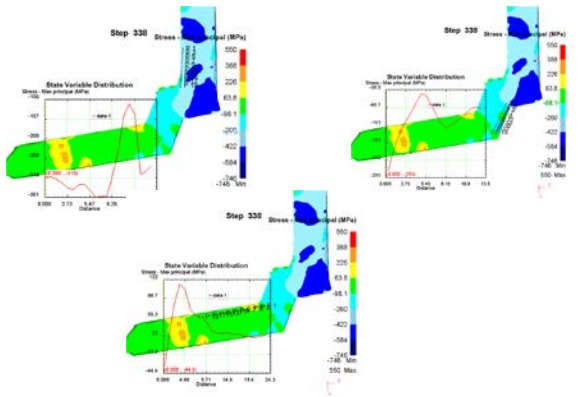


Fig. 2. *Maximum stresses occurring during Multi-ECAP-Conform*

Computer modeling results show that in the billet longitudinal section the strain intensity is e = 4.5…4.7 units, and in the cross section ~ 6 units (Fig. 3). It is known that the level of accumulated strain exceeding e = 4-5 typically results in the UFG structure formation during ECAP [9], therefore, accumulation e=4-5 per processing cycle under Multi-ECAP-Conform is a sufficient factor for the formation of an ultrafine-grained structure. This is also evidenced by the high level of obtained mechanical and functional properties of semi-finished products.

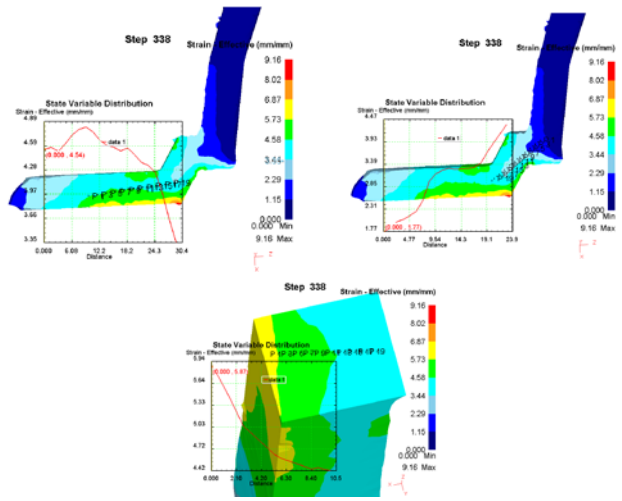


Fig. 3. *Pictures of the intensity distribution in the sample deformation, with Multi-ECAP-Conform*

4. Results of experimental studies

For research we used the aluminum alloy Al 6101 (Al-basis, 0.8 Mg-0.41Si-0.1Cu-0.03Mn-0.5Fe-0.1Zn wt.%) in the cast homogenized state. The billets of 12 mm in diameter and 150 mm in length were cut from the initial ingot.

Before Multi-ECAP-Conform, the billets were subjected to annealing at 540 °C and subsequent quenching in water.

In this study we used the original setup for Multi-ECAP-Conform designed and fabricated in the Institute of Physics of Advanced Materials, USATU [5].

We conducted tensile tests to evaluate the mechanical properties according to GOST 10446-80 at room temperature on Instron 1114. The traverse speed was 1 mm/min. The force measurement accuracy is 1 %. Strength characteristics were determined in accordance with GOST 1497-84, using the tensile test results of samples with the working part of Ø3 mm x 15 mm.

Electrical resistivity (ρ) was determined according to GOST 7229-76 and GOST 12177-79 using test equipment: aspirated psychrometer MV-4M (accuracy ± 2 %), barometer – aneroid BAMM-1 (division value 0.1x103 Pa) and microohmmeter BSZ (accuracy class 0.1).

The measurements were performed on straightened wire samples of 1000 mm in length. The wire sizes were measured by a metal ruler with a scale of 1 mm and micrometer MK-25 with a division value of 0.01 mm. The measurement error was no more than 1%. The ambient temperature was 23.5 °C (with account of the temperature coefficient according to GOST 7229-76 - 0.9745), atmospheric pressure – 100.1 kPa, relative humidity – 55%.

Electrical resistivity (ρ) was calculated using the formula [7, 8]:

$$\rho = \frac{R \cdot l}{S}, \qquad (1)$$

where R – the measured electrical resistance;
S - the cross sectional area of the sample;
l - length of the sample

After ECAP, the billet was subjected at room temperature to drawing to a diameter of 3 mm. The results of tensile tests on the wire made it possible to obtain tensile strength equal to 375 ± 10 MPa, which exceeds standard values of this alloy 60-100 MPa

Electrical resistivity is 30.94 Ohm/km for 1 mm^2 (55.7 %), and total elongation is over 3 %, which is a consequence of the UFG structure formation and is similar to the results of similar studies carried out according to the traditional ECAP scheme [10].

5. Conclusions

1. The stress-strain state of a new method of Multi-ECAP-Conform was investigated:

- it was revealed that at a stage of steady flow the accumulated strain reaches e = 6, which typically ensures the formation of an ultrafine-grained structure and, therefore, has a considerable impact on the increase in mechanical characteristics of semi-products;
- it was established that during Multi-ECAP-Conform mainly compressive stresses are formed in the deformation zones, which contributes to the fabrication of defect-free wires;

2. The obtained values of tensile strength and electrical resistivity of the samples after Multi-ECAP-Conform exceed standard values of semi-products (wires) for electrical purposes, indicating the effectiveness of the new method.

Acknowledgements

The research was supported by the Russian Scientific Foundation grant (project № 14-19-01062) and performed at Ufa State Aviation Technical University.

References:

1. Fridlyander I.N., Sister V.G., Grushko O.E., Berstenev V.V., Sheveleva L.M, Ivanova L.A. Aluminum alloys – the advanced material in automotive industry // Physical metallurgy and thermal treatment of metals. 2002. No 9. P.3-9 (in Russian).

2. Yelagin V.I. Structural nanostructured aluminum-based alloys // Technology of light alloys. 2008. No 2. P.6-20 (in Russian).
3. Alieva S.G., Altman M.B., Ambartsumyan S.M. Commercial aluminum alloys. – M.: “Metallurgy”, 1984. 528p (in Russian).
4. M.Yu. Murashkin, I. Sabirov, V.U. Kazykhanov et al. Enhanced mechanical properties and electrical conductivity in ultrafine-grained Al alloy processed via ECAP-PC // Journal of Materials Science (2013) 48 pp.4501-4509
5. Application for an invention №2013156136 of December 17, 2013 “The method of continuous equal channel angular pressing of metallic rods”. Authors: Raab G.I., Fakhretdinova E.I., Kapitonov V.M., Valiev R.Z.
6. License R.S. SFTS. Key #9190/ Ufa, Russia.
7. Vorontsov L.A., Maslov V.V., Peshkov I.B. Aluminum and aluminum alloys in electrical products. - M.: “Energy”, 1971. 224p.
8. Osintsev O.E., Fedorov V.N. Copper and copper alloys. Russian and foreign grades: reference manuals. – M.: Mechanical Engineering, 2004. 336p.
9. V.M. Segal, V.I. Reznikov, V.I. Kopylov et al. Processes of plastic structuring of metals. - Minsk: Science and Technology, 1994. – 232p.
10. E.V. Bobruk, M.Yu. Murashkin, V.U. Kazykhanov and R.Z. Valiev Aging behavior and properties of UFG aluminum alloys of Al-Mg-Si system // Reviews on Advanced Materials Science 31 (2012) pp.109-115.

DISSIMILAR WELDING AUSTENITIC STAINLESS STEEL S316 WITH FERRITIC STRUCTURAL STEEL GRADE 300NZS

Prof.Dr.Cvetkovski S[1], Dr.Eng. Brkovski D[2] Executive manager,
Faculty of Technology and Metallurgy[1] Skopje, Macedonia, RZ Inter-transped[2] AD Skopje
Macedonia, E-mail: sveto@tmf.ukim.edu.mk, dean_brkovski@intertranssped.com.mk,

ABSTRACT

In this research work, procedure for certification process of dissimilar welding between austenitic stainless steel S316 with structural steel grade 300NZS according EN 15614 standard was explained. Shielded metal arc welding process (SMAW) was used. Welding was performed in PA position with EIS 309 Mo electrode. Qualification test has to confirm that the preliminary welding procedure fulfil quality requirement, and welded joint will satisfy the exploitation conditions. The following investigations were conducted to welded test plate; Visual testing (VT) has to show existence of surface defects in the welded joints. Next step was radiographic testing (RT) in order to check eventually appearing of volumetric defects inside the weld. Finally the plate was cut for mechanical testing. All conducted tests fulfilled requirements except one probe of bend test. Because of that qualification procedure was not successful, and it was completely repeated after two weeks. The repeated welding procedure specification (WPS) was qualified.

KEYWORDS: DISSIMILAR WELDING, S316 AUSTENITIC STEEL, WELDING PROCEDURE, MICROSTRUCTURE, SMAW

Introduction

Welding dissimilar steel is established method in different industrial branches. Many applications exist in industry that requires joining of carbon steels to stainless steels. A typical example can be found in power generation and food process industry. The most common combinations of dissimilar steels involve stainless steel and plain carbon or low alloy structural steel grades [1,2]. Much work has been done to understand the mechanism of dissimilar welding (DW) in such applications. Dissimilar metal welds involving stainless steels can be done using most of the fusion weld methods, including SMAW, TIG and MIG. In selecting the weld filler, the joint is considered as being stainless, rather than the carbon steel. With the progress of steel construction, austenitic/ferritic dissimilar metal joints have become more popular and important [3,4].

In the as-welded condition, a composition gradient develops near the weld interface of the DW due to partial mixing between the two materials. The relatively high hardenability associated with this composition gradient, combined with the high cooling rates associated with fusion welding, produce a thin layer of martensite at the weld interface. It is common to observe hardness differences of more than 200 HV over distances of 250 μm in this transition region. Stainless steel alloys typically have lower carbon levels than the structural steels (0.03–0.08 wt-% C in stainless steels compared to 0.10–0.15 wt-% C in alloy steels). This leads to a carbon concentration gradient across the DW joint. Austenitic stainless steels exhibit a high solubility for carbon and a relatively low diffusivity, while ferritic steels exhibit relatively low solubility and high diffusivity. These differences in carbon solubility and diffusivity, strongly promote carbon migration (i.e., from the high-carbon alloy steel side toward the lower-carbon stainless steel side of the joint). Localized variations in carbon concentration have been measured to be as high as 0.7 wt-% to below about 0.01 wt-%. The hardness in this region can be as high as 500 Vickers. Several hundred microns from this, the carbon denuded ferritic zone can exhibit a reduced hardness on the order of 130 HV.

It is common to observe hardness differences of more than 200 HV over distances of 250 μm in this transition region [5,6]. Stainless steel alloys typically have lower carbon levels than the structural steels. This leads to a carbon concentration gradient across the DW joint. Austenitic stainless steels exhibit a high solubility for carbon and a relatively low diffusivity, while ferritic steels exhibit relatively low solubility and high diffusivity. These differences in carbon solubility and diffusivity, strongly promote carbon migration (i.e., from the high-carbon alloy steel).

Localized variations in carbon concentration have been measured to be as high as 0.7 wt-% to below about 0.01 wt-%. The hardness in this region can be as high as 500 Vickers. Several hundred microns from this, the carbon denuded ferritic zone can exhibit a reduced hardness on the order of 130 HV [5]. Failure of DW in service has been attributed to the sharp microstructural gradients combined with significant differences in thermal expansion between the two materials. In fact, the coefficient of thermal expansion of austenitic stainless steels are ~ 30% higher than alloy steels [7].

A carbon depleted region exists on the ferritic side that has significant localized reductions in tensile and creep strength. Solidification cracking is a significant problem in the austenitic stainless steels welds, particularly in fully austenitic and stabilized compositions. Hot cracking in stainless steel welds is caused by low-melting eutectics containing impurities such as S, P and alloy elements such as Ti, Nb. The WRC- 92 [8,9] diagram can be used as a general guide to maintain a desirable solidification mode during welding [10]. On the contrary, the coarse structures in the HAZ adjacent to the martensite layer are very brittle, so the effect of the martensite layer on the toughness of the joints has to be evaluated properly. The formation of a soft carbon denuded region near the weld interface has been identified as a key factor that leads to accelerated failure under the combined influences of service and thermally induced stresses [11]. Having in mind all negative factors that can influence quality of DW, basic idea in this work is how to avoid them and to obtain welded structure which will satisfy exploitation conditions.

Material and experimental

Two plates were prepared for dissimilar welding (Figure 1). One plate was from austenitic stainless steel S316 and the second plate was from S300NZS structural steel. Prior to welding both plates were machined in order to obtain V groove preparation, Groove angle is 60^0, and groove throat is 2 mm. (Figure 1a), Prepared plates were tack welded with short welds. Welding of plates was performed using SMAW process. EIS 309 Mo stainless electrode was used as filler material. This electrode is recommended for welding of dissimilar austenitic/ferritic steels. The electrodes should be drayed in oven at 300^0/C3h. Chemical composition of filler and base materials are given in table 1. Welding parameters (Table 2) are in accordance with preliminary welding procedure based on personal experience and literature dates. Welding was performed in PA position. Number of passes and order of filing the welding grove is given in Figure 2b. After filling the groove, the plate was turn over and root pass was complete gouged and cleaned. Then, that, new root pass is laid. In this way eventuality for welding defects in the root of welded joints are minimal.

After finishing welding of test plate, investigations of welded joint were performed. As first, visual testing (VT) was done. Characteristic surface defects were not detected. After that

radiographic testing (RT) was performed using X-ray tube type GE ERESCO MF3.1 (figure 3). Radiographic films, AGFA D7 (Vacupac) with dimensions 300x100 mm covered Pb foils are used for recording of weld. Recording of plates was conducted from distance (FFD) of 700 mm. Exposition parameters are160 KV, 5mA and exposing time 0.7 s. Radiographic testing detects pores in the weld, but these defects are acceptable according EN ISO 25817. Next step was mechanical testing. Probes were cute from characteristic position according EN15614. Two probes were prepared for tensile testing. Results of tensile test are given in table 3. In both cases probes were torn in base metal and obtained results were satisfactory.



Figure 1. *Prepared plates for dissimilar welding*

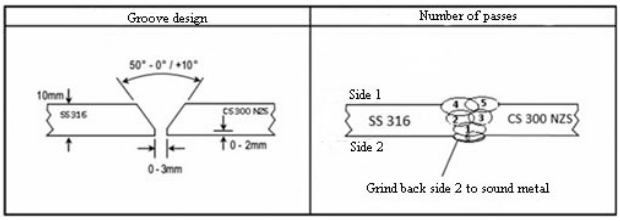


Figure 2 (*a and b) a. Weld groove preparation. b*

According EN15614-1, four probes are prepared for bend testing. Two of them were bended from face side and two from the root side of weld. Bending angle is 180^0, and diameter of former 40 mm. Three probes fulfilled testing requirement but one failed. From the broken surface was concluded that clusters of pores are reason for that (figure 4). So bend testing was not successful.

Table 1 *Chemical composition of base and filler metal*

Elements,%	S316	S300NZS	E309Mo
C	0,08	0,16	0,07
Mn	1,8	1,3	1,0
Si	0,7	0,24	0,8
P	0,015	0,020	-
S	0,020	0,017	-
Cr	17,5	-	22,0
Ni	12,5	-	12,0
Mo	2,6	-	2,5
Ni	0,08	-	-

Table 2 *Welding parameters*

Welding parameters	
Current, A	120-130
Arc voltage, V	75-85
Welding speed, mm/min	220
Heat input, Q, J/mm	235

Impact toughness (Charpy) testing was performed at -15 ^{0}C. Tree probes with standard dimensions 55x55x10 and V-notch in weld root was prepared. Average value from three measurements (64, 60, 56) is 60J. Position of sampling specimen can be seen in figure 5

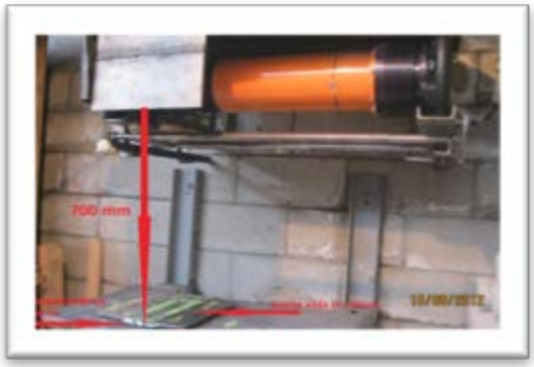


Figure 3 X-ray tube

Table 3 Results of tensile testing

Tensile testing	Probe 1	Probe 2
$Rp_{0.2}$, MPa	341	348
Rm, MPa	475	476

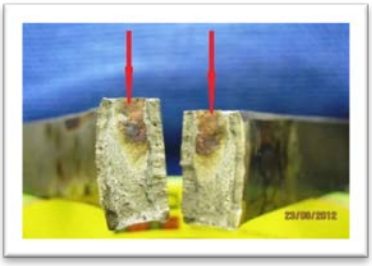


Figure 4 *Bend test pores on broken surface*

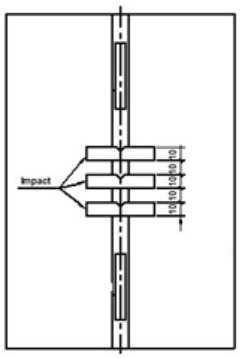


Figure 5 *Sampling of charpy specimens*

Vickers method HV10 was used for hardness measurement. As can be seen from figure 6 these measurement are performed from both sides of welded joints, across the lines two millimetres beneath the surfaces. Measurements include BM, weld and HAZ. Results of measurements are given in table 4.

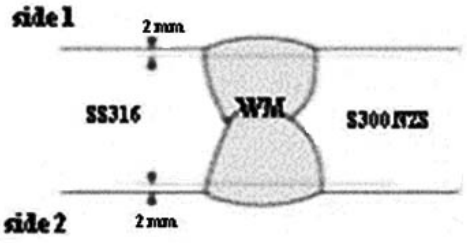


Figure 6 *Hardness (HV10) measurements in dissimilar weld*

***Table 3**. Measured hardness values (HV10}*

Hardness	Side 1	Side 2
BM_{S316}	148	155
$BM_{S300NZS}$	179	176
HAZ_{S316}	158	165
$HAZ_{S300NZS}$	183	186
WM	193	193

Standard metallographic preparation of specimen was performed. Nital (3%) was used for etching of S300NZS steel and V2 etchant for stainless steel S316 and weld metal. Macro photo of welded joints is given in figure 7. Welding defects were not found. Penetration is pretty good. Micro photos of characteristic structures are given in figure 8.



Figure 7 Macro photo of dissimilar weld

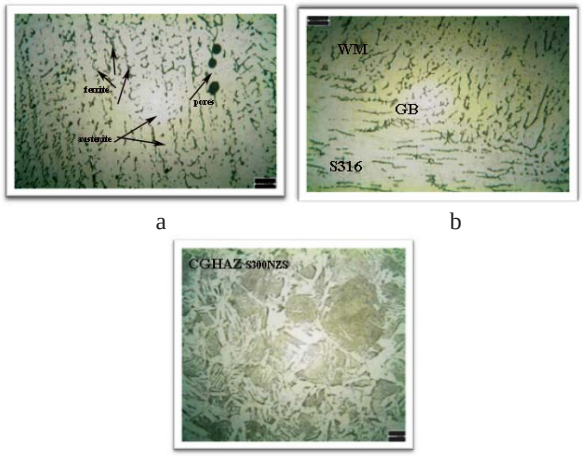


***Figure 8(a-d)** Microstructures in dissimilar austenitic/ferritic weld*

Microstructure of weld metal is given in figure 8a. Its consists of austenite and δ ferrite, Ferrite shape is lacy and vermicular, Transition from weld metal to austenitic S316 steel is given in figure 8b. In figure c is given coarse grain HAZ. Primary austenitic grains are clearly seen. Proeutecoide and Widmanstaten ferrite on grain boundaries can be seen too. Inside the grains microstructure consists of bainite and martensite. Grain boundary between weld metal and plain steel S300NZS can be seen to. Martensitic layer near grain boundary is detected too.

Discussion

Welding of similar structural or similar stainless steels is not some difficult task, but welding of dissimilar austenitic/ferritic steels is always big challenge. The main reason is different chemical and physical properties of both types of steel [11]. Anyhow dissimilar welding is implemented in many industrial sectors long time ago. In our case tank for milk transportation has to be welded to track chassis. S316 steel, together with S304 is the most often implemented for production of food industry equipment. Because of that S316 is chosen as a material for milk tank production. But material for chassis can be ordinary structural steel. It means that dissimilar welding of these materials has to be performed. The first step is qualification of welding procedure. EIS 308 and EIS 309 are recommended as filler materials for SMAW of dissimilar austenitic/ferritic steels; more alloyed E 309 electrode was chosen in this case. Producers of this electrode guarantee about 15% δ ferrite in pure weld metal. As can be seen from Schaefer diagram in our case calculation showed 18%. Presence of δ ferrite in weld metal is necessary to supress appearing of hot cracks in weld metal. But during welding, as result of mixing between base materials and electrode, percentage of δ ferrite in weld will be changed. To check it the following analyse was performed using Schaefer diagram, (figure 9). Ni and Cr equivalent of base materials were determined first; for both base materials and EIS309 electrode. Assuming that dilution of base materials is 50% and 25% is dilution of electrode; it was calculated 9% δ ferrite in the weld metal. Literature dates indicate that 5-10% δ ferrite is useful in weld metal to supress hot cracks [12].

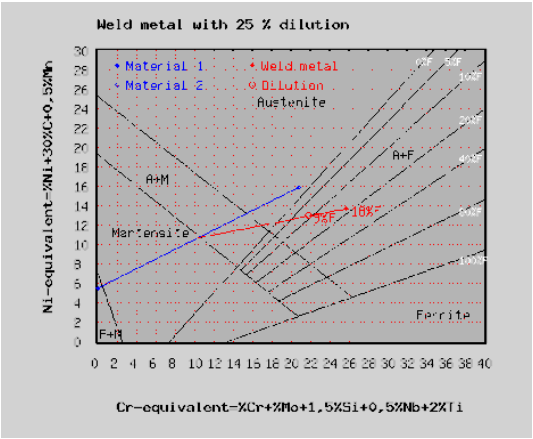


***Figure 9** Calculation % δ ferrite in weld metal*

Metallographic investigations showed that type of crystallisation is AF. It means that during crystallization and cooling of weld, austenite appears first and at lower temperatures δ ferrite forms. It can be seen from the figure 8a that d ferrite appear in the form of lacy and vermicular ferrite. Martensitic layer can be seen on the figure 8d (black arrow), but measurements don't confirm it. To obtain more exact hardness values micro hardness measurements has to be performed

Conclusions

Performed testing of dissimilar welding plates confirmed that welding parameters and filler materials was properly assigned. The reason for failing of one bend probe during the first test is presence of pores in welds. Appearing of pore is not unknown think during SMAW. Porosity is caused by moisture on the work metal ore Moisture in the electrodes, oil ore grease on the plate surface. These reasons can be easily removed and weld without pores can be obtained. This was confirmed during repeated welding procedure. According EN ISO 15614 standard complete procedure was performed and all tests were successful.

Literature

[1] Wei-Chih Chung, Jiunn-Yuan Huang, Leu-Wen Tsay and Chun Chen Microstructure and Stress Corrosion Cracking Behavior of the Weld Metal in Alloy 52-A508 Dissimilar Welds, Materials Transactions, Vol. 52, No. 1 (2011) pp. 12 to 19

[2] Ramazan Kacar, Orhan Baylan, An investigation of microstructure/property relationships in dissimilar welds between martensitic and austenitic stainless steels, Materials and Design 25 (2004) 317–329.

[3] Heinrich, K. F. J. 1986. Microbeam Analysis, Proceedings of 21st International Conference. Eds. A. D. Romig Jr. and W. F. Chambers. 279 to 280.

[4] J. N. DUPONT and C. S. KUSKO, Technical Note: Martensite Formation in Austenitic/Ferritic Dissimilar Alloy Welds,
Welding journal, February 2007, 51s-54s

[5] ZHIHUI WANG, BIYU XU, AND C1QI YE, Study of the Martensite Structure at the Weld Interface and the Fracture Toughness of Dissimilar Metal Joints, Welding Journal, August 1993, 397s-402s.

[6] Sveto Cvetkovski, Rudolf Vallant, Klaus Kerschbaumer, WELDING OF ULTRA HIGH-STRENGTH STEEL (UHSS) WITH AUSTENITIC METAL POWDER WIRE (MPW) Metalurgija-MJoM Vol 17 (4) 2011 p. 199-212

[7] Barnhouse EJ, Lippold JC. Microstructure/property relationship in dissimilar welds between duplex stainless steel and carbon steels. Welding J 1988;(December):477–87.

[8] G. Lothongkum, E. Viyanit, and P. Bhandhubanyong; Study on effects of pulsed TIG welding parameters on delta-ferrite.
content, shape factor and bead quality in orbital welding of AISI 316L stainless steel plate, Journal of Materials Processing Technology, v.110 (2001) 233-238.

[9] American Institute of Chemical Engineers, Guidelines for welding dissimilar steel, Chemical engineering progress, May 1991

[10] Nelson TW, Lippold JC, Mills MJ. Nature and evolution of the fusion boundary in ferritic–austenitic dissimilar metal welds – Part 2: On-cooling transformations. Welding J 2000;(October): 267–77.

[11] Barnhouse EJ, Lippold JC. Microstructure/property relationship in dissimilar welds between duplex stainless steel and carbon steels. Welding J 1988;(December):477–87.

[12] V. Shankar, R.W. Messler Jr., Segregation of phosphorus and sulfur in heat-affected zone hot cracking of type 308 stainless steel. Welding Journal, (2002) 78–84.

[13] G. Madhusudan Reddy, K. Srinivasa Rao, Microstructure and mechanical properties of similar and dissimilar stainless steel electron beam and friction welds, The International Journal of Advanced Manufacturing Technology, December 2009, Volume 45, Issue 9-10, pp 875-888.

COMBINED APPROACH FOR MODELING OF MANUFACTURING EXECUTION SYSTEMS

КОМБИНИРАН ПОДХОД ЗА МОДЕЛИРАНЕ НА СИСТЕМИ ЗА ОПЕРАТИВНО УПРАВЛЕНИЕ НА ПРОИЗВОДСТВОТО

Assoc. Prof. Dr. Eng. Antonova I. D.
Dept. of Industrial Automation, University of Chemical Technology and Metallurgy
Bul. Kl. Ohridski 8, Sofia, Bulgaria

iskra.antonova@uctm.edu

Abstract: *For successful and efficient development of unified modeling framework and software process model (SPM) for MES a new approach is needed. In this paper a modeling framework and SPM that integrates UML profile for system engineering SysML, ANSI/ISA-S95 standard and MES-ML modeling language for MES modeling and specification is presented. The proposed approach is illustrated with a real industrial Pick and Place Unit. Finally some conclusions are made.*

Keywords*:* MES, UML, SysML, ANSI/ISA-S95, MES-ML

1. Introduction

Manufacturing systems are becoming more and more complex and there are many working groups whose research activities are directed in finding new modeling approaches for managing this complexity and for development of software process model (SPM). MES are combined, information, process-oriented and event and time activated software systems which main purpose is to link the automation layer to business planning and logical layer (ERP) [1]. One of the major challenges facing manufacturing today is ability to accurately express the information from multiple disciplines - mechanical, electrical and software engineering used of Manufacturing Execution Systems (MES). Another challenge is connected with the development of unified modeling framework for modeling of the important views of MES components using different modeling languages and standards.

The engineering and specification of MES is an interdisciplinary process which integration requires a modeling language able to represent software, hardware and their interactions. The rapid progress of computer technologies leads the possibilities for development of new methodologies, methods and approaches suitable for development of software and hardware in industrial systems. Some of the most promising and challenging approaches are these of Model Driven Development (MDD) and Model Driven Engineering (MDE) [2], where the systems are presented as models that conform to meta-models, and the model transformations are used to manipulate the various representations. Model Driven Architecture (MDA) [3] is a remarkable MDD initiative of Object Management Group (OMG), consisting in transformation of different platform independent models towards executable applications. In the core of MDA are the open standards - UML, MOF, XMI, etc. UML [4] does not specify a methodology for model driven software or system development but aims to provide an integrated modeling framework, covering structural, functional and behavior descriptions.

The currently available MES, based on traditional approaches, have monolithic architecture, are not flexible enough and have a limited scope. Due to the difficulties in their configuration and adaptation to specific needs, they do not meet the requirements of modern industry. The main trend to overcome these shortcomings is the use of new, advanced software process model (SPM) for MES development.

The main aim of the proposed paper is to suggest an approach for development of unified modeling framework and SPM for development of the important views of MES components and coupling their established modeling notations, based on the combined use of UML profile - SysML and ANSI/ISA-S95 standard models.

The paper is organized in 4 parts. After the introduction, in part 2 the related work about existing approaches for development of MES is discussed. Part 3 of the paper presents the proposed approach for development of SPM for MES is described. A case study concerning an application of the suggested approach for a real industrial unit is presented in part 4. Finally some conclusions are made.

2. Related work

MES engineering is an interdisciplinary challenge and requires cooperation between plant engineers, MES engineers, plant manager, production manager, IT engineers, solution developer, etc. The development and implementation of MES is a difficult task and the main challenges facing the field of MES are associated with the need of unified modeling framework and SPM that can be used to represent and execute such type of systems. The modeling techniques in the field of MES can be categorized in three basic groups – using of standard models, terminology and consistent set of concepts provided by ANSI/ISA-S95 standard [1, 5, 6]; using of MDE and MDA based approaches [2, 3, 4, 7] and set of approaches based on MES process modeling [8, 9].

2.1. Approaches using ANSI/ISA-S95

ANSI/ISA-S95 standard provides standard models, terminology and a consistent set of concepts for defining the interfaces between an enterprise's business systems and its manufacturing control systems, and the activities of manufacturing operations management [1]. The suggested functional enterprise-control model is composed of 12 classes of different set of functions as shown in fig. 1. The information flows between the different functions are defined and categorized in three main areas: information required producing a product, information about the capability to produce a product and information about actual production of the product. A general activity model for all these categories is proposed, with the purpose to identify all possible data flows within manufacturing operations. As shown in fig. 1, eight main activities are defined: detailed scheduling, dispatching, resource management, tracking, definition management, data collection, execution management and analysis.

The object models of these functions are depicted using the Unified Modeling Language (UML) notational methodology. An extended approach based on ANSI/ISA-S95 series of standards integrates ontologies in order to achieve interoperability of the internal and external systems.

2.2. MDE and MDA based approaches

The UML [4] as a general purpose modeling language and an open standard supports the MDE and MDA. It does not specify a methodology for software or system design but aims to provide an integrated modeling framework, covering structural, functional and behavior descriptions. The UML notations support the development

of various diagrams that reflect different aspects of the system in order to capture the full complexity in the phases of detailed analysis and system design. Different object-oriented approaches based on UML and its profile for system engineering SysML [10] for development of control systems, which are applicable in different industry areas, are investigated. Detailed description and analysis of the different suggestions may be found in [11, 12]. The approach for MES modeling, based on SysML provides either an interaction between software components of MES and software and hardware components of the manufacturing system or possibilities for abstract and detailed modeling of MES activities.

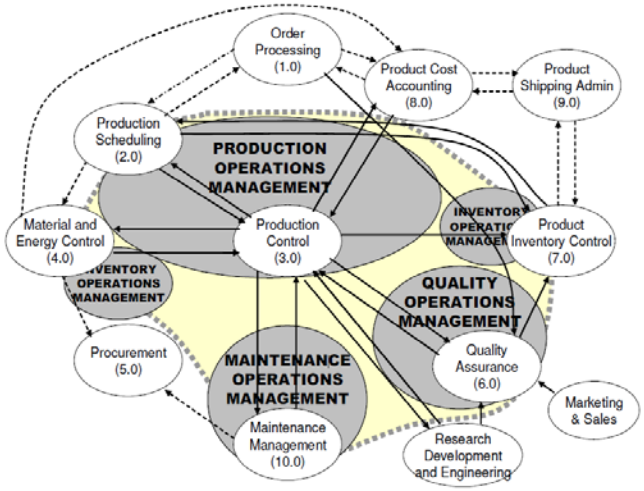


Fig.1: *Manufacturing operations management model [1]*

2.3. Approaches using MES process modeling

The modeling techniques in this group can be categorized into three sub-groups: approaches for MES process modeling using traditional process modeling languages, approaches for MES process modeling using process decomposition and approaches for MES process modeling using hybrid techniques. Various modeling languages and notations are used for modeling of interdisciplinary processes in MES, such as Business Process Modeling Notation (BPMN), Business Process Execution Language (BPEL), and SysML. The BPMN standard offers a number of structural elements, which are missing in other technologies and the information for MES specification is spared among multiple co-workers who have different view for technical and business process, know different details about the processes and have different requirements. BPMN is insufficient for modeling of complex systems but enables to present MES system as a collection of separate processes (which represent the MES functions), and so it is possible to model these processes separately under one large model [13, 14].

In [15] M. Witsch and B. Vogel-Heuser suggest a modeling framework that integrates the different important views for MES specification by coupling their established modeling notations. The main contribution of this framework is the integration of a technical system model, a production process model and an MES functional model with their interconnections and dependencies by a formal link model. MES-ML proposes a graphical MES modeling language. The technical system model represents the static technical systems that perform MES functions. This model either could be on the abstraction level of an entire plant, or detailed to atomic function units depending on the needs. The second model is the production process model, which represents the manufacturing systems in MES. The authors propose to use UML activity diagram or flow chart as the modeling notation.

3. Short description of suggested approach

The existing modeling approaches in the area of MES are not sufficient to satisfy the users and system requirements and for development of the important views of MES components. MES are not flexible enough; they have a limited scope and monolithic architecture and may not be reused in new manufacturing applications.

The success of UML and SysML in unifying many different object-oriented approaches and the graphical modeling language support of MES-ML to the required engineering process of MES led to the idea of their combined use for development of unified modeling framework and software process model for MES components. Supplementary a separation of functions/activities of business processes from production processes by using of ANSI/ISA-S95 standard models and terminology is undertaken.

The proposed model-driven approach is shown in fig.2. The basic cycles for task flow development process included in the proposed methodology, such as – requirements analysis, system functional analysis, architectural design and hardware/software specification are the stages from Harmony SE based methodology for software development processes, described in details in [11, 12]. The suggested approach uses different kinds of ANSI/ISA S95 standard models, modeled through SysML modeling constructs.

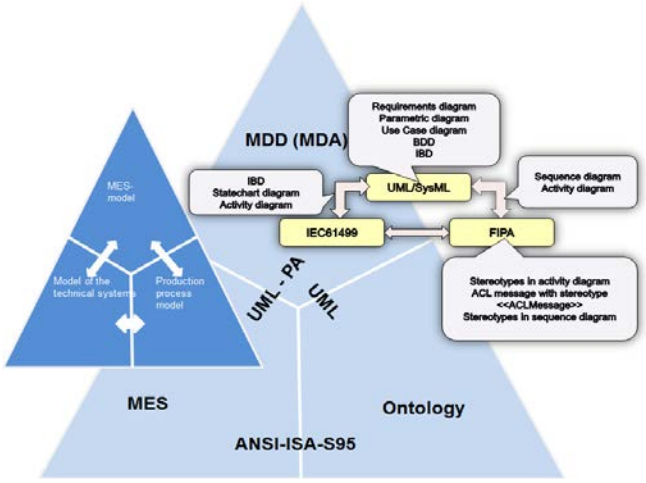


Fig.2: *Approach for development of MES*

The first step in the development of MES using the proposed approach is creating on UML/SysML profile extended with new predefined stereotypes based on MES-ML modeling notations. According MES-ML the stereotypes are divided in several groups representing MES functional model activities, MES functional model events, MES functional model data objects and getaways and MES functional model connecting objects, swim lines and artifacts. To each stereotype an icon from MES-ML modeling notations is assigned.

The development process of the MES requirements and performance analysis function is divided into two main steps – define the concrete customer functional requirements and selection of MES functions represented through the Requirements Diagram (RD) and Requirements table (RT); and MES functionality definition using Use Case Diagram (UCD) and Block Definition Diagram (BDD). The performance analysis function is based on the follow steps – analysis of the MES domain to define the environment of the MES, analysis of the MES structure and manufacturing system and analysis of customer requirements and specification. BDD is used to perform analysis of the MES domain and the MES structure and manufacturing system and in order to present customer requirements RD, RT and UCD are used.

The description and analysis of MES processes and the definition of the interfaces between an enterprise's business systems and its manufacturing control systems, and the activities of manufacturing operations management are sub-stages from next stage in the proposed methodology - architecture design. This stage includes the design of ANSI/ISA 95 models using BDD which are customized through the MES-ML stereotypes and design of the different views for MES system - technical system model, a

production process model and MES functional model modeled with Block Definition Diagram, Internal Block Diagram and Activity Diagram customized through the MES-ML stereotypes. In order to model the physical structure of the manufacturing control system (technical system model), BDD is used. The processes in the manufacturing systems (production process model), Activity Diagrams in different level of decomposition are used. The functions of MES embedded in interacting IT functionalities and systems can be modeled in MES functional model using activity diagram separated with swim lines presenting respectively the ERP, the MES and the process control system functions.

4. Case Study

To show some of the advantages of the suggested approach, a real industrial Pick and Place Unit (fig.3) constructed by Technical University Munich [16] is used. The PPU consists of a stack (1), working as a work piece input storage, a conveyor (2) working as a work piece output storage, a stamp (3) for stamping work pieces and a crane (4) for transporting work pieces by picking and placing them between three working positions – for black, white and metallic work pieces. The PPU may work in various different manifestations called Scenarios.

Fig.4 shows the UML/SysML meta-model of Production Operation Management functions according ANSI/ISA-95 [1] modeled using Papyrus plug-in of the Eclipse platform. The production operation management model is extended with product definition, product capability, product schedule, product performance, operation definition, operation capability, operation schedule and operation performance models presented like blocks. The characteristics of each model are presented with attributes. The meta-models of the Quality operation management function, Maintenance operation management function and Inventory operation management function may be modeled according their equal UML models.

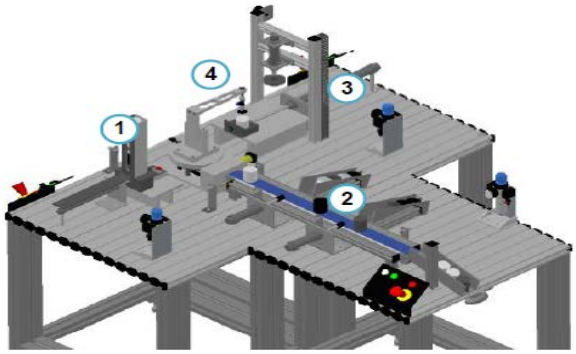


Fig.3: *Pick and Place unit*

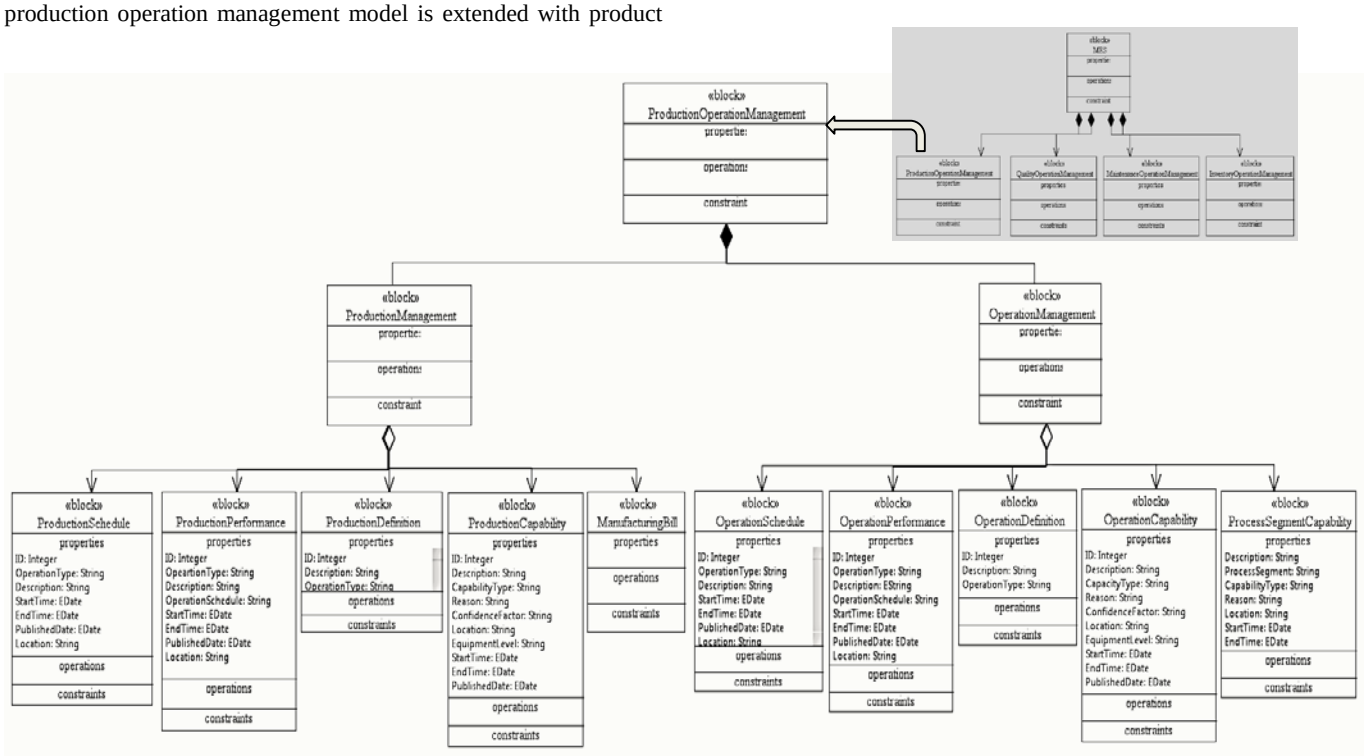


Fig.4: *Meta-model of Production Operation Management functions*

The operation schedule (fig.5), operation definition (fig.6) and operation performance models (fig.7) for PPU are presented using BDD. The Operation schedule model for PPU (fig.5) consists of blocks named according ANSI/ISA-95's model "PPU-Request", "Requirement", "Equipment Requirement" and "PPU-Material". The information needed for model elements is presented as attributes with appropriate data type and constraints defined using OCL (Object Constraint Language). The attributes in block "PPU-Request" show that the plant execute Scenario 0 [16], type of operation is production, start and stop time of the process. The block "Requirement" contains information about earliest start time of the process, latest end and duration of the process. The required equipment for execution of Scenario 0 is Micro switch, Motor, Vacuum switch, Monostable Cylinder, Turning table, Stack, Crane, Ramp and Binary Sensors are defined as attributes in block "Equipment Requirement". The information about material is assigned with attribute named "WP", presenting the number of work pieces for PPU.

In fig.6 the operation definition model for PPU is shown. The model consists of blocks with names "PickUp&Place", "Operation Material Bill", "PPU", "Operation Definition Dependency", "Parameter Specification", "Equipment Specification" and "Material Specification". In block "Operation Definition Dependency" the operations dependency according ANSI/ISA-S95 specifications g dependency types: B can not follow A; B may run in parallel to A; B may not run in parallel to A; start B no later than T (Timing Factor) after A start; etc. are defined. Timing factor is also defined as constraint in block "PPU" and attribute "Duration". The operation definition constraints are assigned using OCL. The type and number of required equipment is defined in "Equipment Specification".

Fig.7 shows the operation performance model for PPU which consist form blocks named "PPU-Operation Response", "Response", "Equipment Actual" and "Material Actual". Due the possibility to use metallic or plastic (black and white) work pieces in block "Material Actual" two attributes – WP color and WP material are defined.

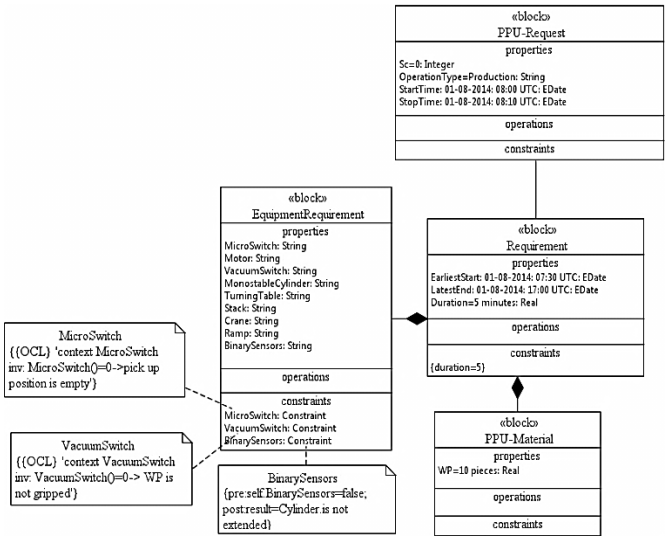


Fig.5: Operation schedule model for PPU

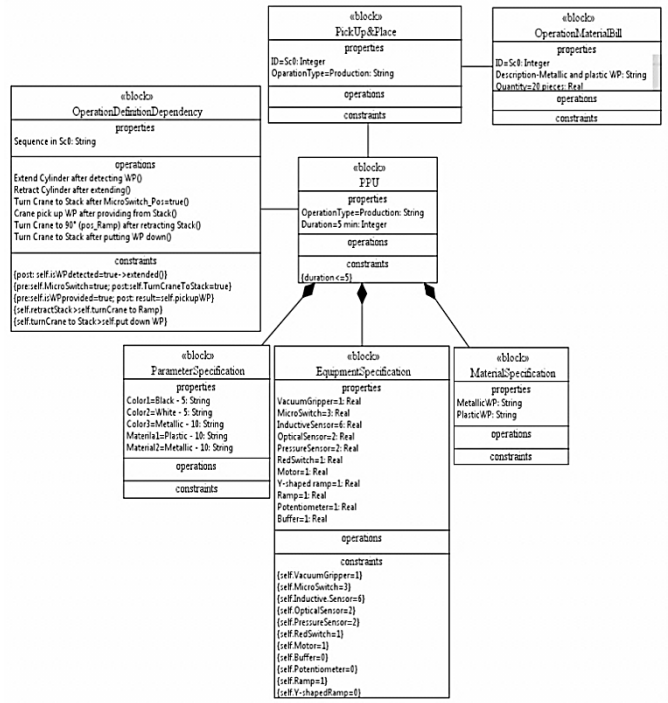


Fig.6: Operation definition model for PPU

5. Conclusions

The paper presents an approach for development of unified modeling framework and SPM for modeling of important views of MES and their components. The UML/SysML profile is extended and at the same time restricted with different stereotypes from MES-ML and ANSI/ISA S95 standard models. The benefits of using this approach are summarized as follow: development of open, flexible and reusable components, faster specification of MES functionality, improvement of capabilities for requirements definition, etc.

The proposed approach is partial realized for modeling of a real industrial Pick and Place Unit. The meta-model and the models of Production Operation Management functions are created.

The future research activities are concentrated mainly on applying the suggested approach to continuous and batch systems as well as application of the suggested approach in industry.

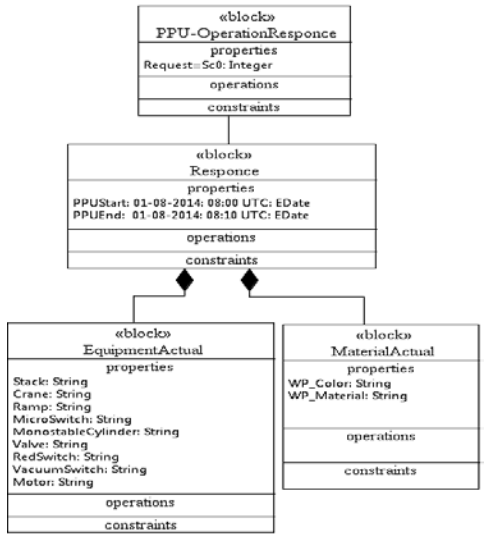


Fig.7: Operation performance model for PPU

6. References

1. ANSI/ISA-S95.00.03-2005, Enterprise-Control System Integration Part 3: Models of Manufacturing Operations Management. ISA, Raleigh, North Carolina, USA
2. Kent, S., Model Driven Engineering. In Proceedings of IFM, 2002, LNCS 2335, Springer.
3. OMG-MDA. MDA Guide version 1.0.1. OMG document omg/2003-06-01, 2003.
4. OMG-UML, 2010. OMG. http://www.omg.org/
5. ANSI/ISA-S95.00.01-2000, Enterprise-Control System Integration Part 1: Models and Terminology, ISA, Raleigh, North Carolina, USA.
6. ANSI/ISA-S95.00.02-2001, Enterprise-Control System Integration Part 2: Object model attributes. ISA, Raleigh, North Carolina, USA.
7. Pietrac L., Leleve A., Henry S., On the use of SysML for Manufacturing Execution System design, IEEE 16th Conference on Emerging Technologies & Factory Automation (ETFA), 2011, 5-9 Sept., Toulouse, pp.1 – 8.
8. Vogel-Heuser B., Erhöhte Verfügbarkeit und transparente Produktion, 2011, ISBN:978-3-86219-178-9.
9. Fang M., Process Modeling and Execution in Non-Enterprise System Integration, Master Thesis Software Engineering, Thesis no: MSE-2012:107, 05 2012
10. OMG-SysML (2006). The OMG Systems Modeling Language, http://omgsysml.org/index.htm,
11. Batchkova I., Antonova I. (2011), Improving the Software Development Life Cycle in Process Control using UML/SysML, Preprints of the 18th IFAC World Congress, pp. 14133÷14138, August 28 - September 2, Milano, Italy.
12. Antonova I., Batchkova I., Development of Multi-Agent Control Systems using UML/SysML, book capter, pp.67-90, InTech, 2011, ISBN: 978-953-307-174-9.
13. Mili H., Tremblay G., Jaoude G.B., Lefebvre E., Elabed L., Boussaidi G.E., Business process modeling languages: Sorting through the alphabet soup. ACM Computing Surveys (CSUR), 43(1):4, 2010.
14. Michalik P., Štofa J., Zolotová I., The use of BPMN for modelling the MES level in information and control systems, Quality innovation prosperity XVII/1 – 2013, ISSN 1335-1745, pp.39-47.
15. Witsch M., Vogel-Heuser B., Modeling of Manufacturing Execution Systems: an Interdisciplinary Challenge, 15th IEEE International Conference on Emerging Technologies and Factory Automation, 2010.
16. Institute of Automation and Information Systems. The Pick and Place Unit – Demonstrator for Evolution in Industrial Plant Automation, 2013. http://www.ais.mw.tum.de/ppu/.